8-10-2021

Post-translational SUMOylation dynamically regulates voltage-gated potassium channel, Kv4.2

Meghyn Welch

Post-translational SUMOylation dynamically regulates voltage-gated potassium channel, Kv4.2

by

Meghyn Welch

Under the Direction of Deborah Baro, PhD

A Dissertation Submitted in Partial Fulfillment of the Requirements for the Degree of

Doctor of Philosophy

in the College of Arts and Sciences

Georgia State University

2021

ABSTRACT

The family of voltage-gated Kv4 ion channels (Kv4.1-3) mediates the transient A-type potassium currents, IA, and is an important regulator of neuronal signaling. Aberrations in Kv4 channel expression and/or function are associated with several disease states, including chronic pain, epilepsy, Alzheimer's disease, Huntington's disease and major depressive disorder. Kv4 channels exist as ternary complexes with potassium channel interacting proteins and dipeptidyl peptidase-like proteins. Multiple ancillary proteins also associate with the Kv4 ternary complex throughout its lifetime. Little is known about the regulation of protein-protein interactions within Kv4 macromolecular complexes. Small ubiquitin-like modifier (SUMO) is a peptide that is post-translationally conjugated to lysine (K) residues on target proteins. This post-translational modification dynamically regulates protein-protein interactions. It can either promote or prevent a given interaction. This dissertation research investigated if/how post-translational SUMOylation moderated Kv4.2 protein-protein interactions to tune IA. Kv4.2 has several putative SUMOylation sites. Two conserved sites were examined in this work: K437 and K579. SUMOylating K579 increased IA when Kv4.2 existed in the ternary complex but decreased IA when Kv4.2 was expressed alone. Studies to identify the mechanism indicated that K579 SUMOylation increased IA by promoting ternary complex recycling after endocytosis, most likely by blocking an interaction with a ubiquitin ligase and thereby reducing a ubiquitin lysosome sorting signal. In contrast, when Kv4 was not incorporated into a ternary complex, K579 SUMOylation blocked an unknown protein-protein interaction that altered channel gating to reduce IA. SUMOylation at the second site, K437, had no effect when Kv4.2 was incorporated into the ternary complex, but increased the insertion of electrically silent channels when Kv4.2 was expressed alone. The mechanism underpinning increased surface expression was not

examined. These dissertation findings were the first to demonstrate that Kv4.2 can be SUMOylated to regulate IA, that SUMOylation modulates Kv4.2 internalization and that the effect of SUMOylation depends upon the available interactome.

INDEX WORDS: Small ubiquitin-like modifier (SUMO), Ion channel, Voltage-gated potassium channel, Kv4, A-type potassium current, Trafficking

Post-translational SUMOylation dynamically regulates voltage-gated potassium channel, Kv4.2

by

Meghyn Welch

Committee Chair: Deborah Baro

Committee: Chun Jiang

Aaron Roseberry

Electronic Version Approved:

Office of Graduate Services

College of Arts and Sciences

Georgia State University

August 2021

DEDICATION

This work is dedicated to my family, especially my Mom, Dad and sister. I would not have been able to accomplish this without you all. Thank you!

ACKNOWLEDGEMENTS

First, I would like to thank my Ph.D. advisor, Dr. Deborah Baro. You have helped me become a confident researcher and have provided invaluable support and guidance over the years.

Second, I would like to thank my dissertation committee – Dr. Chun Jiang and Dr. Aaron Roseberry. Thank you for your advice and support throughout my Ph.D.

I would also like to thank the current and former members of the Baro lab – Lori Forster, Leslie-Anne Jansen, Anna Parker, Selin Atlas, Debasmita De, Janhavi Dubhashi, Sarah Tasneem, Justin Serna, Brenda Okonkwo, and Sasha Guillory. Specifically, I would like to say thank you to Anna Parker, Lori Forster and Leslie-Anne Jansen. You all have provided so much encouragement throughout the years. Thank you all for letting me run ideas by you, your advice, your willingness to always help, and your friendship!

I would also like to thank members of the Jiang and Roseberry labs for your technical help over the years.

Finally, thank you to the Brains and Behavior Fellowship program for the support over the years.

TABLE OF CONTENTS

LIST OF TABLES

LIST OF FIGURES

1 INTRODUCTION

1.1 Role of the transient A-type potassium current in the nervous system

Potassium channels are grouped into several families, including two-pore domain channels, inward-rectifier channels, ligand-gated channels, and voltage-activated channels (Coetzee et al., 1999; Kuang, Purhonen, & Hebert, 2015). Twelve subfamilies of voltage-activated potassium channels (Kv1-12) have been identified and classified according to function: delayed rectifying (Kv1.1-3, Kv1.5-8, Kv2, Kv3.1-2 Kv7, Kv10.1), A-type (Kv1.4, Kv3.3-4, Kv4), outwardly rectifying (Kv10.2), inwardly rectifying (Kv11) slowly activating (Kv12), or modifier/silent (Kv5, Kv6, Kv8, Kv9) (Gutman et al., 2005).

The Kv4 subfamily comprises Kv4.1, Kv4.2 and Kv4.3. Transcripts can be alternately spliced to create additional isoforms. Four Kv4 pore-forming α-subunits assemble to form a channel. Each subunit has a cytoplasmic N- and C-terminus and six transmembrane spanning regions (S1-S6). Kv4 channels have a highly conserved tetramerization domain (T1), which immediately precedes S1 and assists in tetrameric assembly of the α-subunits. S1-S4 make up the voltage sensing domain (VSD), while the p-loop between S5 and S6 constitute the pore-forming domain (Birnbaum et al., 2004).

Kv4 channels are widely expressed throughout the central and peripheral nervous systems (CNS/PNS), and in neurons Kv4 channels are largely expressed in somatodendritic compartments (Birnbaum et al., 2004; Sheng, Tsaur, Jan, & Jan, 1992). Kv4 channels play key roles in controlling neuronal excitability (Jerng & Pfaffinger, 2014). For example, Kv4 channels control neuronal firing rates (Carrasquillo, Burkhalter, & Nerbonne, 2012; Lin, Sun, Kung, Dell'Acqua, & Hoffman, 2011). Kv4 channels modulate back propagating action potentials. In CA1 pyramidal neurons, the density of the Kv4.2 channels increases with distance from the

soma. The high density of Kv4.2 channels in the distal dendrites prevents back propagating action potentials from infiltrating this region (Hoffman, Magee, Colbert, & Johnston, 1997). Kv4 channels regulate synaptic plasticity. For example, Kv4.2 knock out mice have a lowered threshold for LTP induction (X. Chen et al., 2006), and Kv4.2 channels are internalized during LTP induction to facilitate synaptic plasticity (J. Kim, Jung, Clemens, Petralia, & Hoffman, 2007).

A plethora of extracellular signals can modulate IA. In many cases, modulatory effects are mediated by protein kinases, and several different protein kinases are known to phosphorylate Kv4 channels. Protein kinase A (PKA) directly phosphorylates Kv4.2 channels at threonine 38 (T38) and serine 552 (S552) on the N- and C-termini, respectively (A. E. Anderson et al., 2000). PKA phosphorylation at S552 has multiple effects that vary with system. For example, in *Xenopus* oocytes expressing Kv4.2 and potassium channel interacting protein (KChIP), PKA phosphorylation at S552 decreases current amplitude by causing a rightward shift in the voltage of half-activation and increasing the inactivation time constant. In hippocampal dendritic spines, PKA phosphorylation at S552 reduces IA current density and channel surface expression by increasing Kv4.2 internalization (Hammond, Lin, Sidorov, Wikenheiser, & Hoffman, 2008). Protein kinase C (PKC) directly phosphorylates Kv4.2 at two additional C-terminal sites, S447 and S537, and reduces IA current density and surface expression (Schrader et al., 2009). ERK is a downstream target of both PKA and PKC, and ERK phosphorylates Kv4.2 at T602 and T607 to downregulate IA (Adams et al., 2000; H. J. Hu, Alter, Carrasquillo, Qiu, & Gereau, 2007; Schrader et al., 2009; Yuan, Adams, Swank, Sweatt, & Johnston, 2002). Glycogen synthase kinase 3 (GSK3) beta phosphorylation of Kv4.2 at S616 downregulates IA and augments spike-timing dependent LTP (Aceto et al., 2020). Calcium-calmodulin-dependent

kinase (CaMKII) phosphorylates Kv4.2 at two C-terminal sites, S438 and S459, and CaMKII phosphorylation increases channel surface expression and IA current amplitude (Varga et al., 2004).

Aberrant Kv4 expression and function have been implicated in several neurological diseases, including fragile X syndrome, epilepsy, Huntington's disease, Alzheimer's disease, chronic depression, and chronic pain. Fragile X syndrome is caused by loss of fragile X mental retardation protein (FMRP) and is associated with neuronal hyperexcitability. Normally, FMRP associates with Kv4.2 mRNA and positively regulates its translation and protein expression, and in cortical neurons and hippocampal slices from Fmr1 knockout (KO) mice, a reduction in total Kv4.2 protein levels and Kv4.2 surface expression is observed, and this increases neuronal excitability (Gross, Yao, Pong, Jeromin, & Bassell, 2011). Different studies report either a decrease or increase in Kv4.2 expression following a seizure. In the hippocampus, Kv4.2 surface expression is decreased following kainate-induced status epilepticus (SE) (Joshi, Rajasekaran, Hawk, Chester, & Goodkin, 2018; Lugo et al., 2008), while Kv4.2 surface expression is increased following lithium-pilocarpine-induced SE (Joshi et al., 2018). Autosomal dominant lateral temporal epilepsy (ADTLE) is an inherited epilepsy disorder associated with mutations in leucine-rich glioma-inactivated-1 (LGI1). LGl1 is necessary for trafficking Kv4.2 channels to the surface after a pilocarpine induced seizure, and this homeostatic response attenuates phasic firing in thalamocortical neurons (Smith, Xu, Kasten, & Anderson, 2012). Deficits in indirect spiny projection neurons (iSPNs) is linked with the hyperkinetic phenotype seen in Huntington's disease (HD). Distal dendrites of iSPN neurons from symptomatic HD mice are hypoexcitable due to an increased association of Kv4 with KChIP (Carrillo-Reid et al., 2019). In several Alzheimer's disease models neuronal excitability is enhanced by down regulation of Kv4

channels (Hall et al., 2015; K. R. Kim et al., 2021; Ping et al., 2015; Scala et al., 2015). In a mouse model of chronic depression there is an increase in spike timing-dependent long-term potentiation (LTP) in the medium spiny neurons of nucleus accumbens caused by a down regulation of Kv4 channels due to phosphorylation of the channel by GSKbeta (Aceto et al., 2020). Blocking GSKbeta ameliorates depressive-like behaviors in these animals. Chronic pain is associated with nociceptor hyperexcitability and this hyperexcitability is caused by reduced IA and Kv4 expression in these neurons (Kanda et al., 2021; C. Wang et al., 2021; Zemel, Ritter, Covarrubias, & Muqeem, 2018).

1.2 **Kv4 macromolecular complex**

Kv4 α-subunits form functional channels that mediate IA; however auxiliary proteins that interact with the α-subunit can modulate channel function. Co-expressing two auxiliary proteins, potassium channel interacting protein (KChIP1-4) and dipeptidyl peptidase like protein (DPLP; DPP6 and DPP10) is necessary to recapitulate native IA in heterologous expression systems (Amarillo et al., 2008; Jerng, Kunjilwar, & Pfaffinger, 2005; Jerng & Pfaffinger, 2012). This fundamental unit is termed a ternary complex (Figure 1.1).

KChIPs belong to the neuronal calcium sensor (NCS) gene family, and in mammals, four KChIP (KCNIP1-4) genes encode the four families of KChIP proteins (KChIP1-4), and multiple KChIP isoforms exist due to alternative splicing (An et al., 2000; Jerng & Pfaffinger, 2014; Morohashi et al., 2002). KChIPs have four conserved EF-hands that can bind Mg^{2+} or Ca^{2+}. EF-1 is unbound, EF-2 binds Mg^{2+}, and EF-3 and EF-4 bind Ca^{2+} (Chen, Lee, & Chang, 2006; Osawa et al., 2005). KChIPs are cytosolic proteins that have a variable N-terminus attached to a conserved C-terminal core, which contains the 4 EF-hands. Some KChIP isoforms can associate with the plasma membrane via N-myristoylation (O'Callaghan, Hasdemir, Leighton, &

Burgoyne, 2003), S-palmitoylation (Takimoto, Yang, & Conforti, 2002), or a transmembrane segment on the variable N-terminus (Jerng & Pfaffinger, 2008, 2014).

Cytosolic KChIPs first interact with the cytosolic termini of Kv4 α-subunits at the ER (An et al., 2000; Hasdemir, Fitzgerald, Prior, Tepikin, & Burgoyne, 2005; Shibata et al., 2003). Structural models show a 4:4 stoichiometry of Kv4: KChIP subunits, and high-resolution structural information obtained from a crystalized rat or human Kv4.3 N-terminal domain and human KChIP1 describes two KChIP binding sites on the Kv4 N-terminus. A hydrophobic binding pocket on KChIP interacts with a stretch of ~40 N-terminal hydrophobic amino acids on the α-subunit (site 1), and that same KChIP binds to the T1 domain on an adjacent Kv4 subunit and "clamps" two α-subunits together (site 2) (Pioletti, Findeisen, Hura, & Minor, 2006; H. Wang et al., 2007) (Figure 1.2). KChIPs also bind to the Kv4 C-terminus. High-resolution X-ray crystallography studies detailing the interaction between KChIP and the Kv4 C-terminus have yet to be resolved; however, C-terminal deletion mutants show that an intact C-terminus facilities KChIP binding (Callsen et al., 2005; W. Han, Nattel, Noguchi, & Shrier, 2006).

KChIPs increase Kv4 surface levels and steady-state Kv4 protein expression and reduce Kv4 internalization at the cell surface (Foeger, Marionneau, & Nerbonne, 2010; Shibata et al., 2003). In addition, KChIPs exert significant effects on channel biophysical properties, including increasing IA current density, slowing channel inactivation, shifting the voltage dependence of activation and steady-state inactivation to more depolarized values and accelerating recovery from inactivation (An et al., 2000; Bahring et al., 2001; Foeger et al., 2010; Shibata et al., 2003).

DPLPs are single-pass transmembrane proteins belonging to a family of serine proteases that lack the active-site serine and the molecular structure for catalytic activity. DPLP proteins are encoded by two homologous genes, DPP6 and DPP10, and multiple isoforms exist due to

alternative splicing. DPLPs have a short variable cytoplasmic N-terminus, conserved transmembrane segment and large extracellular globular C-terminus (Jerng, Qian, & Pfaffinger, 2004; Nadal, Amarillo, Vega-Saenz de Miera, & Rudy, 2006; Nadal et al., 2003; Takimoto, Hayashi, Ren, & Yoshimura, 2006).

The DPLP transmembrane domain binds to S1 and S2 on the Kv4 α-subunit (Ren, Hayashi, Yoshimura, & Takimoto, 2005); however, high-resolution structural data regarding the binding is lacking. There are conflicting reports about how many DPLPs bind to Kv4 channels. Kv4-DPP6 shows a preference for a 4:4 stoichiometry (Soh & Goldstein, 2008), while Kv4-DPP10 shows a preference for a 4:2 stoichiometry (Kitazawa, Kubo, & Nakajo, 2015).

Like KChIPs, DPLPs also interact with Kv4 α-subunits at the ER and facilitate forward trafficking to the plasma membrane (Lin, Long, Hatch, & Hoffman, 2014; Nadal et al., 2003; Zagha et al., 2005), and this increase in Kv4 surface expression is mediated by N-glycosylation of the DPLP extracellular domain (Cotella et al., 2010; Cotella et al., 2012). DPLPs exert a profound effect on channel gating, increasing single channel conductance, accelerating channel activation, inactivation, and recovery from inactivation, and shifting the voltage dependence of activation and steady-state inactivation to more hyperpolarized values (Jerng et al., 2004; Kaulin et al., 2009; Nadal et al., 2003).

In addition to KChIP and DPLP, multiple ancillary proteins interact with Kv4 α-subunits to influence trafficking and gating. Recently, tandem affinity purification of exogenously expressed Kv4.2 followed by mass spectrometry identified over 120 endogenous HEK cell proteins that associate with the α-subunit (J. H. Hu et al., 2020). In the ER, J-proteins interact with Kv4 α-subunits to facilitate tetramerization, and recruit chaperone protein Hsp70 to prevent the channel from misfolding and aggregating (Li et al., 2017). The Kv4 α-subunit can traffic in

distinct pathways from the ER to the Golgi depending on which KChIP isoform the channel interacts with. For example in HeLa cells, Kv4 channels that associate with KChIP1 traffic from the ER to the Golgi in non-COPII vesicles that do not contain the usual ER-Golgi SNARE proteins, but instead are positive for Vtila and VAMP7 (Flowerdew & Burgoyne, 2009; Hasdemir et al., 2005; B. L. Tang, 2020). Cardiomyocytes express KChIP2 and not KChIP1, and in these cells, Kv4 traffics through a conventional ER-Golgi pathway in COPII containing vesicles, and trafficking requires Rab1 and Sar1 (T. Wang et al., 2012). Soluble N-ethylmaleimide-sensitive factor attachment protein receptor (SNARE) protein, syntaxin 1A binds to the N-terminus of Kv4.2α and this interaction decreases channel surface expression and reduces IA current density in HEK cells (Yamakawa et al., 2007). A di-leucine motif on the C-terminus of Kv4α is necessary and sufficient for dendritic transport of the channel (Rivera, Ahmad, Quick, Liman, & Arnold, 2003), and Kif7 binding to a sequence of amino acids downstream of this motif facilitates dendritic transport (Chu, Rivera, & Arnold, 2006). Potassium channel-associated protein (KChAP, aka PIAS3) associates with Kv4 and increases IA in a transcription-independent fashion (Kuryshev, Gudz, Brown, & Wible, 2000; Pourrier, Schram, & Nattel, 2003). The mechanism of action was not identified, but PIAS proteins were subsequently determined to be SUMO E3 ligases (Johnson & Gupta, 2001; Kahyo, Nishida, & Yasuda, 2001). Actin binding protein filamin interacts with the Kv4 C-terminus to increase IA current density (Petrecca, Miller, & Shrier, 2000). The C-terminus of Kv4 channels associate with Kvβ2 in the rat brain to increase total Kv4 protein levels and IA (Yang, Alvira, Levitan, & Takimoto, 2001). In the mouse brain, Kv4 interacts with Navβ1 and this association stabilizes Kv4.2 protein levels and increases channel surface expression and increase IA current density (Marionneau et al., 2012). Kv4 channels interact with two members of the membrane-associated

guanylate kinase (MAGUK) family, SAP97 and PSD95, and both of these proteins bind the Kv4 C-terminus (Gardoni et al., 2007; Wong, Newell, Jugloff, Jones, & Schlichter, 2002). In the hippocampus, SAP97 is important for Kv4 trafficking from the ER to the post-synaptic sites, while PSD95 is an important anchoring element once the channel arrives to the synaptic compartment (Gardoni et al., 2007). Scaffolding protein AKAP79/150 binds SAP97 and PSD95 and also directly interacts with the C-terminus of Kv4 α-subunits and anchors PKA and calcineurin close to the channel to facilitate dynamic (de)-phosphorylation (Colledge et al., 2000; Lin et al., 2011). Finally, the Kv4 macromolecular complex includes other ion channels. For example, in cerebellar stellate cells, Kv4.2 forms a complex with KChIP3 and Cav3. Calcium influx from Cav3 binds to KChIP3 and this modulation is important for shifting the voltage-dependence of half-inactivation into a physiological range to control spike output (D. Anderson, Mehaffey, et al., 2010; D. Anderson, Rehak, et al., 2010).

Little is known about how interactions with Kv4 are regulated. Previous studies have looked at mechanisms targeting the Kv4α-KChIP or Kv4α-DPLP interaction. Calcium binding to KChIP influences its binding to the α-subunit. Mutating KChIP EF-hands blocks the ability of KChIP4 to co-immunoprecipitate (co-IP) with Kv4.2 in COS cells and attenuates the KChIP4 mediated increase in IA current density and recovery from inactivation (Morohashi et al., 2002). In HEK cells expressing KChIP3 and Kv4.2, more KChIP3 co-IPs with Kv4.2 in the presence of Ca^{2+}; and in whole-cell recordings using a Ca^{2+} -free pipette solution, KChIP3 failed to increase recovery from inactivation and shift the steady-state voltage of half-inactivation to more a positive value (C. Seifert, Storch, & Bahring, 2020). Ceroid lipofuscinosis neuronal 3 (CLN) protein interacts with KChIP3 and modulates the Kv4.2-KChIP3 interaction. Overexpressing CLN3 with Kv4.2 and KChIP3 in HEK cells, reduces the amount of KChIP3 that co-IPs with

Kv4.2 channels, abolishes the KChIP3-mediated increase in IA current density, and attenuates the ability of KChIP3 to slow the time constant of inactivation, shift the voltage of steady-state inactivation to more depolarized value, and speed recovery from inactivation (C. Seifert et al., 2020). N-glycosylation of DPP10 is essential for interaction with Kv4.3. In CHO cells, preventing N-glycosylation of DPP10 disrupts its binding to Kv4.3 and blocks the DPP10 mediated increase in Kv4.3 surface expression, and impairs the ability of DPP10 to hasten inactivation, shift the voltage of activation and steady-state inactivation to more negative values, and accelerate recovery from inactivation (Cotella et al., 2012). In hippocampal CA1 neurons proyl cis/trans isomerase Pin1 modulates the Kv4.2-DPP6 interaction to adjust IA. Seizure or enriched environment exposure leads to phosphorylation of Kv4.2 at T607, and Pin1 binding to phosphorylated T607 reduces the amount of DPP6 that co-IPs with Kv4.2. Pharmacological block of Pin1 or mutating the Pin1 binding site on Kv4.2 increases IA current density and speeds recovery from inactivation in out-side out somatic patches from CA1 pyramidal neurons, suggestive of more Kv4.2 channel in a complex with DPP6 (J. H. Hu et al., 2020). Identifying the mechanisms controlling these protein-protein interactions is important for understanding how IA is dynamically regulated.

1.3 Small ubiquitin-like modifier is a dynamic modification that organizes protein-protein interactions

Small ubiquitin-like modifier is an 11kD peptide post-translationally added to lysine (K) residues on a target protein (Flotho & Melchior, 2013; Henley, Carmichael, & Wilkinson, 2018; Henley et al., 2021)**.** In some cases, SUMO can be SUMOylated to create a polySUMO chain on a protein. In mammals, there are 5 SUMO isoforms (SUMO1-5). SUMO-2 and SUMO-3 are 98% identical and share 47% sequence homology with SUMO-1. Post-translational modification

by SUMO1-3 is widely studied. (Celen & Sahin, 2020; H. M. Chang & Yeh, 2020; Flotho & Melchior, 2013; Henley et al., 2018; Henley et al., 2021). SUMO-2 and SUMO-3 can form poly-SUMO chains on internal K residues (Tatham et al., 2001). Little is known about the function of SUMO-4 and SUMO-5 as post-translational modifiers (Liang et al., 2016; Owerbach, McKay, Yeh, Gabbay, & Bohren, 2005).

SUMO is added to K residues using a series of enzymes similar to those used for conjugating ubiquitin. First, the carboxy terminal of immature SUMO is cleaved by a family of Sentrin/SUMO-specific proteases (SENPs) to expose a C-terminal di-glycine residue, and mature SUMO is transferred to the SAE1/UBA2 heterodimer (E1) and is then transferred to the sole E2 conjugating enzyme Ubc9 (Desterro, Thomson, & Hay, 1997). Approximately 65% of SUMOylation occurs at a SUMO consensus motif, ψKXE/D, where ψ is a hydrophobic residue, x is any amino acid, D is aspartic acid and E is glutamic acid. Ubc9 can directly recognize and SUMOylate a K residue within a SUMO consensus motif (Matic et al., 2010; Sampson, Wang, & Matunis, 2001), or recruit an E3 ligase which helps stabilize the interaction and catalyze conjugation. In the cases where SUMO is added to a non-consensus site, the E3 ligase can direct SUMO to a K residue or provides substrate specificity (Uzoma et al., 2018). Alternatively, a SUMO interacting motif (SIM) can capture a SUMO attached to Ubc9 and SUMO can be added to a nearby K residue (Meulmeester, Kunze, Hsiao, Urlaub, & Melchior, 2008; Zhu et al., 2008). SUMO is a reversible modification, and the main SUMO de-conjugating enzymes are the SENPs (Hickey, Wilson, & Hochstrasser, 2012; Nayak & Muller, 2014) **(Figure 1.3).**

SUMOylation organizes protein-protein interactions, and there are several non-mutually exclusive consequences of protein SUMOylation. (1) SUMO can compete with another post-translational modification, such as ubiquitination, methylation, or acetylation, for the same K

residue (D. D. Anderson, Eom, & Stover, 2012; Armando et al., 2014). (2) SUMO can interact with phosphoinositols in the trans-Golgi (PI(3)P) or plasma membrane (PI(3,4,5)P3) (Kunadt et al., 2015). (3) SUMO can block a protein-protein interaction through steric hindrance. For example, CRMP2 SUMOylation blocks its interaction with endocytic proteins Numb, Esp15, and E3 ubiquitin ligases Nedd4-2 and Itch (Dustrude et al., 2016). (4) SUMO can facilitate target protein interactions with other proteins when the SUMO moiety on the target protein attaches to a SUMO binding domain on an interacting partner protein, the most common being the SIM domain (Hecker, Rabiller, Haglund, Bayer, & Dikic, 2006). The SUMO-SIM interaction is weak, and most protein pairs have additional, stronger sites of interaction. Thus, SUMO is useful for recruitment or for stabilizing protein interactions. Often a single protein will have multiple SIM domains and SUMOylation sites, and large multi-protein complexes can be stabilized by multiple SUMO-SIM interactions (Figure 1.4). This is widely observed in the nucleus, where SUMOylation has been extensively studied.

SUMO is predominately expressed in the nucleus where it controls transcription, replication, DNA repair, and transport. The ability of SUMO to co-regulate a set of functionally related nuclear proteins is well documented. For example, during heat shock, transcription regulatory proteins are recruited to ~1300 gene regulatory sites, mostly at promoters. Although these proteins have binding sites that allow them to form a complex, normally these proteins would disperse after a few minutes. However, SUMOylation of the proteins in these complexes is increased as a part of the heat shock response. As a result, the multi-protein complexes are stabilized on the DNA for 30min, and this drives the gene expression necessary for the heat shock response (A. Seifert, Schofield, Barton, & Hay, 2015). Similarly, when there is a break in DNA, repair proteins are recruited to the site of the break on the DNA. The proteins in the

complex are SUMOylated, and the multiprotein complex is stabilized on the DNA until the repair can be performed (Jentsch & Psakhye, 2013; Psakhye & Jentsch, 2012) (Figure 1.4). In these cases, mutating SUMOylation sites on one individual protein does not alter its functional effect, as long as the other proteins in the network remain SUMOylated.

Extranuclear proteins can also be SUMOylated. Though studies on extra-nuclear SUMOylation began relatively recently, there is a preponderance of data indicating that neurons are tuned by the SUMOylation of ion channels, receptors, transporters for neurotransmitter re-uptake, synaptic proteins, signaling proteins, cytoskeletal-associated proteins, and RNA-binding proteins (Henley et al., 2018; Henley et al., 2021; Wasik & Filipek, 2014). SUMOylation regulates multiple cellular processes in neurons including membrane protein trafficking (Cartier et al., 2019; Dustrude et al., 2016; Kunadt et al., 2015; Ma et al., 2016; Odeh, Coyaud, Raught, & Matunis, 2018; Zhou et al., 2018), translation (Ford, Ling, Kandel, & Fioriti, 2019), signal transduction (Henley et al., 2021), protein localization (Huang et al., 2012), ion channel biophysical properties (see below), synaptic vesicle trafficking and exocytosis (Craig, Anderson, Evans, Girach, & Henley, 2015; Girach, Craig, Rocca, & Henley, 2013; L. T. Tang, Craig, & Henley, 2015). As a result, SUMOylation influences most aspects of neuronal function including neuronal excitability and firing properties, synaptic transmission and plasticity, spine maturation and density, and the stress response (Henley et al., 2021). While an expanding repertoire of targets and functions of extra-nuclear SUMOylation continues to be identified, the regulatory mechanisms involved remain elusive. SUMOylation can be regulated by the phosphorylation status of the target protein (Flotho & Melchior, 2013). Neuronal activity can also modify SUMOylation profiles by altering the behavior of the SUMOylation machinery and/or its location and/or abundance (Craig et al., 2012; Feligioni, Mattson, & Nistico, 2013; Hickey et al.,

2012; Jaafari et al., 2013; Loriol et al., 2014; Loriol, Khayachi, Poupon, Gwizdek, & Martin, 2013; Mendes, Grou, Azevedo, & Pinto, 2016; Nayak & Muller, 2014; Watts, 2013).

Research over the last fifteen years suggests that ion channel SUMOylation serves as a mechanism to dynamically adapt the electrophysiological properties of neurons. SUMOylation silences K2P1 channels (Plant et al., 2010; Rajan, Plant, Rabin, Butler, & Goldstein, 2005). Kv1.5 channel SUMOylation results in a 15mV hyperpolarizing shift in the voltage of dependence of steady-state inactivation (Benson et al., 2007). SUMOylation of Kv2.1 enhances the firing rate of rat hippocampal neurons by shifting the channel's voltage dependence of activation up to 35mV (Plant, Dowdell, Dementieva, Marks, & Goldstein, 2011). Hyper-SUMOylation of Kv7.2 and Kv7.3 diminishes the hyperpolarizing M-current in hippocampal CA3 neurons leading to neuronal hyperexcitability (Qi et al., 2014). Kv11.1 channel SUMOylation reduces current amplitude by reducing the time constant of inactivation (Steffensen, Andersen, Mutsaers, Mujezinovic, & Schmitt, 2018). SUMOylating TRPV1 lowers the temperature coefficient and temperature threshold for channel activation (Y. Wang et al., 2018). Hypoxia induces Nav1.2 SUMOylation which shifts the voltage-dependence of channel activation so that depolarizing current steps evoke larger Na^+ currents (Plant, Marks, & Goldstein, 2016). Hypoxia also increases the late Na^+ current in myocytes by inducing rapid SUMOylation of $Na_V1.5$ channels so they reopen when normally inactive, late in the action potential (Plant, Xiong, Romero, Dai, & Goldstein, 2020). HCN2 SUMOylation increases channel surface expression and Ih Gmax (Parker et al., 2016), and nociceptor HCN2 SUMOylation is altered during chronic pain (Forster, Jansen, Rubaharan, Murphy, & Baro, 2020; Jansen et al., 2021). Enhanced Kainate receptor (GluK2) SUMOylation increased its internalization (Konopacki et al., 2011). SUMOylating an auxiliary subunit of NaV1.7, CRMP2,

reduces its binding to NaV1.7 and results in reduced current density and surface expression (Dustrude et al., 2016). Continued research in this field is likely to reveal that the function of most ion channels can be dynamically regulated by SUMOylation. Furthermore, it is reasonable to think that the behavior of a battery of ion channels can be locally organized by dynamic SUMOylation because, the level of SUMOylation in a compartment is determined by a single SUMO-conjugating enzyme and additional enzymes that have multiple targets including E3 ligases, SENPs, kinases and/or phosphatases. Thus, changing the activity of one of these enzymes should alter a network of proteins. Identifying the effects of ion channel SUMOylation, the molecular mechanisms that mediate these effects and the regulatory mechanisms controlling dynamic SUMOylation will provide important insight into how adaptations in neuronal excitability and/or firing properties are orchestrated.

1.4 **Hypothesis**

The work presented here seeks to addresses the question, How are interactions within the Kv4 macromolecular complex organized? This work uses a heterologous expression system to test the hypothesis that post-translational SUMOylation modulates Kv4 interactions to tune IA. In Chapter 2, SUMOylation of Kv4.2 is characterized, and the effects of SUMOylation on IA mediated by Kv4.2 were identified. In Chapter 3, the effects of Kv4.2 SUMOylation was examined for IA mediated by the ternary complex, and the molecular mechanisms mediating these effects were investigated.

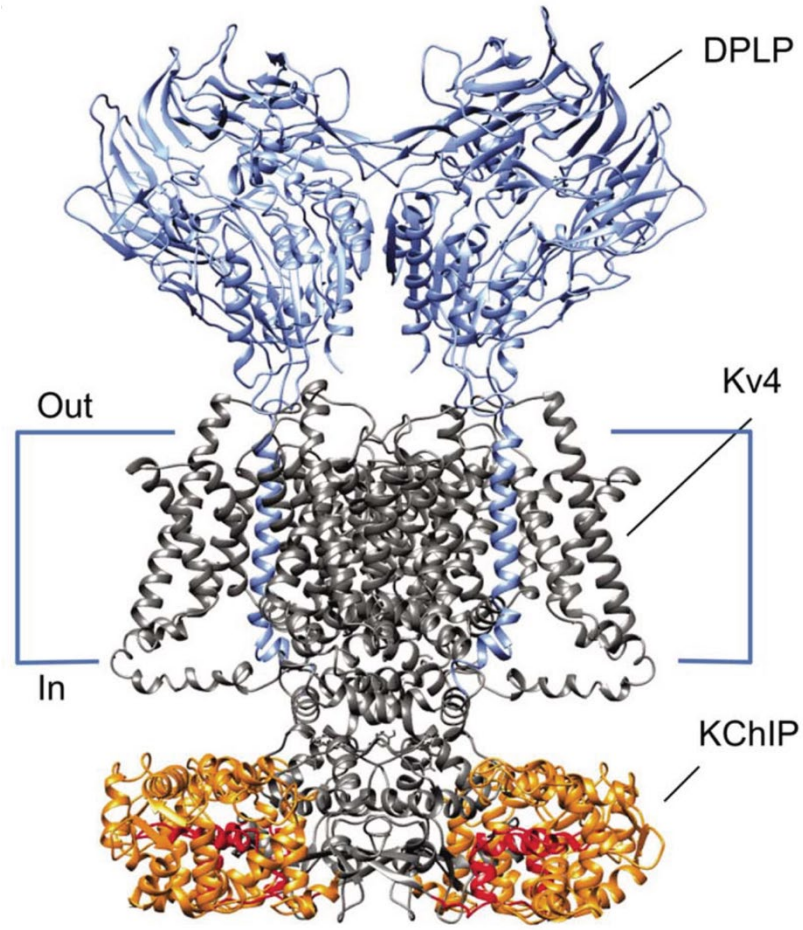

Figure 1.1 The Kv4 ternary complex

The ternary complex is comprised of 4 Kv4 pore-forming α-subunits, 4 KChIPs, and 4 DPLPs. The N- and C-termini of Kv4 channels interact with cytoplasmic KChIPs, and the transmembrane domain of DPLPs interacts with S1 and S2 on Kv4α. Black helices, Kv4α; red helices, Kv4 N-terminus; purple helices, DPLP; orange helices, KChIP. Only 6 of the 12 subunits are shown for clarity. Adapted from Jerng and Pfaffinger 2014.

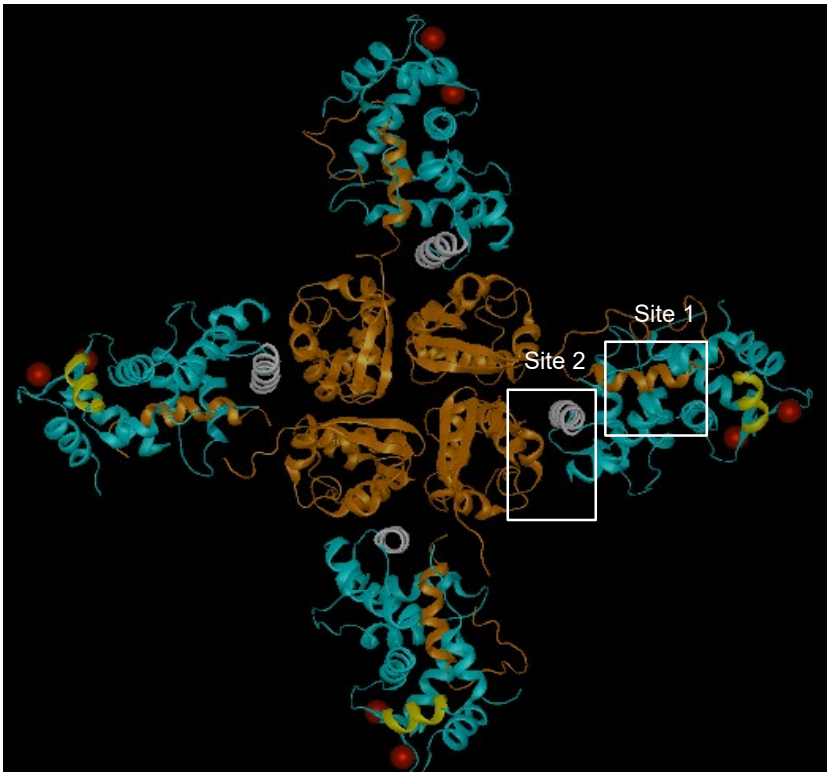

Figure 1.2 KChIP1-Kv4.3 N-terminal binding sites

KChIP1 interacts with 2 sites on the Kv4.3 N-terminus. At Site 1 hydrophobic residues on the Kv4 N-terminus anchor to a hydrophobic pocket in KChIP1 that is revealed when KChIP helix 10 is displaced. Site 2 involves KChIP helix 2 binding to the T1 domain of an adjacent Kv4α subunit, "clamping" two α-subunits together. Orange helices, Kv4.3 N-terminus; blue helices, KChIP1; yellow helices, KChIP1 helix 10; gray helices KChIP1 helix 2; red spheres, calcium. Adapted from Pioletti et al., 2006. Protein databank 2I2R.

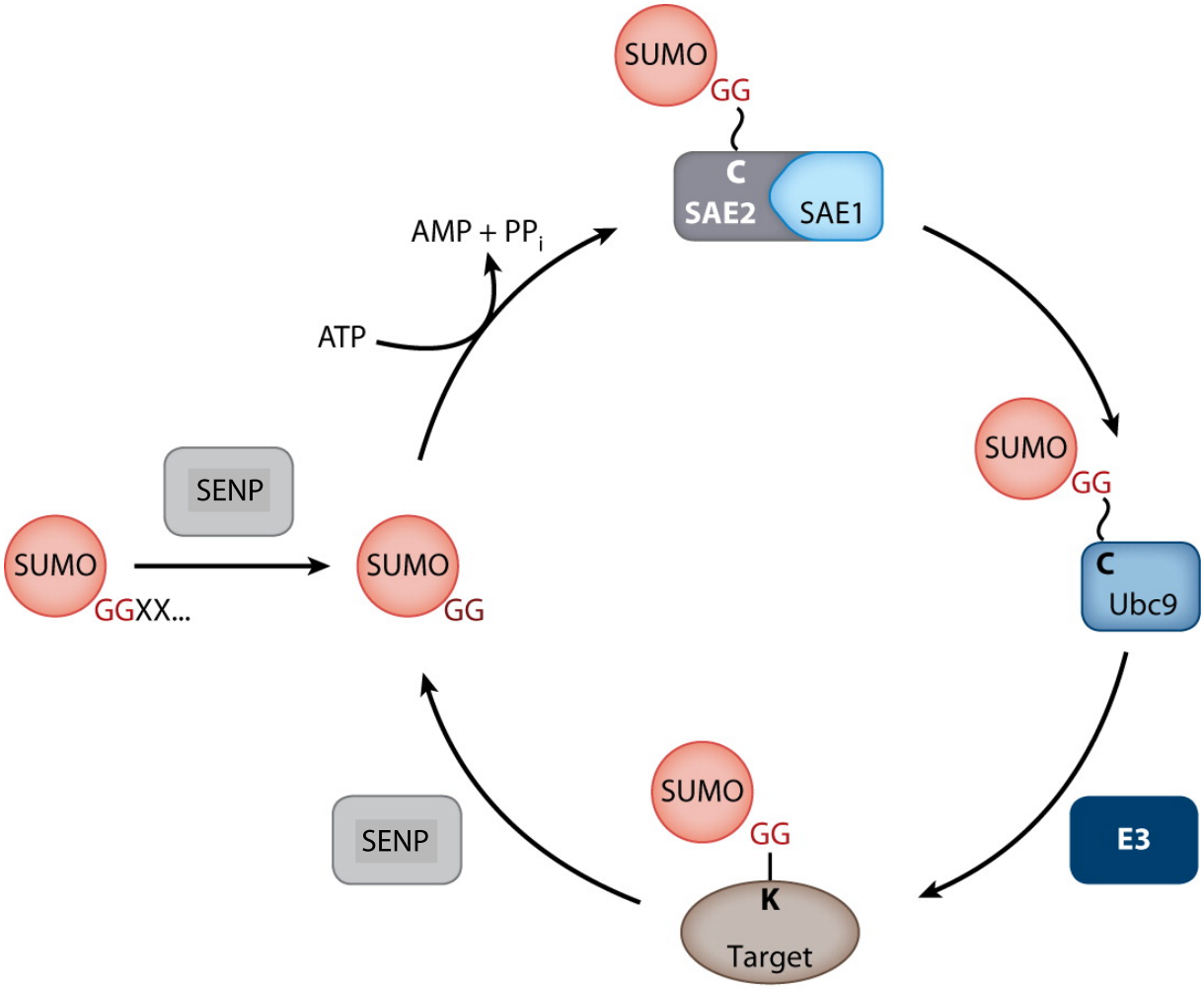

Figure 1.3 SUMOylation pathway

Immature SUMO is cleaved by SENP to reveal a C-terminal di-glycine residue. SUMO is transferred to the E1 conjugating enzyme (SAE1/SAE2) in an ATP-dependent manner and is then added to the sole E2 conjugating enzyme, Ubc9. Ubc9, often in conjunction with E3 SUMO ligases, adds SUMO to K residues on a target protein via an isopeptide bond. SUMO is a reversible modification and the isopeptide bond can be cleaved by SENP. Modified from Flotho and Melchior 2013.

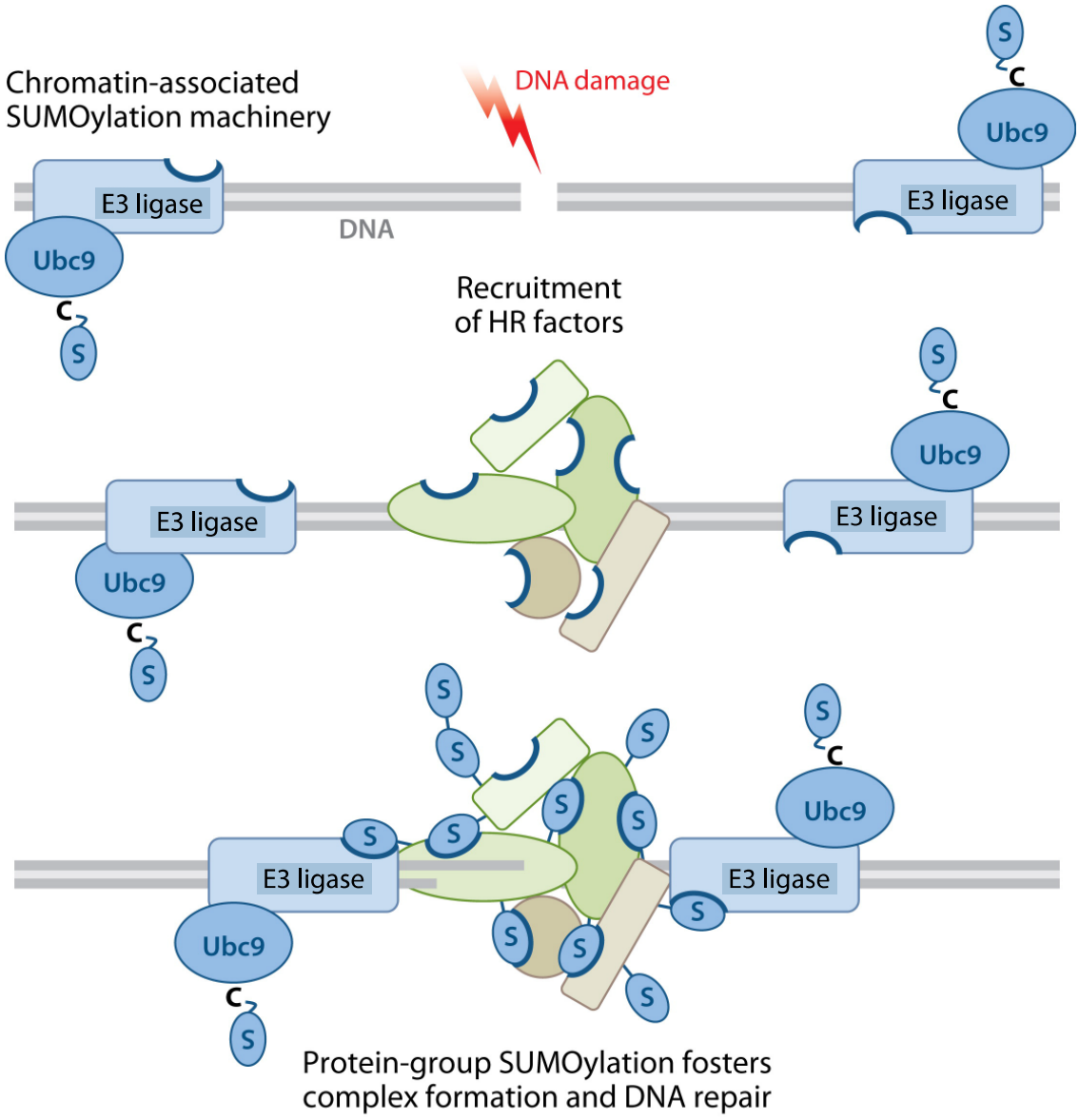

Figure 1.4 Group protein SUMOylation

Group protein SUMOylation facilitates DNA repair by homologous recombination (HR) following a double stranded break. The SUMOylation machinery which includes Ubc9 and an E3 SUMO ligase is bound to the chromatin via a binding domain on the E3 ligase. Upon DNA damage, homologous recombination factors assemble on the single stranded DNA and the E3 ligase initiates group protein SUMOylation of the HR proteins. There is a SUMO-interacting motif (SIM) (dark blue curved circle) on the E3 ligase to allow stable binding of the ligase to the HR complex. It is the combination of multiple SUMO-SIM interactions that stabilize the HR complex and ultimately promotes DNA repair. Modified from Jentsch and Psakhye, 2013.

.

2 CHAPTER 1: SUMOYLATING TWO DISTINCT SITES ON THE A-TYPE POTASSIUM CHANNEL KV4.2, INCREASES SURFACE EXPRESSION AND DECREASES CURRENT AMPLITUDE

Publication: **Welch, M. A.**, Forster, L. A., Atlas, S. I., & Baro, D. J. (2019). SUMOylating Two Distinct Sites on the A-type Potassium Channel, Kv4.2, Increases Surface Expression and Decreases Current Amplitude. *Front Mol Neurosci, 12*, 144. doi:10.3389/fnmol.2019.00144

Contribution Disclosure: Authors M. Welch and D. Baro were responsible for the conception and design of the research presented. Authors M. Welch, D. Baro, L. Forster, and S. Atlas contributed to the acquisition and analysis of the data. Authors M. Welch and D. Baro were responsible for drafting the manuscript, and all authors were involved in revising the manuscript.

2.1 Abstract

Post-translational conjugation of Small Ubiquitin-like Modifier (SUMO) peptides to lysine (K) residues on target proteins alters their interactions. SUMOylation of a target protein can either promote its interaction with other proteins that possess SUMO binding domains, or it can prevent target protein interactions that normally occur in the absence of SUMOylation. One subclass of voltage-gated potassium channels that mediates an A-type current, I_A, exists as a ternary complex comprising Kv4 pore forming subunits, Kv channel interacting proteins (KChIP) and transmembrane dipeptidyl peptidase like proteins (DPPL). SUMOylation could potentially regulate intra- and/or intermolecular interactions within the complex. This study began to test this hypothesis and showed that Kv4.2 channels were SUMOylated in the rat brain and in human embryonic kidney (HEK) cells expressing a GFP-tagged mouse Kv4.2 channel (Kv4.2g). Prediction software identified two putative SUMOylation sites in the Kv4.2 C-terminus at K437 and K579. These sites were conserved across mouse, rat, and human Kv4.2 channels and across mouse Kv4 isoforms. Increasing Kv4.2g SUMOylation at each site by ~30% produced a significant ~22-50% decrease in I_A G_{max}, and a ~70-95% increase in channel surface expression. Site-directed mutagenesis of Kv4.2g showed that K437 SUMOylation regulated channel surface expression, while K579 SUMOylation controlled I_A G_{max}. The K579R mutation mimicked and occluded the SUMOylation-mediated decrease in I_A G_{max}, suggesting that SUMOylation at K579 blocked an intra- or inter-protein interaction involving K579. The K437R mutation did not obviously alter channel surface expression or biophysical properties, but it did block the SUMOylation-mediated increase in channel surface expression. Interestingly, enhancing K437 SUMOylation in the K579R mutant roughly doubled channel surface expression, but produced no change in I_A G_{max}, suggesting that the newly inserted channels were

electrically silent. This is the first report that Kv4.2 channels are SUMOylated and that SUMOylation can independently regulate Kv4.2 surface expression and I_A G_{max} in opposing directions. The next step will be to determine if/how SUMOylation affects Kv4 interactions within the ternary complex.

2.2 Introduction

The transient A-type potassium current (I_A) is a rapidly activating, subthreshold current that regulates neuronal excitability. In mammals, I_A is mediated by Kv1.4, Kv3.3-4 and Kv4.1-3 α-subunits (Gutman et al., 2005). Kv4 channels are widely expressed in a number of central neurons, and evidence suggests that native Kv4 channels exist in a ternary complex with two well studied auxiliary subunit proteins, cytosolic Kv channel interacting protein (KChIP) and transmembrane dipeptidyl peptidase like protein (DPPL) (Birnbaum et al., 2004; Jerng & Pfaffinger, 2014; W. C. Wang, Cheng, & Tsaur, 2015). Interactions between Kv4α subunits and β auxiliary subunits determine channel surface expression and biophysical properties (An et al., 2000; Holmqvist et al., 2002; Jerng & Pfaffinger, 2014; Jerng et al., 2004; Nadal et al., 2003; Shibata et al., 2003; Zagha et al., 2005). However, how these interactions are regulated remains largely unknown. KChIP EF-hands can bind Mg^{2+} and Ca^{2+}, and there is evidence suggesting Ca^{2+} binding to KChIP can influence its interaction with Kv4α (Bahring, 2018; C. P. Chen et al., 2006; Gonzalez, Pham, & Miksovska, 2014; Lee, Chen, & Chang, 2009; Morohashi et al., 2002; Pioletti et al., 2006). N-glycosylation of DPP10 controls its interaction with Kv4α, and its ability to modulate channel surface expression and the biophysical properties (Cotella et al., 2010; Cotella et al., 2012). It is important to identify additional mechanisms that may govern these interactions. Post-translational modifications like SUMOylation can regulate protein-protein

interactions, and in this work, we begin investigating whether SUMO regulates α-β subunit interactions by studying the role of Kv4 SUMOylation.

Small ubiquitin-like modifier (SUMO), a.k.a. sentrin, represents a family of pro-peptides. There are four SUMO isoforms in mammals (SUMO 1-4). SUMO-1 and SUMO-2 share 47% sequence identity. SUMO-2 and SUMO-3 are 97% identical and are typically referred to as SUMO-2/3 because they are usually not experimentally differentiated. Post-translational modifications by SUMO 1-3 are well studied (Flotho & Melchior, 2013; Henley et al., 2018; Wasik & Filipek, 2014). SUMO-4 is atypical and little is known about its function as a post-translational modifier (Guo et al., 2004; Owerbach et al., 2005; C. Y. Wang, Yang, Li, & Gong, 2009; Wei et al., 2008).

The terminal amino acids of SUMO 1-3 pro-peptides are removed to produce a mature peptide that ends in a di-glycine. The mature peptide can be conjugated to lysine (K) residues on target proteins by the enzyme, Ubc9 (Desterro et al., 1997). In most cases (~65%), Ubc9 recognizes a SUMO consensus sequence on the target protein and SUMOylates the K in that sequence; however, Ubc9 can also act in conjunction with other proteins to SUMOylate K residues at non-consensus sites (Flotho & Melchior, 2013; Hendriks, D'Souza, Chang, Mann, & Vertegaal, 2015; Matic et al., 2010). SUMO modification is reversible, and deconjugation is effected by a family of sentrin-specific proteases (SENP) (Hickey et al., 2012).

SUMO influences diverse cellular functions by controlling protein-protein interactions, and recent work highlights SUMO's role in regulating the surface expression and biophysical properties of ion channels (Gong et al., 2016; Henley et al., 2018; Kruse et al., 2009; Parker et al., 2016; Wasik & Filipek, 2014; H. Wu, Chen, Cheng, & Qi, 2016). Several voltage-gated potassium channels are known to be regulated by SUMO. Kv1.1 channels are modified by

SUMO-1 and SUMO-2/3 and co-localize with SENP2 in hippocampal neurons (Qi et al., 2014). Kv1.5 channels are largely SUMOylated at two K residues, and preventing SUMOylation at these sites causes a hyperpolarizing shift in the voltage of half-inactivation (V_{50} inact) (Benson et al., 2007). SUMOylation of Kv2.1 channels regulates pancreatic β-cell excitability by accelerating the time constant (τ) of inactivation and impairing recovery from inactivation (Dai, Kolic, Marchi, Sipione, & Macdonald, 2009). Additionally, Kv2.1 SUMOylation increases the excitability of rat hippocampal neurons by causing a depolarizing shift in the voltage of half-activation (V_{50} act) (Plant et al., 2011). Kv7.1 channel SUMOylation in neonatal mouse ventricular myocytes results in a depolarizing shift in V_{50} act (Xiong et al., 2017). SENP2 knockout mice display increased excitability in CA3 pyramidal neurons due to hyper-SUMOylation of Kv7.2 channels which diminishes the hyperpolarizing M-current, causing these mice to develop spontaneous convulsive seizures followed by sudden death (Qi et al., 2014). Kv11.1 SUMOylation decreases steady-state current amplitude by increasing the τ of inactivation and modifying deactivation kinetics (Steffensen et al., 2018).

SUMOylation of Kv4 channels has not been reported. Here, we test the hypothesis that Kv4.2 channels are SUMOylated to regulate their surface expression and biophysical properties.

2.3 Materials and Methods

2.3.1 Plasmids and antibodies

A previously described plasmid containing a mouse Kv4.2-GFP fusion protein, here termed Kv4.2g, was generously provided by Dr. Dax Hoffman. Note GFP is attached to the C-terminus of Kv4.2. A plasmid containing mCherry2-C1 was a gift from Michael Davidson (Addgene plasmid #54563). A plasmid containing SUMO-2 (Kamitani, Nguyen, Kito, Fukuda-Kamitani, & Yeh, 1998) was a gift from Edward Yeh (Addgene plasmid #17360). A plasmid

containing Ubc9 (Yasugi & Howley, 1996) was a gift from Peter Howley (Addgene plasmid #14438). All antibodies are described in Table 2.1.

2.3.2 Site-directed mutagenesis

PCR-based site-directed mutagenesis was used to create 2 mutations in the Kv4.2g plasmid described above: K437R and K579R. Typically, 10-100ng of Kv4.2g DNA served as the template in 50µL PCRs containing PrimeSTAR GXL polymerase (Takara), 5X PrimeSTAR GXL buffer (Takara), nucleotides, and the primers described in Table 2.2. The cycling conditions were as follows: 1X 95°C 1min; 30X 98°C 30sec, 68°C 7min; 1X 68°C 5min. Afterward, 20units of DPN1 (Takara) was added to the PCR and incubated at 37°C for 2hrs to digest the template DNA. Then, 2µl of the PCR was added to 50µl of subcloning grade competent XL1 blue cells (Agilent) and incubated on ice for 30min. The cells were heat shocked for 45sec at 42°C and cooled on ice for 2min. 200µl of NZY broth was added and the reaction was incubated at 37°C for 30min to allow for expression of kanamycin resistance. The cells were plated onto NZY plates containing 30µg/ml kanamycin and incubated at 37°C overnight. A single colony was used to inoculate NZY broth containing 30µg/ml kanamycin and incubated at 37°C, shaking at 220rpm, overnight. Plasmid DNA was isolated using the Qiagen Mini Kit, according to the manufacturer's instructions. The isolated plasmid was sequenced at the Georgia State University Cell Protein and DNA Core Facilities, and the sequences were analyzed using Lasergene software (DNAstar) to ensure that only the desired mutation was present. To create a double mutation, a previously mutated Kv4.2g channel served as the template in the PCR reaction.

2.3.3 Rat Brain Membrane preparations

A single whole rat brain was homogenized ~20X on ice in homogenization buffer (0.3M sucrose, 10mM sodium phosphate buffer pH 7.4, 1mM EDTA, and protease inhibitor cocktail [1:100, Sigma cat. #P8340]) supplemented with 20mM *N*-Ethylmaleimide (NEM) to prevent SUMO deconjugation. The homogenate was centrifuged at 5000rpm for 10min at 4°C to spin down cell nuclei. The supernatant was transferred to two Beckman tubes and crude membranes were pelleted by centrifuging at 40,000rpm for 90min at 4°C. The supernatant was removed, the pellets were re-suspended in homogenization buffer (500µl/tube) for 1hr at 4°C with shaking. The resuspended pellets from each tube were combined, and protein concentration was determined by performing a bicinchoninic acid (BCA) assay (Pierce). Rat brain tissue was generously provided by Dr. Chun Jiang. This study was carried out in accordance with the principles of the Basel Declaration and recommendations of Ethical Issues of the International Association for the Study of Pain and National Institutes of Health. The protocol was approved by the Institutional Animal Care and Use Committee at Georgia State University.

2.3.4 Cell culture

Human embryonic kidney 293 (HEK-293) cells were obtained from American Type Culture Collection (ATCC). Cells were maintained at 37°C with 5% CO_2 in Eagle's Minimum Essential Medium (Corning, cat. #10009CV) supplemented with 10% Fetal bovine serum (FBS) (ATCC 30-2020) and 1% Penicillin/Streptomycin (Sigma, cat. #P4333).

2.3.5 Generating cell lines stably expressing wild-type and mutant Kv4.2g

HEK-293 cells were plated on 60mm culture plates at ~90% confluency. 1hr prior to transfection, the media was replaced with EMEM+10% FBS without antibiotics. 10µg of plasmid DNA was combined with 50µl OptiMEM (Gibco). 20µl of Lipofectamine 2000

(Invitrogen) was combined with 50µl OptiMEM. After 5min, DNA and Lipofectamine were combined and incubated for 20min at RT. The mixture was dropped onto HEK-293 cells. After 2 days, cells were harvested and dilute resuspensions were re-plated with EMEM+10% FBS+1% Pen/Strep+G418 (Geneticin, Gibco, 500µg/ml). After ~3 weeks individual colonies were selected using cloning rings. Expression in all cells was confirmed using fluorescence microscopy and whole cell patch clamp recordings.

2.3.6 Transient transfections

Cells were plated onto 60 or 100mm culture dishes at $1.9X10^6$ or $6X10^6$ cells per plate, respectively. The next day, cells were transiently transfected using calcium phosphate. At least 1hr prior to transfection, the media was changed. For 60 or 100mm culture plates, 10 or 25µg of plasmid DNA was prepared in 250 or 440µl of TE buffer (10mM Tris-HCl pH 8, 1mM EDTA), respectively. When multiple plasmids were co-transfected, the total amount of DNA remained the same, and the different plasmids were equally represented by weight within a mixture. Immediately prior to transfection, 30 or 60µl of 2M $CaCl_2$ was added to the DNA, dropwise, flicking to mix. Then 250 or 500µl of 2X HBS (275mM NaCl, 10mM KCl, 12mM dextrose, 1.4mM Na_2HPO_4, 40mM HEPES, pH 7.05-7.1) was added dropwise to the DNA, flicking to mix. The mixture was immediately added to the cells and cells were returned to 37°C with 5% CO_2 for 4hrs followed by a media change. Cells were allowed to grow for ~48hrs to allow for expression of the plasmid DNA. Before using the transfected cells, the transfection efficiency was assessed using fluorescence microscopy. Only plates with >80% transfection efficiency were used in experiments.

2.3.7 Immunoprecipitation

2.3.7.1 Kv4.2 IP from rat brain

Kv4.2 channels were immunoprecipitated from rat brain membranes using the Classic Magnetic IP/Co-IP Kit (Pierce), 1mg of rat brain membrane and 5µg of rabbit anti-Kv4.2 (Table 2.1). The IP product was eluted in a volume of 50µL.

2.3.7.2 GFP IP from HEK cells

Cells on 100mm culture dishes were washed 2X with ice-cold PBS and lysed with 1ml of RIPA buffer (1% NP40, 50mM Tris-HCl pH 7.4, 150mM NaCl, 0.1% SDS, 0.5% DOC, 2mM EDTA, 20mM NEM, 1:100 protease inhibitor cocktail) for 30min on ice. The plate was scraped, the lysate was transferred to a 1.5ml microcentrifuge tube, and cell debris was spun down by centrifuging for 15min at 14,000rpm. Protein concentration in the supernatant was determined with a BCA assay (Pierce). Kv4.2g channels were immunoprecipitated using the Classic Magnetic IP/Co-IP Kit (Pierce) according to the manufacturer's instructions using 5µg of rabbit anti-GFP (Table 2.1) with 1mg of protein. IP product was eluted in a volume of 100µL.

2.3.8 Western Blot

After electrophoresis on 12% SDS-polyacrylamide gels, proteins were transferred for 2hrs at 45mAMP to a PVDF membrane (Immobilon-P, cat. #IPVH00010) using a semidry electroblotting system (OWL). After drying overnight, membranes were blocked in 5% non-fat dry milk in TBS (50mM Tris-HCl pH 7.4, 150mM NaCl) for 1hr at room temperature. Blots were washed 1X for 10min with TTBS (TBS+ 0.1% Tween20), and then primary antibodies prepared in 1% non-fat dry milk in TTBS were added and incubated at 4°C overnight with shaking. Blots were washed 3X, 5min each with TTBS and then incubated with appropriate alkaline phosphatase conjugated secondary antibodies in TTBS with 1% non-fat dry milk for

2hrs at RT with shaking. The membrane was washed 3X with TTBS, 10min each. The blot was incubated with alkaline phosphatase substrate (Bio-Rad) for 5min, and then the membrane was exposed to film (MedSupply Partners), and chemiluminescent signals were captured with a Kodak X-Omat 2000A imager. Optical densities for bands of interest were measured with ImageJ, as previously described (Parker et al., 2016). In some cases, antibodies were stripped from blots as follows: 2X mild stripping buffer, 10min each; 2X PBS, 10min each; 2X TTBS, 5min each. AP substrate was applied for 5min, and the membrane was exposed to film to ensure that the original chemiluminescent signal was gone. In order to compensate for error introduced by technical variabilities such as fluctuating exposure times and loss of protein due to stripping, blots that were stripped and re-probed always contained 0.2µg BSA in one lane. A primary antibody against BSA was always included along with other primary antibodies to detect the BSA signal. The pre- and post-stripping BSA signals were used to normalize other signals of interest on the pre- and post-stripped blot, respectively.

2.3.9 Biotinylation assay to measure surface expression

Cells were washed twice with room-temperature PBS containing 0.2mM $CaCl_2$ and 1.5mM $MgCl_2$ (PBS-CM) and incubated with 2ml of 1mg/ml EZ-link-Sulfo-NHS-SS-Biotin (ThermoFisher, cat. #21331) for 30min at 8°C. Cells were washed twice with room-temperature PBS-CM and residual biotin was quenched using PBS-CM with glycine for 15min at 8°C. Cells were lysed for 30min on ice using 500µL RIPA buffer. Cells were scraped from the plate and the lysate was transferred to a sterile 1.5ml microcentrifuge tube. Cell debris was pelleted by centrifuging for 10min at 14,000rpm. The supernatant was removed, added to a spin column (ThermoFisher, cat. #69725) containing 100µL of NeutrAvidin Agarose Resin (ThermoFisher, cat. #29201), and incubated with shaking for 2hr at 4°C. The lysate/resin was centrifuged at

1000Xg for 2min and the eluate containing intracellular proteins was saved for western blot analysis. The resin was washed 3X with Wash Buffer 1 (1% NP40, 1% SDS, 1X PBS) and 3X with Wash Buffer 2 (0.1% NP40, 0.5M NaCl, 1X PBS). In order to elute extracellular proteins, 50µL of 1X SDS buffer (1X SDS, 0.1% Bromophenol blue, 100mM DTT) was added to the beads and incubated with shaking for 1hr at room temperature. Beads were pelleted by centrifugation at 1000Xg for 2min. The supernatant was recovered and used in western blot analyses.

Western blots containing intracellular and extracellular fractions as well as 0.2µg BSA (~66kD, Sigma cat. #A7517) were cut horizontally at the ~50kD marker. Optical densities for bands on the upper portion of the blot were obtained using primary antibodies against GFP (Table 2.1) and BSA (Table 2.1). After obtaining the optical densities for the Kv4.2g and BSA bands, the upper portion of the blot was stripped and re-probed with primary antibodies against Na^+/K^+-ATPase (Table 2.1) and BSA. The Kv4.2g and Na^+/K^+-ATPase signals were each normalized by their respective BSA signal to remove error introduced by technical variabilities such as fluctuating exposure times and loss of protein due to stripping. Kv4.2g surface expression was then quantified by dividing the normalized Kv4.2g signal by the normalized Na^+/K^+-ATPase signal, which we previously showed did not change when SUMO availability was altered (Parker et al., 2016). In all experiments, the lower portion of the blot was probed with a primary antibody against actin to detect any intracellular contamination in the extracellular fractions. The experiment was excluded if actin was detected in the extracellular fraction.

2.3.10 Whole cell patch clamp electrophysiology

Glass coverslips were prepared by dipping in ethanol, air drying, and coating with 50µg/ml Poly-L-Lysine for 1hr at 37°C. Poly-L-Lysine was removed, coverslips were washed 1X with dH_20, and allowed to air dry before use. Cells were transiently transfected with mCherry or mCherry+SUMO+Ubc9. Approximately 24hrs after transfection, cells were seeded onto 20mm Poly-L-Lysine coated coverslips at a density of $8X10^4$ cells per coverslip, and were incubated for ≥24hrs before use. A coverslip was transferred to the recording chamber and continuously superfused with extracellular saline (in mM: 141 NaCl, 4.7 KCl, 1.2 $MgCl_2$, 1.8 $CaCl_2$, 10 glucose, 10 HEPES, pH 7.4, osmolarity ~300). Cells were visualized using an Olympus IX70 microscope and only cells expressing mCherry, visualized by red fluorescence, were patched. Fire polished borosilicate glass pipettes having a resistance between 2-5MΩ were filled with intracellular saline (in mM: 140 KCl, 1 $MgCl_2$, 1 $CaCl_2$, 10 EGTA, 2 MgATP, 10 HEPES, pH 7.2, osmolarity ~290) and connected to a MultiClamp 700A amplifier (Axon Instruments). To generate a whole cell patch, a GΩ seal was formed by slight negative pressure. After forming a GΩ seal, gentle suction was used to rupture the membrane and only cells that maintained ≥700MΩ seal after breaking through the membrane were used. Fast and slow capacitance transients, and series resistance was compensated. To elicit I_A, a 1sec -90mV pre-pulse was followed by a 250ms test-pulse from -50mV to +50mV in 10mV increments. Offline subtraction of currents evoked following a pre-pulse to -30mV was used to isolate I_A. I_A G_{max} and voltage of half-activation (V_{50} act) were determined by converting peak current amplitude (I_{peak}) to conductance (G) for each voltage step using the equation $G=I_{peak}/(V_m-V_r)$, where V_r= -86mV, plotting G/G_{max} as a function of membrane potential, and fitting the resulting curve with a first-order Boltzmann equation. The steady-state inactivation properties of I_A were determined with a

series of 1.4sec steps from -110mV to -30mV in 10mV increments, each followed by a 200ms test pulse to +20mV. Steady state voltage-dependence of half-inactivation (V_{50} inact) curves were generated by plotting I/I_{max} as a function of pre-pulse voltages and fitting the resulting curve with a first-order Boltzmann equation. To determine the fast (τ_f) and slow (τ_s) time-constants of inactivation a two-term exponential equation was used to fit the decay current elicited by 250ms voltage-step to +50mV following a pre-pulse to -90mV.

2.3.11 Statistical analysis

Data were analyzed using GraphPad PRISM 7 software. Each data set was assessed for normality and homogeneity of variance. Data were analyzed using parametric or non-parametric tests as indicated, including the student's unpaired t-test, the Mann-Whitney U test, and the one-way ANOVA followed by a Tukey's post-hoc comparison when appropriate. In all cases, the significance threshold was set at $p<0.05$. Data points > 2 standard deviations from the mean were considered outliers and were excluded. In all cases, values reported represent the mean±SEM.

2.4 Results

2.4.1 Kv4.2 is SUMOylated in the rodent brain

To determine if Kv4.2 channels were SUMOylated *in vivo*, immunoprecipitation (IP) experiments were performed using rat brain membrane preparations and an antibody against Kv4.2 (Table 2.1) followed by western blot experiments using primary antibodies against Kv4.2, SUMO-1, or SUMO-2/3 (Table 2.1). The antibodies against Kv4.2 and SUMO-2/3, but not SUMO-1, recognized the same 68kD band previously identified as the Kv4.2 channel in rat brain membrane preparations (Figure 2.1, asterisk) (Nadal et al., 2003). This band was not observed when IP experiments were repeated with a non-specific rabbit IgG. These data suggest that a fraction of rat brain Kv4.2 channels were decorated with SUMO-2/3 and that the addition of the

12kD modification did not detectably alter the molecular weight of the channel under our PAGE conditions. A 130kD band likely representing aggregated Kv4.2 channels was also observed (Figure 2.1, arrow) (Jerng et al., 2005; Jerng et al., 2004). The anti-SUMO-2/3 antibody recognized an additional 100kD band that was not recognized by the channel antibody in the anti-Kv4.2 but not the anti-IgG IP product (Figure 2.1, arrow head), and this band may represent a SUMOylated protein(s) that non-covalently interacts with the channel. Two likely candidates are DPP6-S and DPP10 that have predicted molecular weights of ~115kD and ~100kD when glycosylated, respectively (Jerng et al., 2004). SUMO prediction software (see 2.4.6 below) indicates both of these proteins have multiple potential SUMOylation sites. In sum, these results showed that Kv4.2 channels were measurably decorated with SUMO-2/3 but not SUMO-1 in the rat brain.

2.4.2 Kv4.2 channels are SUMOylated in a heterologous expression system

To study the effects of Kv4.2 SUMOylation, we established a Human Embryonic Kidney (HEK)-293 cell line that stably expressed Kv4.2g, which is a mouse Kv4.2 channel tagged with a C-terminal GFP. The stable cell line was called HEK-Kv4.2g. IP experiments using an anti-GFP antibody (Table 2.1) were performed on whole cell lysates from HEK-Kv4.2g cells, and IP products were analyzed with western blotting (Figure 2.2). Antibodies against GFP (Figure 2.2A), Kv4.2 (Figure 2.2B) and SUMO-2/3 (Figure 2.2C) all recognized the same 100kD band (asterisk), which is the predicted size of the Kv4.2-GFP fusion protein. The 100kD band was never observed when a non-specific IgG was used in IP experiments, or on blots containing IP products from HEK parental cells (Figure 2.2). Furthermore, a 70kD band was also detected by all antibodies (arrow head), and it most likely represents cleavage of the channel. This signal was not included in subsequent quantifications, and most likely represents sample degradation. These

data suggest that Kv4.2g channels are SUMOylated in our heterologous expression system under baseline conditions.

2.4.3 SUMOylation of the Kv4.2 channel can be manipulated in a heterologous expression system

SUMOylation can be increased in HEK cells by overexpressing SUMO and its conjugating enzyme Ubc9 (Dai et al., 2009; Parker et al., 2016). SUMOylation can be decreased by application of anacardic acid, which inhibits protein SUMOylation by binding to the SUMO-activating enzyme (E1) and preventing the formation of the E1-SUMO intermediate (Fukuda et al., 2009). To determine if SUMOylation of Kv4.2g could be manipulated in our heterologous expression system, we transiently transfected HEK-Kv4.2g cells with mCherry or mCherry+SUMO+Ubc9 plasmid DNA. For the anacardic acid treatment group, the drug was bath applied (100μM) for 1hr to HEK-Kv4.2g cells that had been transiently transfected with mCherry immediately before cell lysis. Kv4.2g SUMOylation was analyzed with IP followed by western blotting experiments (Figure 2.3). Blots were initially probed with anti-SUMO-2/3 and then stripped and re-probed with anti-GFP (Figure 2.3A). The fraction of SUMOylated Kv4.2g channels in a given experiment was determined by dividing the BSA-normalized optical density (OD) of the SUMO-2/3 band by the BSA-normalized OD of the GFP band, as described in Materials and Methods. All data for control (mCherry), SUMO+Ubc9, and anacardic acid treatment groups were plotted in Figure 2.3B after normalizing each data point by the mean control value. A significant ~60% increase in mean Kv4.2g channel SUMOylation was observed in the SUMO+Ubc9 treatment group relative to control (Figure 2.3B). No significant difference in Kv4.2g channel SUMOylation was observed in cells treated with anacardic acid relative to control (Figure 2.3B). This might be due to a low level of baseline SUMOylation in the HEK-

Kv4.2g cell line. On the other hand, a higher concentration and/or a longer application of anacardic acid might be necessary to observe a decrease in Kv4.2g channel SUMOylation in our heterologous expression system. In sum, overexpressing SUMO+Ubc9 in HEK-Kv4.2g cells produces a significant increase in Kv4.2g SUMOylation, and only this manipulation was performed in subsequent experiments.

2.4.4 Increased SUMOylation of Kv4.2 channels alters the properties of I_A

To test whether altering baseline SUMOylation affected the function of Kv4.2 channels, HEK-Kv4.2g cells were transiently transfected with mCherry (control) or mCherry+SUMO+Ubc9 plasmid DNA, and whole cell patch clamp recording was used to elicit I_A (Figure 2.4A) and steady-state inactivation of I_A (Figure 2.4B). The maximal conductance (G_{max}) (Figure 2.4C), voltage dependence (Figure 2.4D), and time constants (τ) of inactivation (Figure 2.4E-F) in the two treatment groups were measured. Enhancing baseline SUMOylation by ~60% (Figure 2.3) produced a significant ~22% decrease in mean I_A G_{max} (Figure 2.4C; Table 2.3), a small but significant ~4mV depolarizing shift in the voltage-dependence of inactivation (Figure 2.4D, Table 2.3), and a significant ~25% increase in the fast time constant of inactivation (τ_f) (Figure 2.4E; Table 2.3).

2.4.5 Kv4.2 SUMOylation regulates channel surface expression

We hypothesized that a mean ~60% increase in Kv4.2 SUMOylation (Figure 2.3) produced a mean 22% decrease in I_A G_{max} (Figure 2.4) by reducing channel surface expression. To test this, biotinylation experiments were used to measure Kv4.2g channel surface expression in HEK-Kv4.2g cells transiently transfected with mCherry or mCherry+SUMO+Ubc9 plasmid DNA. Briefly, biotin was added to the cells to label extracellular proteins, cells were lysed, and biotinylated proteins were isolated using NeutrAvidin beads. Western blots containing

intracellular and extracellular fractions were probed for GFP, Na^+/K^+-ATPase and actin as described in Materials and Methods. We previously demonstrated that surface expression of Na^+/K^+-ATPase was not altered by increasing SUMO and Ubc9 (Parker et al., 2016), so changes in Kv4.2g surface expression between the two treatment groups were detected as differences in the ratio of extracellular GFP to Na^+/K^+-ATPase signals. A representative experiment is shown in Figure 2.5A. As expected, Kv4.2g and Na^+/K^+-ATPase were observed in intracellular and extracellular fractions, while actin was not. Extracellular Kv4.2g bands appeared higher than intracellular Kv4.2g bands. This could be due to differences in the loading buffers: Intracellular samples were run in 8M Urea loading buffer (8M urea, 20mM Tris-HCl pH 8.0, 1mM EDTA, 0.05% Bromophenol blue, 0.6M DTT), while extracellular samples were run in 1X SDS buffer (1X SDS, 0.1% Bromophenol blue, 100mM DTT). Alternatively, protein concentrations and post-translational modifications could differ between fractions. Experiments were repeated and the extracellular GFP to Na^+/K^+-ATPase ratio was obtained for each experiment as described in Materials and Methods. All data for control (mCherry) and experimental (mCherry+SUMO+Ubc9) treatments were plotted after normalizing each data point by the mean control value (Figure 2.5B). Surprisingly, enhancing Kv4.2g SUMOylation did not decrease channel surface expression as predicted, but rather, significantly increased Kv4.2g surface expression by ~70%.

2.4.6 SUMOylation at K579 is responsible for the decrease in I_A G_{max}, while SUMOylation at K437 mediates the increase in Kv4.2 surface expression when SUMOylation is enhanced.

Enhanced SUMOylation appears to have two opposing effects: (1) to decrease I_A G_{max} (Figure 2.4), and (2) to increase channel surface expression (Figure 2.5). One explanation may be

that Kv4.2g can be SUMOylated at multiple sites, and SUMOylation at each site could produce a distinct effect. Potential Kv4 SUMOylation sites were identified using two free web-based prediction programs: SUMOplot (http://www.abgent.com/sumoplot) and GPS-SUMO (Zhao et al., 2014). Multiple sites were identified, but only two were conserved across species and isoforms, were predicted by both programs and were located within intracellular domains (Figure 2.6). We chose to examine SUMOylation at these two lysine (K) residues, K437 and K579.

To test whether overexpression of SUMO+Ubc9 increased SUMOylation at K437 and K579, we used site-directed mutagenesis to replace K with arginine (R). This mutation will prevent SUMOylation but not electrostatic interactions. Three stable lines were generated: HEK-Kv4.2g K437R+K579R, HEK-Kv4.2g K437R, and HEK-Kv4.2g K579R. SUMOylation was or was not globally enhanced in each line using transient transfection of mCherry+SUMO+Ubc9 or mCherry alone. SUMOylation of the Kv4.2 double mutant was highly similar in the two treatment groups (Figure 2.7A-B). On the other hand, average Kv4.2g SUMOylation was increased in the single mutants, but instead of the significant ~60% increase observed for wild-type channels (Figure 2.3), each single mutant showed a ~30% increase in SUMOylation that was not significantly different from control (Figure 2.7C-D and 7E-F). Together these data suggested that both sites were being SUMOylated and each contributed equally to the ~60% increase observed for wild-type Kv4.2g. It should be noted that Kv4.2g channels were SUMOylated in the double mutant, suggesting that additional sites on the channel or the GFP tag were SUMOylated under baseline conditions and that SUMOylation at these sites was not obviously increased by transient overexpression of SUMO+Ubc9.

Biotinylation experiments were used to measure channel surface expression in mutant cell lines transiently transfected with mCherry or mCherry+SUMO+Ubc9. Whereas over-

expressing SUMO+Ubc9 in the wild-type cell line produced a significant 70% increase in Kv4.2g surface expression (Figure 2.5), globally enhancing SUMOylation in the double mutant or the HEK-Kv4.2g K437R cell lines had no effect on Kv4.2g surface expression (Figure 2.8A-D). In contrast, overexpressing SUMO+Ubc9 produced a significant 94% increase in Kv4.2g surface expression in HEK-Kv4.2g K579R cells relative to mCherry controls (Figure 2.8E-F). A t-test indicates that the 94% increase in the K579R mutant cell line is not significantly greater than the 70% increase observed in the wild-type cell line (t-test, p=0.64).

Electrophysiological experiments were repeated on the mutant cell lines to determine if SUMOylation at K437 and/or K579 was associated with the SUMOylation-mediated changes in Kv4.2g biophysical properties (Figure 2.4). Whole cell patch clamp was used to measure I_A in mutant cells lines transiently transfected with mCherry or mCherry+SUMO+Ubc9 (Figure 2.9; Table 2.3). Whereas over-expressing SUMO+Ubc9 in wild-type HEK-Kv4.2g produced a significant 22% decrease in I_A G_{max} relative to mCherry controls (Figure 2.4B), enhancing SUMOylation did not reduce I_A G_{max} in the double mutant or the HEK-Kv4.2g K579R mutant cell lines; however, a significant decrease was observed in the HEK-Kv4.2g K437R cell line (Figure 2.9). These data suggested that SUMOylation of Kv4.2g at K579 mediates a decrease in I_A G_{max}.

Table 2.3 shows that the SUMOylation-mediated 4mV shift in the V_{50} inactivation seen in the wild-type channel (Figure 2.4C) was lost in cells expressing Kv4.2g channels containing the double-mutation or either of the single-mutations. Similarly, the previously observed SUMO-mediated increase in τ_f (Figure 2.4D) was lost in all 3 mutant cell lines, and a mean ~20% decrease was observed in the double mutant and K579R cell lines. Interpretation of these data is confounded by the fact that the mutations themselves may alter τ_f independent of SUMOylation,

and/or there could be cell-line specific factors contributing to the effects. The latter hypothesis was next tested using transient transfection experiments (see section 2.4.7 below).

In sum, enhanced SUMOylation at K437 increased Kv4.2 channel surface expression while enhanced SUMOylation at K579 decreased I_A G_{max} (Figures 2.8 and 2.9). Enhancing SUMOylation of the wild type channel produced a ~30% increase in SUMOylation at both sites (Figure 2.7), and the net result of the two opposing effects was a ~22% decrease in I_A G_{max} (Figure 2.4B). Interestingly, when the SUMOylation-mediated increase in surface expression was prevented by the K437R mutation, enhanced SUMOylation at K579 produced only a slightly larger decrease in the mean I_A G_{max} (33% instead of 22%) (Table 2.3). Similarly, when the SUMOylation-mediated decrease in I_A G_{max} was prevented by the K579R mutation, enhancing SUMOylation at K437 produced an average 94% increase in surface expression (Figure 2.8E-F), but no change in I_A G_{max} (Figure 2.9E-F; Table 2.3). These data suggest that the channels inserted into the membrane upon enhanced SUMOylation may be mostly silent.

2.4.7 There is a significant decrease in I_A G_{max} in HEK cells transiently transfected with Kv4.2g K579R compared to Kv4.2g.

The mutations K437R and K579R prevented SUMOylation at these sites and the SUMOylation-mediated alterations in surface expression and I_A G_{max}, respectively (Figures 2.8 and 2.9). It was not clear if the mutations blocked, or mimicked and occluded the effects of SUMOylation. Measurements could not be compared between the independently selected stable lines because there could be differences in their proteomes and/or Kv4.2g gene copy number; i.e., different numbers of plasmids stably integrated into the genome in each cell line. In order to address this issue, HEK cells were transiently transfected with wild-type or mutant plasmids, and I_A was recorded using whole cell patch clamp. Figure 2.10 illustrates that HEK cells transiently

transfected with the K579R plasmid had a significantly smaller I_A G_{max} than cells transfected with the wild-type or K437R plasmids, while I_A in the latter two transfections was not significantly different (Kv4.2g, 54.2nS±7.9; Kv4.2g K437R, 62.1nS±5.9; Kv4.2g K579R, 27.6nS±3.6). I_A could not be further reduced by enhancing SUMOylation in cells transfected with K579R plasmid, whereas this treatment did reduce I_A in cells transfected with the wild-type or K437R plasmids (Figure 2.10D). These data suggest that enhancing SUMOylation at K579 had the same effect as removing K579; i.e., the K579R mutation mimicked and occluded the effect of SUMOylation at K579.

Overexpression of SUMO+Ubc9 in the stable HEK-Kv4.2g cell line significantly shifted the V_{50} inact and increased τ_f (Figures 2.4D-E; Table 2.3). It is noteworthy that these significant changes were not observed in transient co-transfections with Kv4.2g+SUMO+Ubc9 (Table 2.4). Also, these parameters were not significantly different among transient transfections using wild-type vs. mutant plasmid DNA (Table 2.4). These data suggest that SUMOylation at K437 or K579 is not sufficient to regulate the V_{50} inact and τ_f. The SUMOylation-mediated changes in the stable HEK-Kv4.2g cell line may have required an additional factor(s) specific to that cell line.

Lastly, we examined whether the K437R mutation blocked, or mimicked and occluded the effect of K437 SUMOylation. HEK cells were transiently transfected with wild-type or mutant plasmids, and biotinylation experiments were performed. Figure 2.11 illustrates that Kv4.2g surface expression was not significantly different among HEK cells transiently transfected with wild-type or mutant plasmids (Kv4.2g 1.0±0.094, Kv4.2g K437R 1.1±0.28, Kv4.2g K579R 0.98±0.18). Thus, the K437R mutation blocks the effect of SUMOylation.

2.5 Discussion

Several ion channels are post-translationally regulated by SUMOylation (Gong et al., 2016; Henley et al., 2018; Kruse et al., 2009; Parker et al., 2016; Wasik & Filipek, 2014; H. Wu et al., 2016). Multiple members of the voltage-gated potassium channel superfamily are known to be SUMOylated including Kv1.1 (Qi et al., 2014), Kv1.5 (Benson et al., 2007), Kv2.1 (Dai et al., 2009; Plant et al., 2011), Kv7.1 (Xiong et al., 2017), Kv7.2 (Qi et al., 2014), and Kv11.1 (Steffensen et al., 2018). In this work, we tested the hypothesis that Kv4 channels can be SUMOylated to regulate their biophysical properties and surface expression. We found Kv4.2 channels were decorated by SUMO-2/3 but not SUMO-1 in rat membrane preparations. *In silico* analysis suggested that Kv4.2 could be SUMOylated at several sites. Two predicted SUMOylation sites, K437 and K579, were conserved across species and Kv4 isoforms. Globally enhancing baseline SUMOylation in HEK cells stably expressing Kv4.2 increased SUMOylation at K437 and K579 by ~30% each. Enhanced SUMOylation at K437 resulted in a mean ~70-95% increase in Kv4.2 surface expression with no change in I_A G_{max}. Enhancing SUMOylation at K579 decreased mean I_A G_{max} by ~25-50% with no change in surface expression. Our data support the hypothesis that post-translational SUMOylation of Kv4 channels can regulate their function through multiple mechanisms.

2.5.1 The function of Kv4 channel SUMOylation

Post-translational modification of Kv4 channels regulates I_A over short time scales. This is the first report that Kv4.2 channels can be post-translationally modified by SUMO. Globally increasing SUMOylation in HEK cells expressing a mouse Kv4.2-GFP fusion protein (Kv4.2g) increased Kv4.2 SUMOylation on the C-terminus at K437 and K579. When both sites were mutated to R, Kv4.2g SUMOylation could no longer be experimentally increased; however,

Kv4.2 was still SUMOylated under baseline conditions. This suggests that SUMOylation occurs at additional sites on the channel and/or the GFP tag.

There are three potential, non-mutually exclusive consequences of protein SUMOylation. First, SUMOylation can prevent protein-protein interactions through steric hindrance (Dustrude et al., 2016). Second, SUMO can compete with other post-translational modifications that occur on the same K residue such as ubiquitination, methylation, or acetylation (D. D. Anderson et al., 2012; W. Wang et al., 2014). The third and most common function of SUMOylation is to promote protein-protein interactions (Psakhye & Jentsch, 2012; A. Seifert et al., 2015). SUMO interacts with specific protein binding domains, and the best studied is the SUMO-interacting motif (SIM) (Aguilar-Martinez et al., 2015; C. C. Chang et al., 2011; Hecker et al., 2006; Jardin, Horn, & Sticht, 2015; Kerscher, 2007; Namanja et al., 2012). In general, the SUMO-SIM bond is relatively weak and serves to increase the affinity between proteins that bind one another through additional contacts. Thus, SUMOylation may stabilize an existing interaction and/or facilitate recruitment of a protein.

In some cases, SUMOylation enzymes can target an entire group of physically or functionally connected proteins. Importantly, a protein that is SUMOylated often possess one or more SIMs. Thus, group SUMOylation can result in a set of interlocking Lego-like interactions for each protein in a complex, and the collection of individually weak SUMO-SIM bonds stabilizes the entire structure (Jentsch & Psakhye, 2013). In native cells, Kv4 channels exist in a ternary complex comprising four α-subunits, four cytoplasmic KChIP subunits, and four transmembrane DPPL subunits (Amarillo et al., 2008; Foeger, Norris, Wren, & Nerbonne, 2012; Jerng et al., 2005; Jerng & Pfaffinger, 2012; W. C. Wang et al., 2015). It is possible that group SUMOylation could stabilize the ternary complex, as prediction software indicates that all Kv4

channels, all KChIPs (1-4) and DPP6/10 possess multiple potential SUMO and SIM domains. In support of this idea, both KChIPs and DPPLs regulate Kv4 surface expression and gating (Jerng & Pfaffinger, 2014), and both have the potential to interact with Kv4 C-terminal SUMOylation sites (Callsen et al., 2005; W. Han et al., 2006; Lin et al., 2014; Ren et al., 2005; Sokolova et al., 2003). It is also possible that cytoplasmic C-terminal SUMOylation could regulate interactions between the Kv4.2 α-subunits, themselves, or C-terminal intra-molecular interactions (Hatano et al., 2004). SUMOylation could also regulate Kv4α interactions outside the ternary complex, as the C-terminus is known to interact with additional proteins, like SAP97 (El-Haou et al., 2009; Gardoni et al., 2007; Jerng & Pfaffinger, 2014).

In HEK cells stably or transiently expressing Kv4.2g, enhancing SUMOylation at K437 increased channel surface expression by up to 95% without altering I_A G_{max}, suggesting SUMOylation increased the number of silent channels in the plasma membrane. The human protein atlas indicates KChIP2-4 are endogenously expressed at a low but detectable level in HEK cells (http://www.proteinatlas.org), and a previous study showed that co-expression of Kv4.2 and KChIP2 in HEK cells produced a 40-fold increase in Kv4.2 surface expression but only a 3-fold increase in Kv4.2 current density (Foeger et al., 2010). These data suggest SUMOylation at K437 could modulate the Kv4.2-KChIP interaction. SUMOylation could also stabilize interactions with endogenous SAP97 which is expressed at high levels in HEK cells (http://www.proteinatlas.org) and has been shown to increase Kv4 surface expression. On the other hand, attachment of a bulky SUMO at K437 might also reduce C-terminal interactions necessary for endocytosis (Nestor & Hoffman, 2012).

In HEK cells stably or transiently expressing Kv4.2g, increasing SUMOylation at K579 reduced I_A G_{max} by ~30-50% without altering channel surface expression. Replacing K with R

had the same effect. Since enhancing K579 SUMOylation produced the same effect as removing K579, SUMOylation most likely blocked an interaction involving K579 that influenced peak current amplitude.

2.5.2 Physiological functions and regulation of SUMOylation

SUMO is emerging as an important physiological regulator of ionic currents. Dopamine gates activity-dependent SUMOylation to regulate the densities of I_A and the hyperpolarization activated current (I_h), and this is necessary to maintain activity homeostasis in a pattern generating neuron (Parker, Forster, & Baro, 2019). In hippocampal neurons, SUMOylation is known to regulate the kainate-receptor-mediated excitatory postsynaptic current (Chamberlain et al., 2012; Martin, Wilkinson, Nishimune, & Henley, 2007), the delayed rectifier (Plant et al., 2011), and the M-current (Qi et al., 2014). SUMOylation is necessary for synaptic plasticity at mossy fiber-CA3 synapses, and hyper-SUMOylation suppresses the M-current and leads to hippocampal neuron hyperexcitability and seizures in a mouse model of sudden death. In dorsal root ganglion (DRG) sensory neurons, SUMOylation increases Na^+ current (I_{Na}) amplitude (Dustrude et al., 2016; Francois-Moutal et al., 2018; Moutal et al., 2017), and lowers the temperature threshold of activation for the TRPV1-mediated current (Y. Wang et al., 2018) and hyper-SUMOylation contributes to pathological pain states. In rat cerebellar granule neurons, SUMOylation increases I_{Na} and reduces the leak current; and, hypoxia acts through SUMOylation to increase I_{Na}, which contributes to hypoxic brain damage (Plant et al., 2016; Plant, Zuniga, Araki, Marks, & Goldstein, 2012). In cardiac myocytes, SUMOylation determines the native attributes of the slow delayed rectifier current (I_{Ks}) (Xiong et al., 2017).

In many of the previous examples, SUMO-mediated regulation of the current was due to SUMOylation of ion channels and/or their auxiliary proteins. In hippocampal neurons GluR2,

Kv1.1, Kv2.1 and Kv7 ion channels are SUMOylated (Chamberlain et al., 2012; Martin, Wilkinson, et al., 2007; Plant et al., 2011; Qi et al., 2014). In DRG sensory neurons, auxiliary subunit Collapsin Response Mediator Protein 2 (CRMP2) is SUMOylated to increase its association with the voltage-gated sodium channel 1.7 ($Na_V1.7$) (Dustrude et al., 2016; Dustrude, Wilson, Ju, Xiao, & Khanna, 2013). $Na_V1.2$ α-subunits and two-P domain, acid sensitive K^+ (TASK) channels are SUMOylated in cerebellar granule neurons (Plant et al., 2016; Plant et al., 2012). In cardiac myocytes, KCNQ1 subunits are SUMOylated to shift their voltage dependence (Xiong et al., 2017). An appreciation for the regulation of ion channel SUMOylation is guiding the design of small molecules to prevent SUMO dysregulation in disease states (Cox & Huber, 2018; Francois-Moutal et al., 2018).

SUMOylation is highly regulated. In this study, target protein SUMOylation was experimentally enhanced by transient overexpression of the SUMO substrate and the SUMO conjugating enzyme, Ubc9. In native cells, SUMOylation can be regulated at the level of the target protein and/or the SUMOylation machinery. The target protein phosphorylation status gates its ability to be SUMOylated (Dustrude et al., 2016; Flotho & Melchior, 2013) and neuromodulators have been shown to act through kinases to gate SUMOylation (Parker et al., 2019). In addition, neuronal activity can regulate the SUMOylation machinery abundance, localization and level of activity (Craig et al., 2012; Feligioni et al., 2013; Hickey et al., 2012; Lee et al., 2014; Loriol et al., 2014; Loriol et al., 2013; Lu et al., 2009; Nayak & Muller, 2014). Modulators and activity regulate I_A in native neurons (J. Kim et al., 2007; Lei, Deng, & Xu, 2008; Parker et al., 2019; Rodgers, Krenz, Jiang, Li, & Baro, 2013; Shah, Hammond, & Hoffman, 2010; Shen, Zhou, Yang, Xu, & Wang, 2008). It will be important to test whether SUMO post-translational modification of Kv4.2 channels contributes to this regulation.

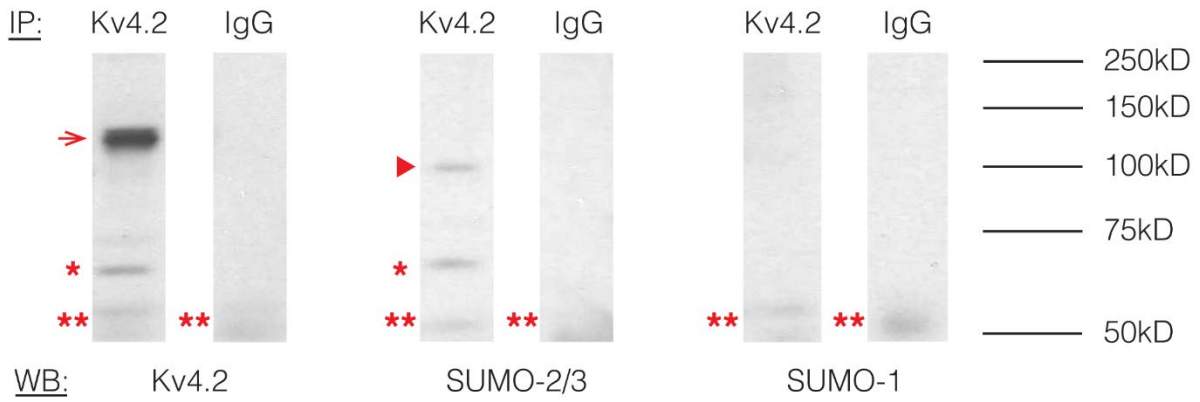

Figure 2.1 Kv4.2 channels are SUMOylated in the rodent CNS.
Immunoprecipitation (IP) experiments were followed by western blot analysis. Antibodies are as indicated. The experiment was repeated three times using the brains from three different rats. A 68kD band, representing the Kv4.2 channel is indicated by an asterisk. A 130kD band representing aggregated Kv4.2 channels is indicated by an arrow. A 100kD band that most likely represents a protein that non-covalently interacts with the Kv4.2 channel is indicated by an arrowhead. A 50kD band (double asterisk) most likely represents the IP antibody.

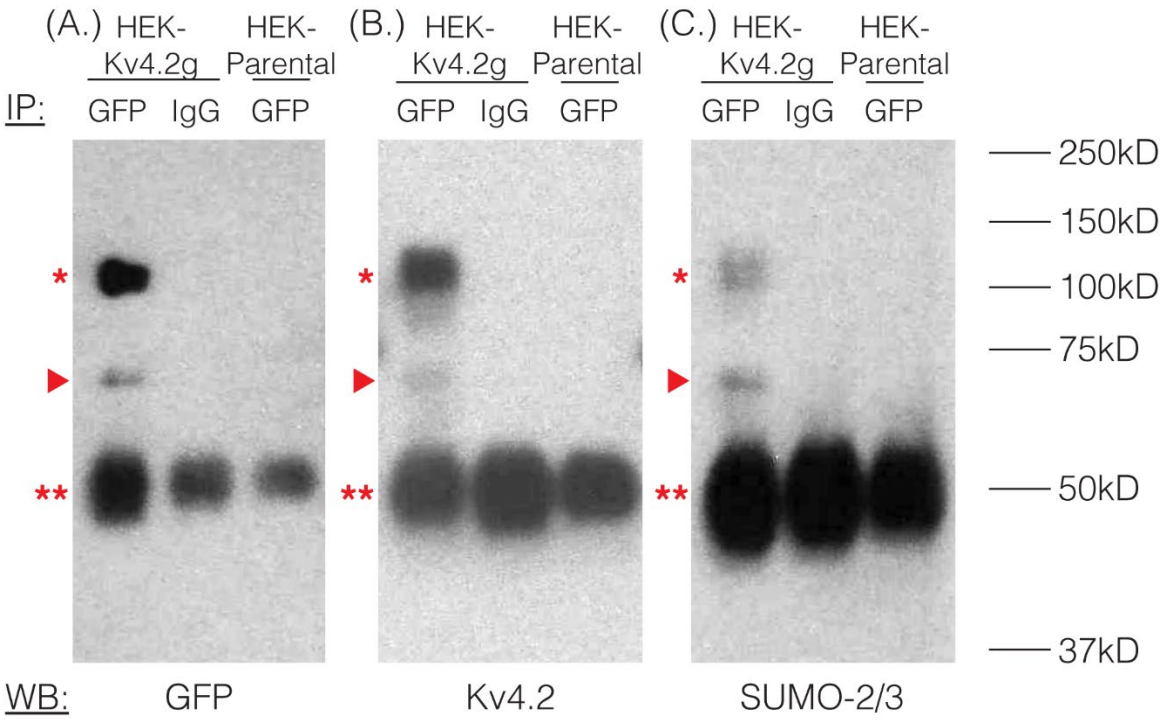

Figure 2.2 Kv4.2 channels are SUMOylated in a heterologous expression system.

A mouse Kv4.2 channel with a C-terminal GFP tag (Kv4.2g) was stably expressed in Human Embryonic Kidney (HEK) cells (HEK-Kv4.2g). IP experiments were performed on cell lysates from HEK-Kv4.2g cells or HEK parental cells using an anti-GFP or a negative control IgG antibody. Western blots containing IP product were probed using an **(A)** anti-GFP, **(B)** anti-Kv4.2, or **(C)** anti-SUMO-2/3 antibody. Experiments were repeated three times. The Kv4.2-GFP protein was detected as a 100kD band (asterisk) using antibodies against GFP, Kv4.2, and SUMO-2/3. This band was never observed when a negative control IgG or HEK parental cells were used in the IP. A 70kD band was also detected by all antibodies (arrow head), and it most likely represents cleavage of the channel. This signal was not included in subsequent quantifications. This most likely represents sample degradation. The 50kD band observed in all lanes (double asterisk) likely represents the IP antibodies.

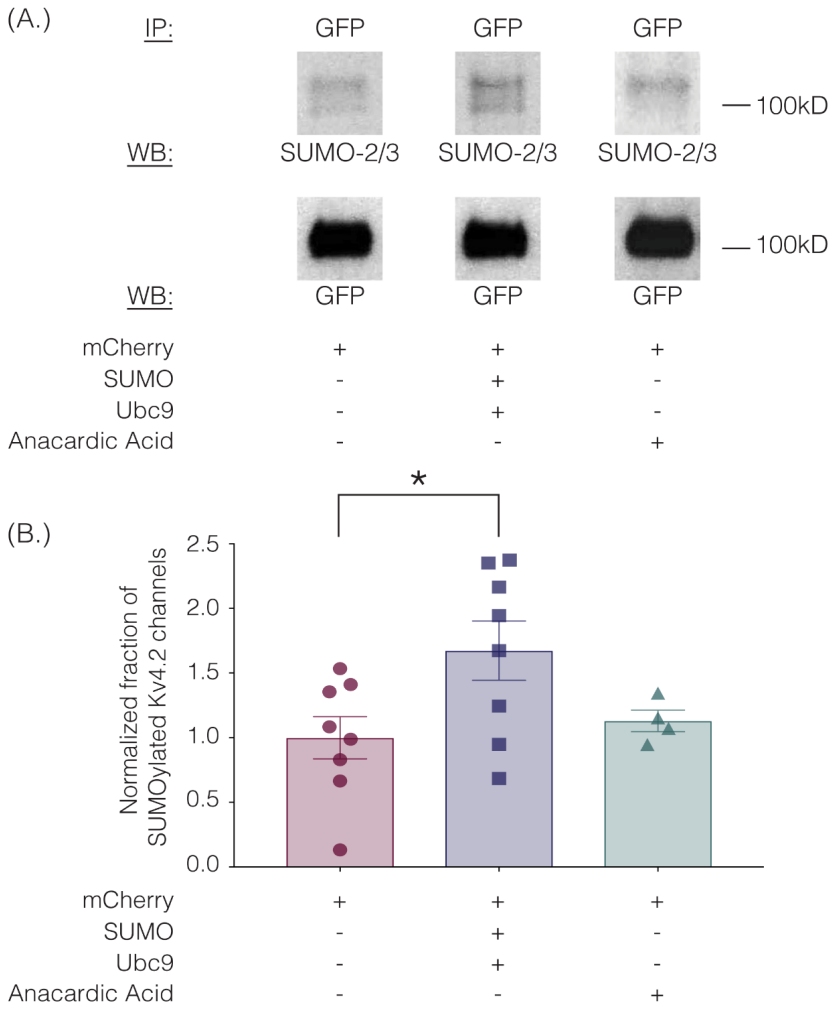

Figure 2.3 Kv4.2 channel SUMOylation can be manipulated in a heterologous expression system.

HEK-Kv4.2g cells were transiently transfected with mCherry or mCherry+SUMO+Ubc9 plasmid DNA. Two days after transfection, cells were lysed and used in IP experiments. In some cases, HEK-Kv4.2g cells transiently transfected with mCherry were treated with anacardic acid (100μM, 1hr) prior to cell lysis and IP. Western blots containing IP product were probed for SUMO-2/3 and then stripped and re-probed for GFP. The fraction of SUMOylated Kv4.2 channels was determined. **(A)** Representative western blots for each treatment group. Note that two bands are resolved with anti-SUMO-2/3, but not anti-GFP, suggesting that shorter exposure times or lower amounts of input protein would reveal two bands with anti-GFP. **(B)** Plots showing the fraction of SUMOylated Kv4.2 channels in control, SUMO+Ubc9, and anacardic acid treatment groups. Each symbol represents one independent experiment, and all data points were normalized by the mean value for the control treatment group. Asterisk, significant differences in the fraction of SUMOylated Kv4.2 channels among treatment groups. One-way ANOVA with Tukey's post-hoc, $F(2,17)=3.68$, $p=0.047$; control, 1.0±0.16; SUMO+Ubc9, 1.6±0.23; anacardic acid, 1.1±0.083.

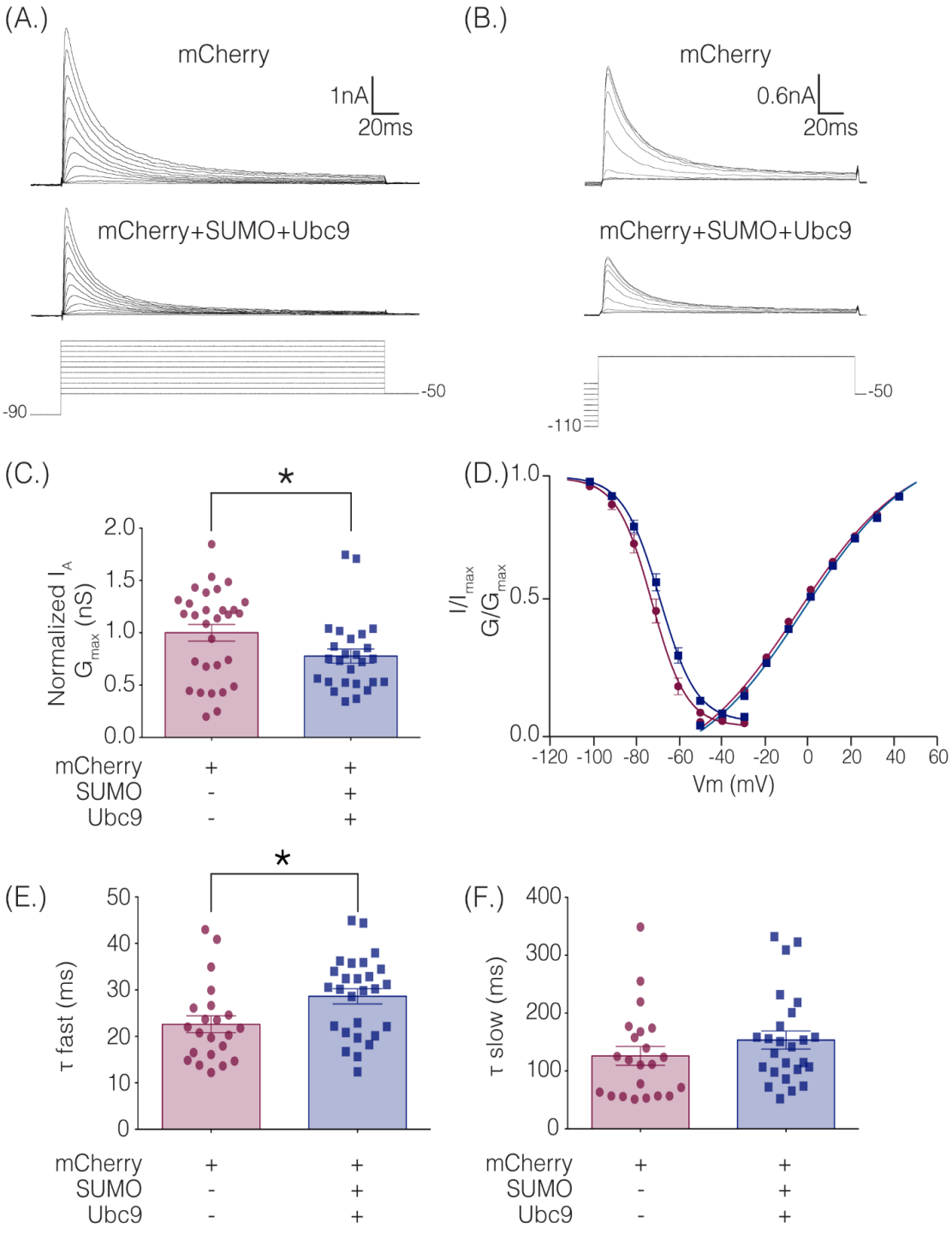

Figure 2.4 I_A G_{max} is significantly decreased in HEK-Kv4.2g cells transiently transfected with SUMO+Ubc9 compared to control.

Whole cell patch clamp experiments were performed on HEK-Kv4.2g cells that were or were not transiently transfected with SUMO+Ubc9 to produce a ~60% increase in mean Kv4.2 SUMOylation. **(A)** Representative current traces (upper panel) and voltage steps (lower panel)

used to obtain the voltage dependence of activation. **(B)** Representative current traces (upper panel) and voltage steps (lower panel) used to obtain the voltage dependence of steady-state inactivation. **(C)** Plots of normalized I_A G_{max} for control and SUMO+Ubc9 treatment groups. Each data point represents one cell. Cells in each treatment groups were obtained from ≥3 independent transfections. All data points were normalized by the mean value for the control treatment group. Asterisk, significantly different; control, 1.0±0.079; SUMO+Ubc9, 0.78±0.068; Mann-Whitney U p=0.044. **(D)** Activation and steady-state inactivation curves for control and SUMO+Ubc9 treatment groups. Each point represents the mean±SEM for all cells shown in panel 4C. **(E-F)** Inactivation τ for all cells shown in panel 4C. Asterisk, significantly different; t-test p=0.018.

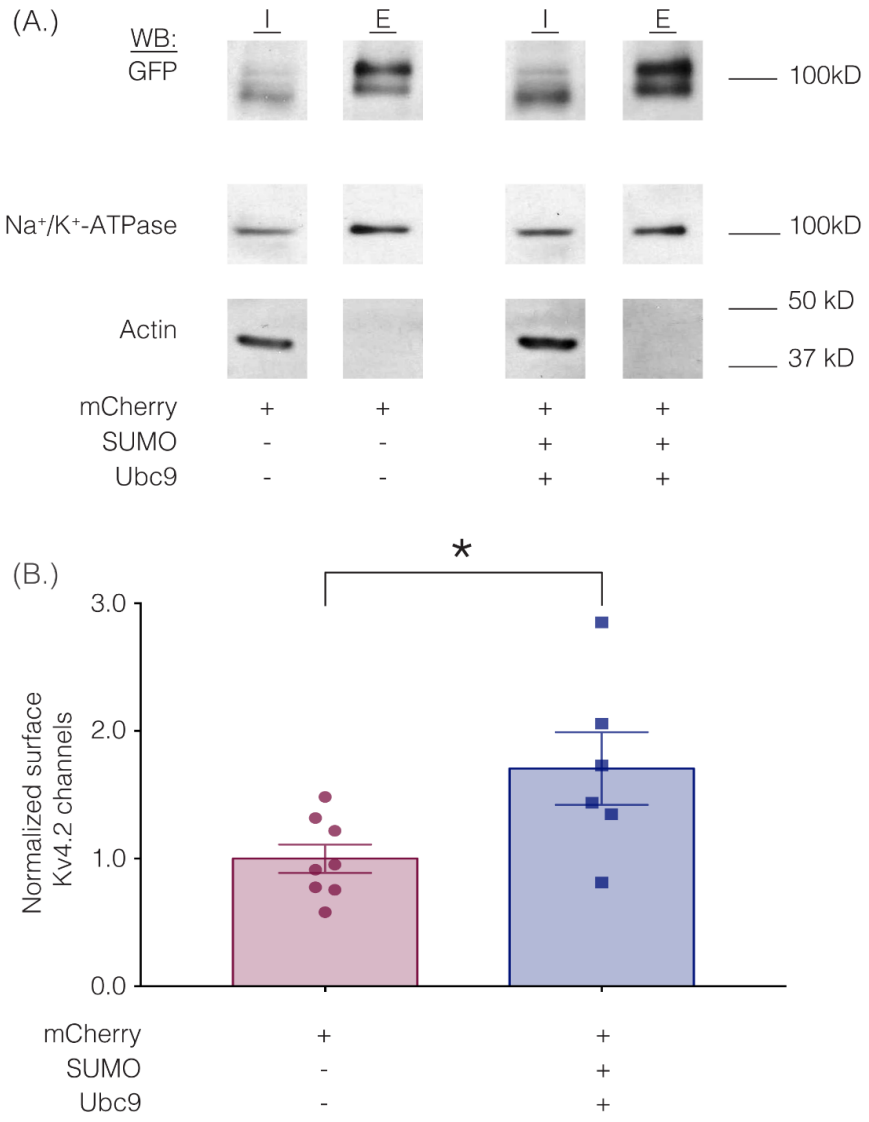

Figure 2.5 Increased SUMOylation mediates an increase in Kv4.2 surface expression.
(A) Representative western blots for each treatment group. HEK-Kv4.2g cells were transiently transfected with mCherry or mCherry+SUMO+Ubc9. Extracellular proteins were biotinylated, and cells were lysed. Surface proteins were isolated using NeutrAvidin beads (E for extracellular). Unbound proteins were assumed to be intracellular (I for intracellular). The upper portion (above 50kD) of a western blot containing I and E fractions was probed for GFP and then stripped and re-probed for Na^+/K^+-ATPase, and the lower portion of the blot (below 50kD) was probed for actin. Intracellular bands appeared to run slightly lower than extracellular. There are several potential explanations including distinct loading buffers, different protein concentrations and differences in post-translational modifications. **(B)** Plots of normalized Kv4.2g channel surface expression. The blots were used to measure channel surface expression as described in Materials and Methods. Each data point is one independent experiment. Each data point was normalized by the mean value for the control treatment group. Asterisk, significantly different; control, 1.0±0.11; SUMO+Ubc9, 1.7±0.28; t-test p=0.025.

Figure 2.6 Identification of Kv4.2 SUMOylation sites.

The amino acid sequences for mouse Kv4.1 (NP_032449.1), Kv4.2 (NP_062671.1) Kv4.3 (NP_001034436), rat Kv4.2 (Q63881.1), and human Kv4.2 (NP_036413.1) channels were aligned. Two putative, evolutionarily conserved SUMOylation sites predicted by SUMOplot and GPS-SUMO are located on intracellular domains. The probability that the site is SUMOylated is indicated, and transmembrane domains are highlighted in red.

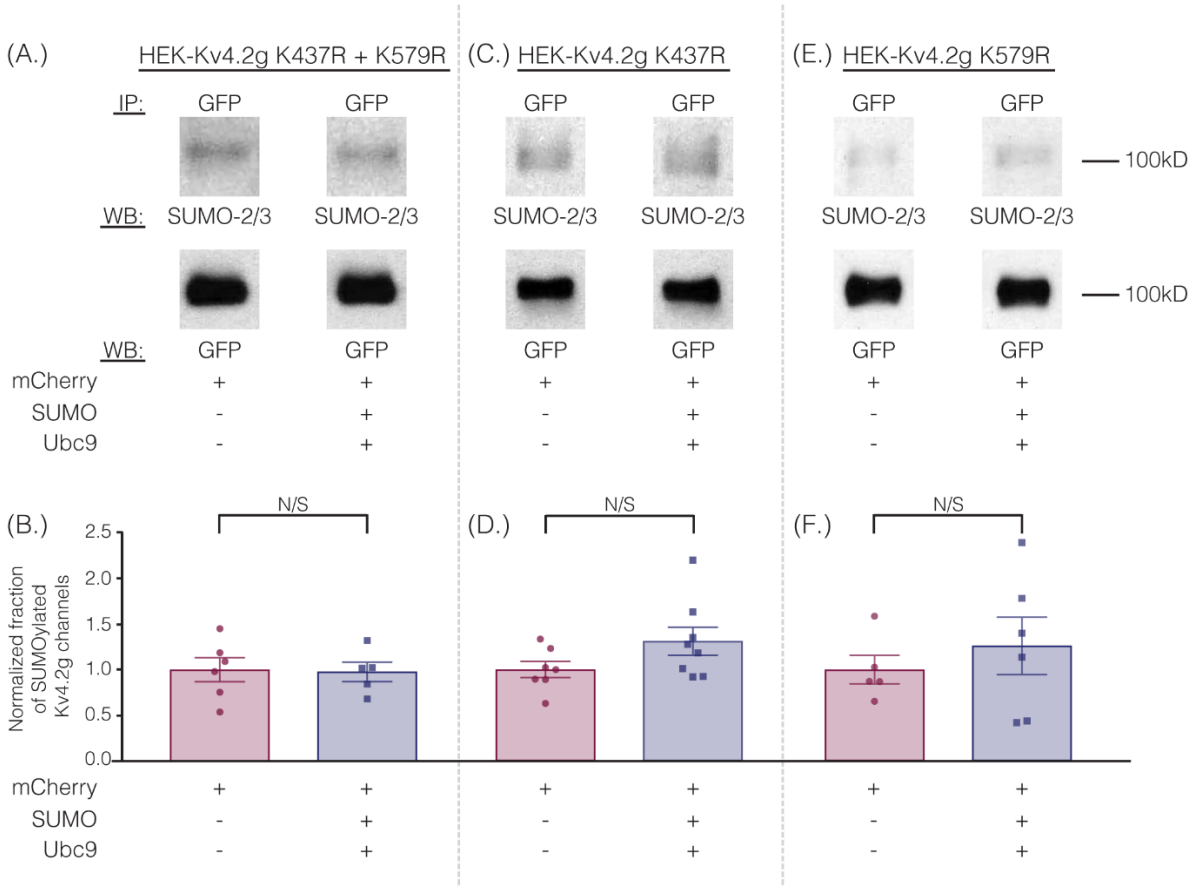

Figure 2.7 The ability to manipulate Kv4.2 channel SUMOylation is lost when K437 and K579 are mutated to R.

(A, C, and E) Representative experiments using the indicated stable mutant cell line. **(B, D, and F)** Bar graphs showing normalized fraction of SUMOylated Kv4.2 channels. Each data point represents one independent experiment. All data points were normalized by the mean value for the mCherry treatment group. **Kv4.2g K437R+K579R:** control, 1.0±0.13; SUMO+Ubc9, 0.98±0.11; t-test p=0.90. **Kv4.2g K437R:** control, 1.0±0.088; SUMO+Ubc9, 1.3±0.15; t-test p=0.11. **Kv4.2g K579R:** control, 1.0±0.16; SUMO+Ubc9, 1.3±0.31; t-test p=0.51.

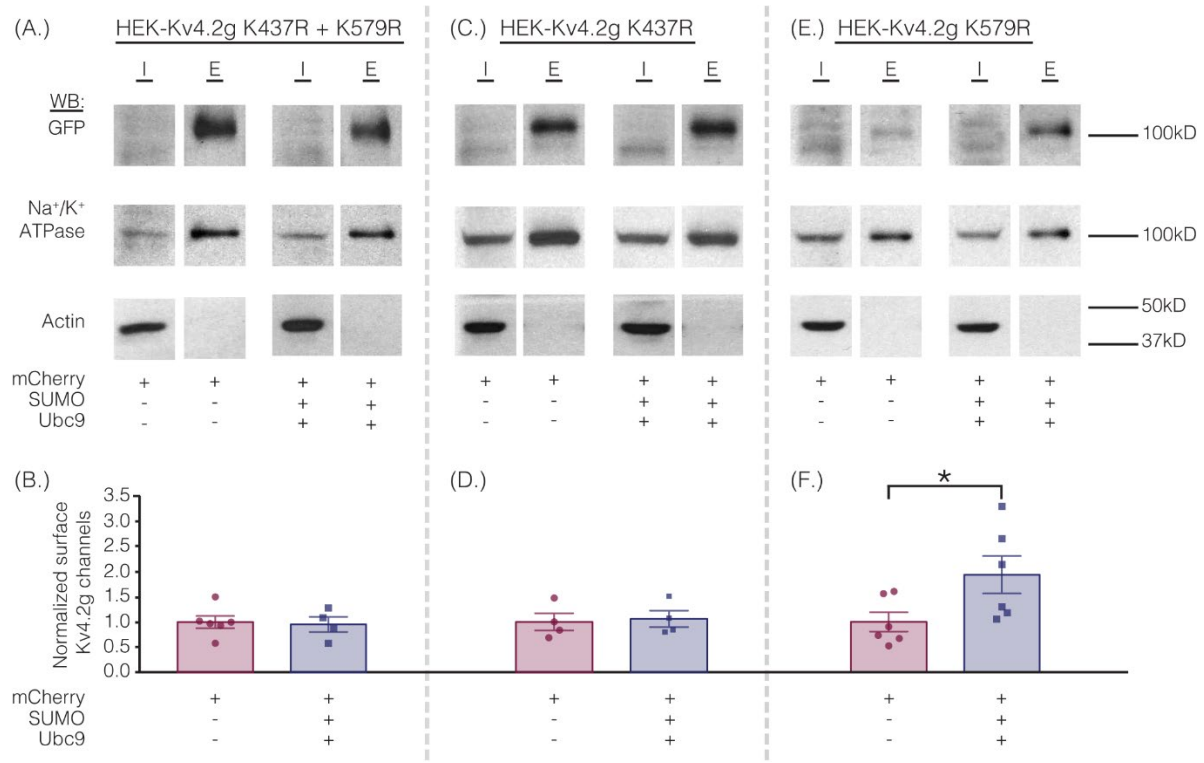

Figure 2.8 Increased SUMOylation at K437 mediates the increase in Kv4.2 surface expression.

(A, C, and E) Representative experiments. **(B, D, and F)** Bar graphs showing normalized Kv4.2 surface expression. Each data point is one independent experiment. All data points were normalized by the mean value for the mCherry treatment group. Asterisk, significant difference. **Kv4.2g K437R+K579R:** control, 1.0±0.12; SUMO+Ubc9, 0.95±0.15; t-test p=0.82. **Kv4.2g K437R:** control, 1.0±0.17; SUMO+Ubc9, 1.1±0.16; t-test p=0.81. **Kv4.2g K579R:** control, 1.0±0.19; SUMO+Ubc9, 1.9±0.37; t-test p=0.049.

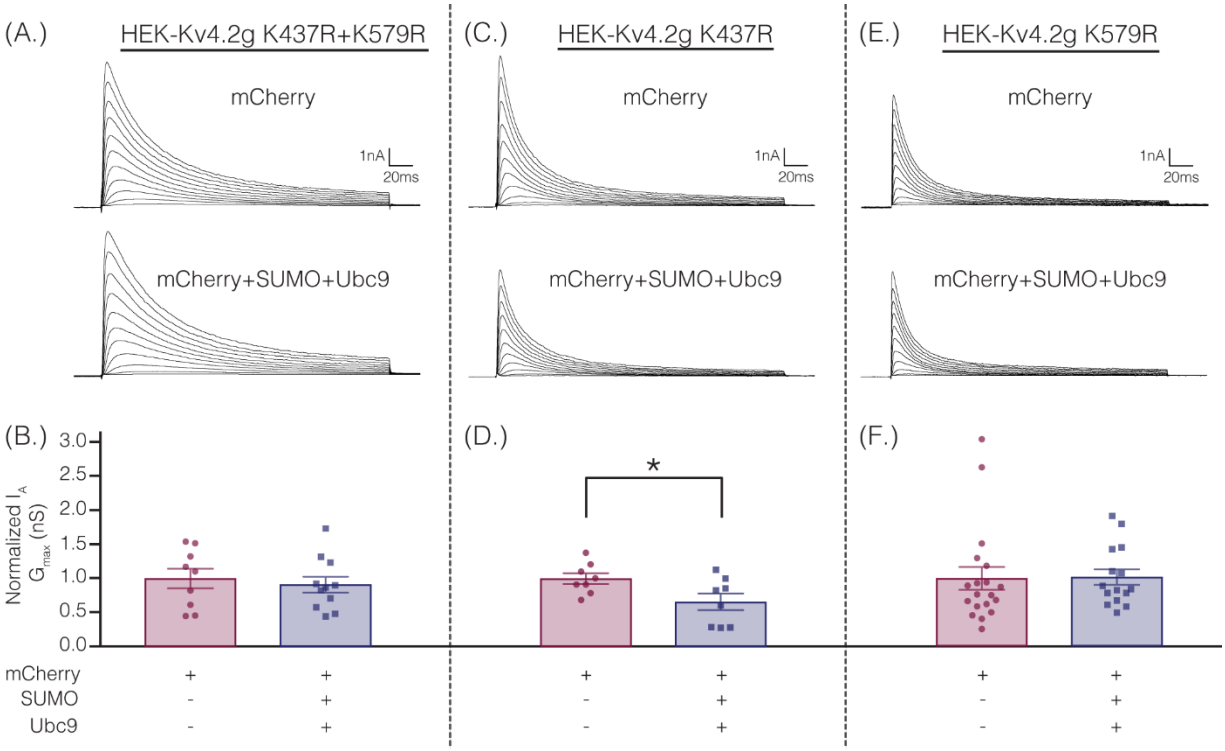

Figure 2.9 Increased SUMOylation at K579 mediates the decrease in I_A G_{max}.
(A, C, and E) Representative current traces for the indicated stable mutant cell line in each treatment group. **(B, D, and F)** Bar graphs representing normalized I_A G_{max}. Each data point is one cell, and cells in each treatment group were obtained from ≥3 independent transfections. All data points were normalized by the mean value for the mCherry treatment group. Asterisk, significantly different. **Kv4.2g K437R+K579R:** control, 1.0±0.14; SUMO+Ubc9, 0.91±0.12; t-test p=0.63. **Kv4.2g K437R:** control, 1.0±0.080; SUMO+Ubc9, 0.66±0.12; t-test p=0.035. **Kv4.2g K579R:** control, 1.0±0.1656; SUMO+Ubc9, 1.02±0.1141; Mann-Whitney U p=0.4715.

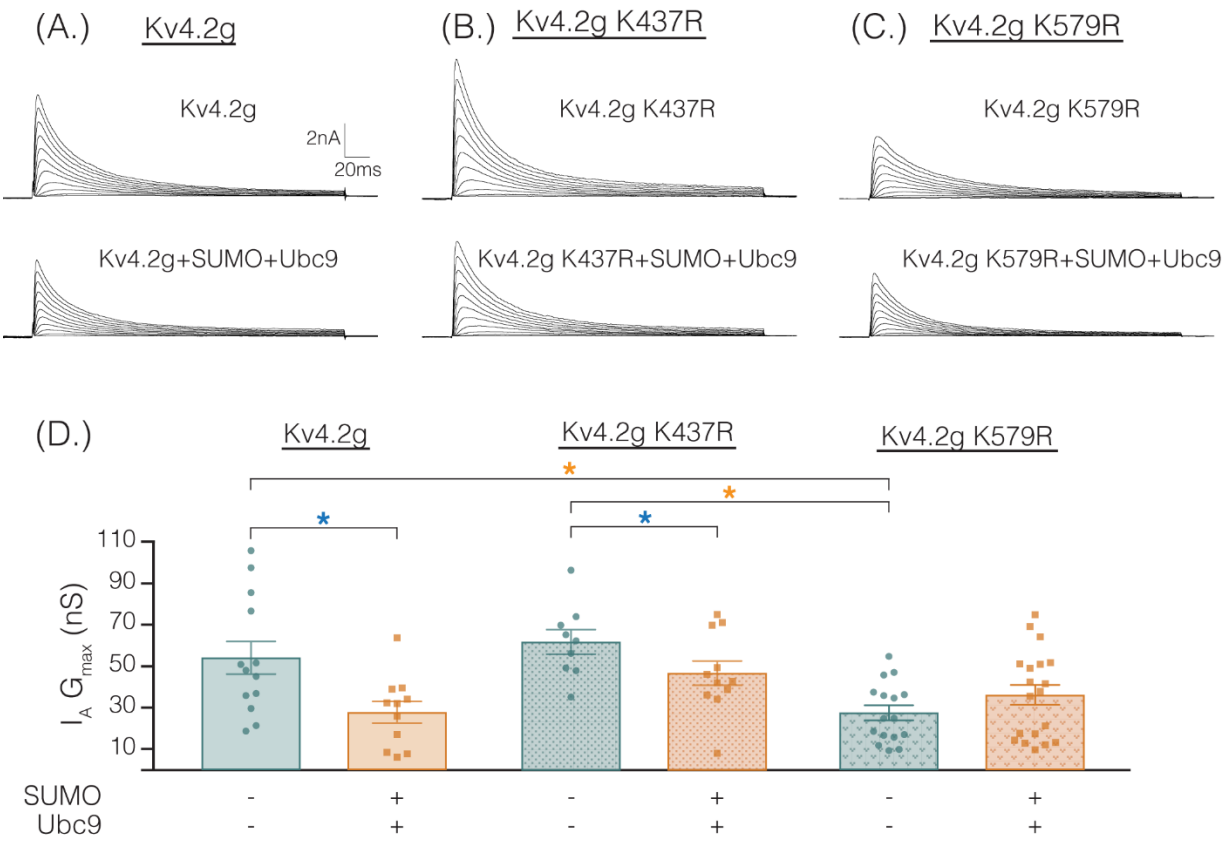

Figure 2.10 Transiently transfecting HEK cells with Kv4.2g K579R significantly decreases I_A G_{max} compared to control.

(A-C) Representative current traces for each treatment group. Each data point represents one cell, and data for each treatment group was pooled from ≥3 independent transfections. **(D)** Plots showing I_A G_{max}. Orange asterisks, significant differences in I_A G_{max} among HEK cells expressing Kv4.2g, Kv4.2g K437R, and Kv4.2g K579R. One-way ANOVA with Tukey's post-hoc, $F(2,35)=9.75$, $p=0.0004$. Blue asterisks, significant differences in I_A when SUMO+Ubc9 was co-transfected. **Kv4.2g:** control, 54.2nS±7.9; SUMO+Ubc9, 27.8nS±5.2; t-test p=0.014. **Kv4.2g K437R:** control, 62.1nS±5.9; SUMO+Ubc9, 46.9nS±5.9; t-test p=0.049. **Kv4.2g K579R:** control, 27.6nS±3.59; SUMO+Ubc9, 36.2nS±4.84; t-test p=0.18.

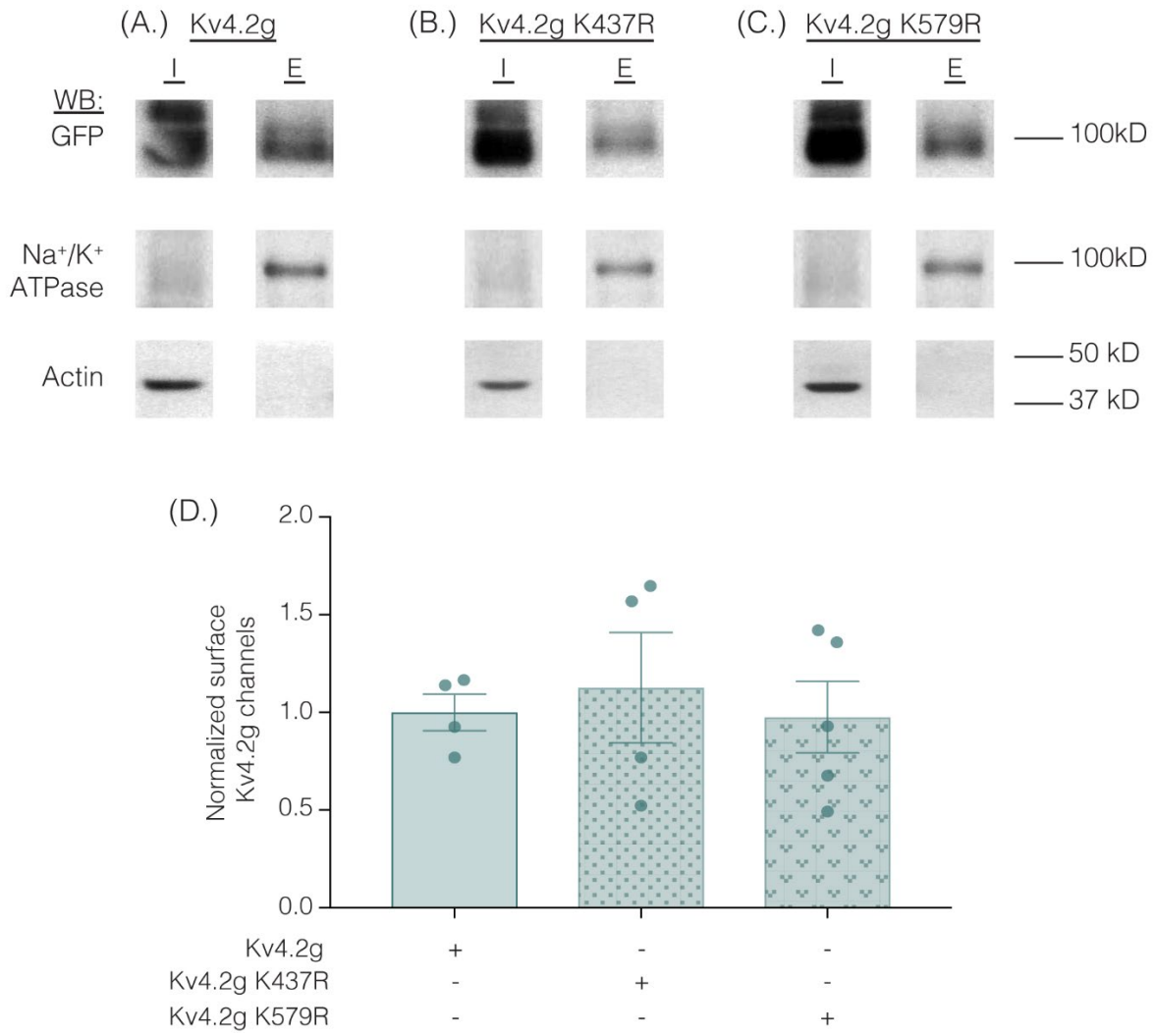

Figure 2.11 Transiently transfecting HEK cells with wild-type or mutant Kv4.2g does not significantly alter surface expression.

HEK cells were transiently transfected with Kv4.2g, Kv4.2g K437R, or Kv4.2g K579R plasmid DNA and cell surface biotinylation experiments were performed. **(A-C)** Representative western blots for each treatment group. **(D)** Plots of normalized surface Kv4.2g channels. Each data point is one independent experiment and was normalized by the mean wild-type value. One-way ANOVA with Tukey's post-hoc, $F(2,10)=0.16$, $p=0.85$.

Table 2.1 Primary antibodies

Antigen:	Verified by:	Species, manufacturer and catalogue number:	Concentration used:
Kv4.2	Specificity verified by the company. WB analysis of rat membranes probed with anti-Kv4.2 (1:200) revealed a 68kD band.	rabbit, alomone labs, #APC-023	IP: 8.3µL antibody per 1000µg protein; WB: 1:750
GFP (IP)	Specificity verified by the company. Ab detects 5ng recombinant GFP expressed in HEK293 cells.	rabbit, abcam, ab290	IP: 1µL antibody per 500µg protein
GFP (WB)	Specificity verified by the company. WB analysis of untransfected COS and COS cells transfected with pCruz GFP-Lac Z	rabbit, Santa Cruz Biotechnology, sc-8334	WB: 1:3000
SUMO-1	Specificity verified by the company. WB analysis of HEK293 expressing SUMO-1.	rabbit, Santa Cruz Biotechnology, sc-9060	WB: 1:1000
SUMO-2/3	Specificity verified by the company. WB analysis of HEK293 cells transfected with SUMO-2	rabbit, Santa Cruz Biotechnology, sc-32873	WB (HEK cells): 1:3000; WB (rat brain): 1:1000
SUMO-2/3	Specificity verified by the company. Ab recognizes 15 and 18kD bands in HeLa extract on WB.	rabbit, abcam, ab3742	WB (HEK cells): 1:1000; WB (rat brain): 1:750
Na^+/K^+-ATPase	Specificity verified by the company. Positive signal on WB using HEK293 whole cell lysate.	mouse, abcam, ab7671	WB: 1:3000
Actin	Specificity verified by the company. WB analysis of C32 whole cell lysate	rabbit, Santa Cruz Biotechnology, sc-1616-R	WB: 1:2000
BSA	Specificity verified by the company. BSA was loaded onto a gel. WB analysis revealed a 68kD band when probed with anti-BSA antibody.	rabbit, ThermoFisher, A11133	WB: 1:20,000

Table 2.2 Site-directed mutagenesis primers

Primer name:	Primer sequence:
For-Kv4.2K437R	CGAGCAGCCAgAAGCGGGAGTGCAAATGCCTACATGC
Rev-Kv4.2K437R	GCATGTAGGCATTTGCACTCCCGCTTcTGGCTGCTCG
For-Kv4.2K579R	CAGCCGATCCAGCTTAAATGCCAgAATGGAAGAGTGTGTTAAAC
Rev-Kv4.2K579R	GTTTAACACACTCTTCCATTcTGGCATTTAAGCTGGATCGGCTG

Table 2.3 Whole-cell patch clamp physiology data for stable lines

Stable Lines								
	HEK-Kv4.2g		**HEK-Kv4.2g K437R**		**HEK-Kv4.2g K579R**		**HEK-Kv4.2g K437R+K579R**	
	mCherry	mCherry+ SUMO+ Ubc9	mCherry	mCherry+ SUMO+ Ubc9	mCherry	mCherry+ SUMO+ Ubc9	mCherry	mCherry+ SUMO+ Ubc9
G_{max} (nS)	32.7±2.6	25.5±2.2^{T}	75.2±6.0	49.5± 9.2^{TT}	26.2±4.3	26.7±3.0^{NS}	92.8±13.3	84.5±10.9^{NS}
V_{50} Actvation (mV)	-4.9±2.0	-2.8±1.7	-2.5±1.9	-5.1±1.6	-6.5±1.5	-4.3±2.6	-19.3±3.8	-15.2±4.3
V_{50} Inactivation (mV)	-72.2± 1.2	-67.8± 0.7^{T}	-73.5± 1.1	-75.8±1.7^{NS}	-72.8±1.0	-71.2±1.1^{NS}	-69.3±1.6	-69.4±1.9^{NS}
Slope Activation	29.0±1.3	25.6±1.1	31.1±1.9	29.8±1.8	25.0±1.3	26.4±1.0	26.1±2.0	29.3±2.2
Slope Inactivation	-7.3±0.3	-7.4±0.3	-6.7±0.2	-6.7±0.2	-7.8±0.3	-6.7± 0.2	-6.5±0.4	-6.7±0.3
τ_{Fast} (ms)	22.6±1.8	28.6±1.6^{T}	16.6±0.9	18.3±2.0^{NS}	29.4±1.8	23.2± 1.7^{TTT}	26.8±2.8	18.3±2.9^{NS}
τ_{Slow} (ms)	126.1± 16.3	153.4± 15.7	64.1±3.0	72.0±8.9	229.8± 29.3	121.4± 12.9	81.04±7.2	77.9±10.9

^{T} HEK-Kv4.2g mCherry significantly different from mCherry+SUMO+Ubc9 (G_{max}, Mann-Whitney U, p=0.044; V_{50} inactivation, t-test, p=0.0019; τ_{fast}, t-test, p=0.018)

^{TT} HEK-Kv4.2g K437R mCherry significantly different from mCherry+SUMO+Ubc9 (t-test, p=0.035)

^{TTT} HEK-Kv4.2g K579R mCherry significantly different from mCherry+SUMO+Ubc9 (t-test, p=0.019)

Table 2.4 Whole-cell patch clamp physiology data for transient transfections

Transient transfections						
	Kv4.2g		**Kv4.2g K437R**		**Kv4.2g K579R**	
	Kv4.2g	Kv4.2g+ SUMO+Ubc9	Kv4.2g K437R	Kv4.2g K437R+ SUMO+Ubc9	Kv4.2g K579R	Kv4.2g K579R+ SUMO+Ubc9
G_{max} (nS)	54.2±7.9^{TTT}	27.8±5.2^{T}	62.1±5.9^{TTT}	46.9±5.9^{TT}	27.6± 3.6	36.2±4.8
V_{50} Activation (mV)	-2.6±1.8	2.5±2.5	-5.1±3.3	-0.7±2.1	2.6±1.8	-4.3±3.4
V_{50} Inactivation (mV)	-71.5±1.5	-72.9±1.0 ^{NS}	-69.6±1.7	-70.8±1.3	-73.5±0.9	-70.9±0.8
Slope Activation	26.1±0.8	23.0±1.0	27.1±1.8	28.2±1.4	27.2±0.8	28.7±1.1
Slope Inactivation	-6.4±0.2	-7.0±0.2	-6.2±0.2	-6.3±0.2	-7.1± 0.2	-6.5±0.2
τ_{Fast} (ms)	22.1±2.4	27.4±3.1 ^{NS}	17.1±1.7	17.1±1.0	26.1±2.1	26.9±2.0
τ_{Slow} (ms)	76.2±8.0	105±20.5	68.3±6.9	60.9±3.7	93.2±10.1	138.4±32.4

^{T} Kv4.2g significantly different from Kv4.2g+SUMO+Ubc9 (t-test, p=0.014)
^{TT} Kv4.2g K437R significantly different from Kv4.2g K437R+SUMO+Ubc9 (t-test, p=0.049)
^{TTT} Significantly different from Kv4.2g K579R (One-way ANOVA with Tukey's post-hoc, F(2,35)=9.75, p=0.0004)
^{NS} Significant differences produced by enhanced SUMOylation previously observed in the Kv4.2g stable line are not observed when Kv4.2g is transiently expressed (V_{50} inactivation, t-test p=0.48; τ_{Fast}, t-test p=0.19)

3 CHAPTER 2: SUMOYLATION OF THE KV4.2 TERNARY COMPLEX INCREASES SURFACE EXPRESSION AND CURRENT AMPLITUDE BY REDUCING INTERNALIZATION

In review, Journal of Biological Chemistry: **Welch, M. A.**, Jansen, L-A. R., & Baro, D. J. (2021). SUMOylation of the Kv4.2 ternary complex increases surface expression and current amplitude by reducing internalization.

Contribution Disclosure: Authors M. Welch and D. Baro were responsible for the conception and design of the work presented. All authors contributed to acquiring and/or analyzing the data. Authors M. Welch and D. Baro drafted the manuscript, and all authors were involved in revising the manuscript.

3.1 Abstract

Kv4 α-subunits exist as ternary complexes with potassium channel interacting protein (KChIP) and dipeptidyl peptidase-like protein (DPLP), and multiple ancillary proteins also interact with the α-subunits throughout the channel's lifetime. How interactions within the Kv4 macromolecular complex are modulated is poorly understood. Small ubiquitin-like modifier (SUMO) is a 11kD peptide post-translationally added to lysine (K) residues to regulate protein-protein interactions. SUMO is a dynamic modification, and it could be the case that SUMOylation modulates interactions within the Kv4.2 macromolecular complex to control IA. In this manuscript, we begin testing this hypothesis by examining the effect of SUMOylation when a Kv4.2 GFP (Kv4.2g) fusion protein was co-expressed with KChIP2a and DPP10 in human embryonic kidney cells (HEK). Increasing SUMOylation in HEK cells expressing Kv4.2g+KChIP2a+DPP10 produced a significant ~35-70% increase in IA maximum conductance (Gmax) and a significant ~30-50% increase in Kv4.2g surface expression that was accompanied by a 65% reduction in ternary complex internalization. Blocking clathrin-mediated endocytosis in HEK cells expressing the Kv4.2g ternary complex mimicked and occluded the effect of SUMO on IA Gmax, however the amount of adaptor protein 2 (AP2) associated with Kv4.2g channels was not SUMO dependent. We previously generated Kv4.2g constructs containing K to arginine (R) substitutions at two evolutionarily conserved SUMOylation sites, K437 and K579. Experiments in HEK cells overexpressing Kv4.2g mutant ternary complexes revealed SUMOylation of Kv4.2g K579 was responsible for the increase in IA Gmax and surface expression and the reduction in internalization, while SUMOylation of Kv4.2g K437 had no effect on any parameter tested. Interestingly, we also found that the effect of Kv4.2g SUMOylation depended on the available interactome.

3.2 Introduction

The transient potassium current (IA) is a rapidly inactivating subthreshold current mediated by Kv1.4, Kv3.3-4 and Kv4.1-3 α -subunits (Gutman et al., 2005). These α -subunits exist in macromolecular complexes. Kv4 channels play a key role in shaping neuronal excitability, action potential firing rate, synaptic integration and synaptic plasticity; and, dysregulation of Kv4 channels is associated with neurological disorders, including epilepsy, Alzheimer's disease, major depressive disorder, Huntington's disease and chronic pain (Aceto et al., 2020; Carrillo-Reid et al., 2019; Hall et al., 2015; Kanda et al., 2021; K. R. Kim et al., 2021; Kohling & Wolfart, 2016; Noh, Pak, Choi, Yang, & Yang, 2019; Scala et al., 2015; C. Wang et al., 2021; Zemel et al., 2018).

Kv4 channels form a ternary complex with potassium channel interacting protein (KChIP1-4) and dipeptidyl peptidase-like protein (DPLP; DPP6 and 10). The ternary complex is the fundamental unit that reproduces native IA in heterologous expression systems (Amarillo et al., 2008; Jerng et al., 2005; Jerng & Pfaffinger, 2012). The Kv4 ternary complex is anchored in distinct, dynamic macromolecular complexes at different stages in the channel's lifespan. Tandem affinity purification of exogenously expressed Kv4.2 followed by mass spectrometry identified over 120 endogenous HEK cell proteins that associate with the α subunit (J. H. Hu et al., 2020).

Dynamic interactions with several proteins contribute to Kv4 trafficking and function at the plasma membrane (Jerng & Pfaffinger, 2014). Kv4 channels are translated and inserted in the ER membrane, and ER-located J proteins recruit Hsp70 to properly fold and stabilize Kv4 monomers and facilitate tetrameric assembly of Kv4 channels (Li et al., 2017). Cytosolic KChIPs interact with the cytosolic N- and C-termini of Kv4α subunits at the ER, which facilitates

tetrameric assembly and masks a hydrophobic stretch of amino acids at the Kv4 N-terminus, allowing Kv4 to efficiently traffic to the plasma membrane (Kunjilwar, Strang, DeRubeis, & Pfaffinger, 2004; Shibata et al., 2003). Kv4-KChIP2 containing vesicles traffic through a conventional ER-Golgi pathway in ventricular myocytes, while Kv4-KChIP1 traffics in non-COPII containing vesicles in HeLa cells, and different combinations of SNAREs and GTPases likely interact with the Kv4 complex depending on the route taken (Flowerdew & Burgoyne, 2009; Hasdemir et al., 2005; J. H. Hu et al., 2020; B. L. Tang, 2020; T. Wang et al., 2012). The transmembrane domain and the short intracellular N-terminus of DPLP interacts with Kv4 S1 and S2 to promote exit from the ER (Cotella et al., 2012; Lin et al., 2014; Ren et al., 2005). Both DPLPs and KChIPs modulate channel gating at the plasma membrane (An et al., 2000; Bahring et al., 2001; Foeger et al., 2010; Jerng et al., 2004; Nadal et al., 2003; Shibata et al., 2003). A conserved di-leucine motif on the Kv4.2 C-terminus is necessary and sufficient to traffic Kv4.2 channels to the dendrites (Rivera et al., 2003), and kinesin isoform Kif17 interacts with the Kv4.2 C-terminus downstream of the di-leucine motif to facilitate this transport (Chu et al., 2006). The Kv4.2 C-terminus also interacts with the actin binding protein, filamin, and this interaction results in a robust increase in IA current density (Petrecca et al., 2000). Phosphorylation controls Kv4 surface expression, and in hippocampal neurons, the scaffolding protein AKAP79/150 anchors PKA and calcineurin in the Kv4 macromolecular complex (Lin et al., 2011). The Kv4 macromolecular complex can include other ion channels, such as Cav3.1-3 (D. Anderson, Mehaffey, et al., 2010; D. Anderson, Rehak, et al., 2010).

Little is known about what modulates these dynamic protein-protein interactions with and within the ternary complex. Previous work has shown calcium binding to KChIP stabilizes its binding to Kv4 (Morohashi et al., 2002; C. Seifert et al., 2020). Ceroid lipofuscinosis neuronal 3

(CLN3) protein interacts with KChIP3 and disrupts the Kv4.2-KChIP3 interaction (C. Seifert et al., 2020). N-glycosylation of DPP10 is essential for its interaction with Kv4.3 (Cotella et al., 2012). Prolyl cis/trans isomerase Pin1 disrupts the interaction between Kv4.2 and DPP6 (J. H. Hu et al., 2020). Expanding our knowledge of the mechanisms regulating protein-protein interactions within the Kv4 macromolecular complexes is key for understanding how IA is dynamically adapted.

Post-translational SUMOylation regulates protein-protein interactions. Small ubiquitin like modifiers (SUMO1-5) are 11kD peptides that can be conjugated to lysine residues on target proteins (Celen & Sahin, 2020; H. M. Chang & Yeh, 2020; Flotho & Melchior, 2013; Henley et al., 2021). SUMOylation is a dynamic modification, and the SUMOylation status of a target is determined by the opposing activities of the sole SUMO conjugating enzyme, Ubc9, and proteases that cleave SUMO from a target (Desterro et al., 1997). There are several non-mutually exclusive consequences of protein SUMOylation. 1.) SUMOylation can promote protein-protein interactions usually by an association between the SUMO moiety and a specific SUMO binding domain on the interacting partner (Psakhye & Jentsch, 2012; A. Seifert et al., 2015). 2.) SUMOylation can block protein-protein interactions usually through steric hindrance (Dustrude et al., 2016). 3.) SUMOylation can compete with another post-translational modification such as methylation, acetylation, and ubiquitination for the same K reside on a target protein (D. D. Anderson et al., 2012; W. Wang et al., 2014). 4.) SUMO can interact with phosphoinositols concentrated in the trans-Golgi (PI(3)P) and plasma membrane ($PI(3,4,5)P_3$) (Kunadt et al., 2015). In this work, we begin to test the hypothesis that post-translational SUMOylation modulates interactions within the Kv4.2 macromolecular complex to tune IA.

Kv4.2 channels can be SUMOylated. Increasing baseline SUMOylation in HEK cells expressing a mouse Kv4.2 GFP fusion protein (Kv4.2g) increased channel SUMOylation at two evolutionarily conserved K residues, K437 and K579, to produce a significant 22-50% decrease in IA maximal conductance (Gmax) and a significant 70-95% increase in surface expression (Welch, Forster, Atlas, & Baro, 2019). SUMOylation at K437 increased surface expression of electrically silent channels while SUMOylation at K579 mediated the significant decrease in IA Gmax without altering surface expression. In the previous study, Kv4.2g was expressed alone (Welch et al., 2019). This study examines the effect of SUMOylation on IA mediated by the Kv4.2 ternary complex.

3.3 Materials and Methods

3.3.1 Chemical and antibodies

All chemicals were purchased from Sigma unless stated otherwise. All antibodies are described in Table 3.1.

3.3.2 Cell culture

Human Embryonic Kidney 293 (HEK) cells were obtained from American Type Culture Collection (ATCC) and were cultured at 37°C and 5% CO_2 in Eagle's Minimum Essential Medium (MEM) (Corning, cat no. 10009CV) supplemented with 10% fetal bovine serum (ATCC, cat no. 30-2020) and 1% penicillin/streptomycin (Sigma, cat no. P4333).

3.3.3 Plasmids

A previously described plasmid containing the mouse Kv4.2 channel with GFP fused to the c-terminus (Kv4.2g) was provided by Dax Hoffman. PCR-based site directed mutagenesis was performed as previously described to generate two mutations in the Kv4.2g plasmid, K437R and K579R (Welch et al., 2019). A plasmid containing SUMO-2 (Kamitani et al., 1998) was

provided by Edward Yeh (Addgene plasmid #17360). A plasmid containing Ubc9 (Yasugi & Howley, 1996) was a gift from Peter Howley (Addgene plasmid #14438). pCMV6-KChIP2a (NM_145703) was purchased from Origene Technologies. PCR was used to add SalI and XhoI restriction sites at the beginning and end of the KChIP2a open reading frame (ORF) using the primers: SalI_KChIP2aFor: ATATATGTCGACGATGCGGGGCCAAGGCCGAAAGG and XhoI_KChIP2aRev: GAGTTTCTGCTCGAGCGGCCGCGTACGCGTCTAGATGAC. The KChIP2a ORF was subcloned into pCMV-HA-N vector (Clontech) at the SalI and XhoI restriction sites to generate the vector pCMV-HA-N-KChIP2a. pCMV3-DPP10 (NM_199021) was purchased from Sino Biological. PCR was used to add SalI and XhoI restriction sites at the beginning and end of the DPP10 ORF using the primers: SalI_DPP10For: ATATATGTCGACGATGACAGCCATGAAGC and XhoI_DPP10Rev: ATATATCTCGAGTTATTCATCTTCTTCT. The DPP10 ORF was subcloned into pCMV-HA-N vector (Clontech) at the SalI and XhoI restriction sites to generate the vector pCMV-HA-N-DPP10. All constructs were sequenced to ensure that PCR did not introduce mutations.

3.3.4 Transfection

HEK cells were transfected using the calcium phosphate transfection method. HEK cells were plated at $1.9X10^6$ cells/plate or $6X10^6$ cells/plate onto 60mm or 100mm plates, respectively, and incubated for 24 hr. 10µg or 25µg of DNA were prepared in 250µl or 440µl TE buffer (10mM Tris-HCl pH 8, 1mM EDTA), and immediately before transfection 30µl or 60µl of 2M $CaCl_2$ followed by 250µl or 500µl 2X HBS (275mM NaCl, 10mM KCl, 12mM dextrose, 1.4mM Na_2HPO_4, 40mM HEPES, pH 7.05-7.1) was added dropwise to the DNA mixture, respectively. The transfection solution was added dropwise to the cells, and the cells were returned to 37°C/5% CO_2 for 4hrs followed by a media change. Equal amounts of each plasmid were used

when co-transfecting multiple plasmids. Transfection efficiency was assessed 48hrs later using fluorescence microscopy and only plates with >80% efficiency were used in experiments.

3.3.5 Western Blot assay

Proteins were resolved on 10% SDS-polyacrylamide gels and transferred for 1hr at 90V to a PVDF membrane (Immobilon-P, cat# IPVH00010) using a wet electroblotting system (BioRad, Mini Trans-Blot cell) and instructions provided by the manufacturer. Membranes were dipped in methanol and dried for 30min. Membranes were blocked in 5% non-fat dry milk in TBS (50mM Tris-HCl pH7.4, 150mM NaCl) for 1hr at room temperature. Membranes were washed 1X with T-TBS (TBS+0.1% Tween20) for 10min. The membrane was incubated with primary antibodies (Table 3.1) in 1% non-fat dry milk in T-TBS overnight at 4°C with shaking. Membranes were washed 3X 5min each with T-TBS. Membranes were incubated with the appropriate alkaline phosphatase conjugated secondary antibodies in 1% non-fat dry milk in T-TBS for 2hr at room temperature. Membranes were washed 3X with T-TBS for 10min each. Alkaline phosphatase substrate was placed on the membrane for 5min. Membranes were exposed to film (Research Products International) and chemiluminescent signals were visualized with a Kodak X-Omat 2000A imager. The optical density (OD) of a protein(s) of interest was measured using ImageJ software, as previously described (Parker et al., 2016; Welch et al., 2019).

In some cases, membranes were stripped and re-probed. In these cases, membranes were washed 2X in mild stripping buffer (20mM glycine, 0.1%SDS, 1% Tween 20, 50mM KCl, 20mM Magnesium acetate, pH 2.2) for 10min each. Membranes were then washed, 2X with PBS for 10min each, and 2X with T-TBS for 5min each. To ensure that the chemiluminescent signal was gone, alkaline phosphatase substrate was added to the membrane for 5min and the membrane was exposed to film for 10min. To account for technical variabilities such as

differences in exposure time or loss of protein due to stripping, 0.1µg or 0.2µg BSA protein was always included in one lane on every gel and a primary antibody against BSA was always included for detection. The signal for the protein of interest on the pre- and post-stripped blot was always normalized by the BSA signal on the pre- and post-stripped blot, respectively.

In some cases, SYPRO Ruby Protein Blot Stain (BioRad) was used to assess total protein. Whole cell lysates (10µg) were resolved with PAGE and transferred to a PVDF membrane, as described above. Dried PVDF membranes were incubated protein side face-down in 7% acetic acid/10% methanol for 15min and then washed 4X, 5min each with dH_2O. Membranes were placed protein side face-down in SYPRO Ruby Protein Blot Stain for 15min and then washed 3X, 1min each with dH_2O. Stained protein was visualized using an Omega Ultra Lum 10gD imaging system using blue light transillumination. The optical density of the total protein signal was measured using ImageJ.

3.3.6 Electrophysiology

For whole-cell patch clamp experiments, HEK cells were transfected with the appropriate DNA and incubated for 24hr. Cells were then passaged on to 100mm coverslips coated with Poly-L-Lysine (50µg/ml) and incubated. The next day, coverslips were transferred to a recording chamber and superfused continuously with extracellular saline (in mM: 141 NaCl, 4.7 KCl, 1.2 $MgCl_2$, 1.8 $CaCl_2$, 10 glucose, 10 HEPES, pH 7.4, osmolarity ~300). Cells were visualized on an IX70 Olympus microscope, and transfected cells were identified with fluorescence microscopy. Fire polished borosilicate glass pipettes having a resistance of ~2MΩ were filled with intracellular saline (in mM: 140 KCl, 1 $MgCl_2$, 1 $CaCl_2$, 10 EGTA, 2 MgATP, 10 HEPES, pH 7.2, osmolarity ~290) and connected to a MultiClamp 700A amplifier (Axon Instruments). After forming a GΩ seal, a slight negative pressure was used to break through the membrane, and only

cells that maintained >700MΩ seal following rupture and had less than 15MΩ access resistance were examined. Fast and slow capacitance and series resistance were compensated. IA was elicited with a series of 1sec pre-pulses to -90mV each followed by a 250ms test-pulse ranging from -50 to +50mV in 10mV increments. The leak current from a pre-pulse to -30mV was subtracted offline. Current (I) was converted to conductance (G) using the equation G=I/Vm-Vr, with Vm being the membrane potential and Vr being the reversal potential for potassium, -86mV. The maximal conductance (Gmax), the voltage of half-activation (V50 act), and the slope of the activation curve were determined by plotting conductance against voltage and fitting the data with a first-order Boltzmann equation. The fast and slow time constants of inactivation (τfast and τslow) were determined by fitting the decay current for the +50mV test-pulse with a two-term exponential equation. The voltage of half-inactivation (V50 inact) was measured with a series of 1.4sec pre-pulses from -110 to -30mV in 10mV increments, each followed by a 200ms test pulse to +20mV. Current was plotted against voltage and the data were fitted with a first-order Boltzmann equation to determine V50 inact and the slope of the inactivation curve.

In some experiments, clathrin-mediated endocytosis was blocked with Pitstop2 (abcam, ab120687). Cells were treated with 20µM Pitstop2 for 20min at 37°C/5%CO_2 before transferring the coverslip to the recording chamber and Pitstop2 (20µM) was included in the superfusate. Pitstop2 was prepared as a 30mM stock in DMSO, where the working concentration of DMSO was 0.7%. Application of 0.7% DMSO for 20min at 37°C/5%CO_2 prior to transferring the cells to the recording chamber and inclusion of 0.7% DMSO in the superfusate did not affect IA Gmax (n=3; Gmax, control: 87.44nS vs. DMSO: 90.55nS). In experiments using Pitstop2, enhanced SUMOylation was not achieved by co-transfecting SUMO and Ubc9; rather, SUMO-2 and/or SUMO-3 peptide (4.2µM, Boston Biochem, #K-700) was dissolved in the intracellular

saline in the patch pipette and delivered to the cell after whole-cell configuration was achieved. SUMO peptides were used at a concentration previously shown regulate the amplitude of kainate evoked current in HEK cells expressing GluK2 (Konopacki et al., 2011).

3.3.7 Immunoprecipitation

For experiments to measure steady-state Kv4.2g levels, transfected HEK cells on 100mm culture dishes were washed 1X with ice-cold PBS and lysed in 1ml RIPA buffer (1% NP40, 50mM Tris-HCl pH7.4, 150mM NaCl, 0.1% SDS, 0.5% DOC, 2mM EDTA) supplemented with 20mM N-Ethylmaleimide (NEM) and protease inhibitor cocktail (1:100, Sigma cat no. P8340) on ice for 30min. Plates were scraped, and lysates were transferred to a 1.5ml centrifuge tube. Cell debris was pelleted by centrifugation at 14,000rpm for 15min. Bicinchoninic acid (BCA) assay was performed to determine protein concentration, and 1mg of protein was added to 2µl anti-GFP antibody (Table 3.1). The lysate was incubated with the antibody at 4°C overnight with shaking. IP was carried out using the Pierce Classic Magnetic IP/Co-IP kit (ThermoFisher cat no. 88804) according to manufacturer's instructions. IPs were eluted in 100µl of elution buffer.

For experiments quantifying the amount of adaptin α that co-immunoprecipitated (co-IP) with Kv4.2g, transfected HEK cells on 60mm culture plates were washed 1X PBS. Cells were then lysed for 30min on ice with IP/lysis buffer supplied with the Pierce Classic Magnetic IP/Co-IP kit and supplemented with 20mM NEM and protease inhibitor cocktail (1:100). Cells were scraped, transferred to a 1.5ml centrifuge tube, and cell debris was pelleted for 10min at 14,000rpm. Protein concentration was determined with BCA, and 0.5mg of protein was added to 1µl anti-GPF (Table 3.1). The lysate was incubated with the antibody at 4°C with shaking overnight, and IP was performed with the Pierce Magnetic IP/Co-IP kit. IP was eluted in 50µl elution buffer.

3.3.8 Biotinylation of cell surface proteins

NeutrAvidin resin (300µL) (ThermoFisher cat no. 29201) was placed in a Pierce Snap Cap Spin Column (ThermoFisher cat no. 69725) and was equilibrated by washing 3X with PBS. Transfected HEK cells were washed 2X with PBS supplemented with 1.5mM $MgCl_2$ and 0.2mM $CaCl_2$ (PBS-CM) and incubated with EZ-Link Sulfo-NHS-SS-Biotin (1mg/ml) (ThermoFisher cat no. 21331) in PBS-CM for 30min at 4°C. Unreacted biotin was quenched with PBS-CM +100mM glycine at 4°C for 15min, and cells were lysed for 30min on ice in 500µL RIPA buffer supplemented with protease inhibitor cocktail. Plates were scraped. The lysate was transferred to a clean 1.5ml centrifuge tube. Cell debris was pelleted by centrifugation for 10min at 14,000rpm, and the supernatant was added to the washed NeutrAvidin resin and incubated for 2hr at 4°C with shaking. The column was placed in a clean 1.5ml microcentrifuge tube and centrifuged for 2min at 1000xg. The flow-through containing the unbiotinylated proteins was considered to be the intracellular fraction. The resin was washed 3X with Wash Buffer 1 (1% NP40, 1% SDS, 1X PBS) and 3X with Wash Buffer 2 (0.1% NP40, 0.5M NaCl, 1X PBS). Biotinylated, cell surface proteins were eluted from the NeutrAvidin resin by incubating with 75µl of 1X SDS buffer (50mM Tris HCl pH 6.8, 2% SDS, 10% glycerol, 0.1% Bromophenol Blue, 100mM DTT) with gentle shaking for 1hr at room temperature followed by centrifugation for 2min at 1000xg. Intracellular and extracellular fractions along with 0.2µg of BSA were used in western blot assays. Blots were cut horizontally at ~50kD. The lower portion of the blot was incubated with an antibody against actin. The upper portion of the blot was incubated with antibodies that recognized BSA and GFP. After measuring the OD for BSA and GFP, the blot was stripped and incubated with antibodies that recognize BSA and the Na^+/K^+-ATPase, whose surface expression did not change when SUMOylation was increased above baseline in HEK cells (Parker et al.,

2016). The ODs of the extracellular GFP and Na^+/K^+-ATPase signals were normalized to their respective BSA signals, and then the normalized GFP signal was divided by the normalized Na^+/K^+-ATPase signal to determine Kv4.2 surface expression.

3.3.9 Internalization assay

Three plates of cells were used for each internalization experiment. One plate was used to measure internalization, one was used to measure total surface expression, and one was used to measure stripping efficiency. Cells were biotinylated and quenched as described above. The remainder of the experiment varied according to the plate.

Cells on the internalization plate were washed 1X in MEM. Fresh MEM was added, and the plate was incubated for 2.5hr at 18°C to allow for internalization with reduced degradation (Le, Yap, & Stow, 1999). Cells were then washed 1X with NT buffer (150mM NaCl, 1mM EDTA, 0.2% BSA, 20mM Tris pH8.6). Surface-bound biotin was removed by incubating with 100mM sodium 2-mercaptoethanesulfonate (MESNA) in NT buffer for 30min at 4°C. Cells were washed 3X in NT buffer, 3X in PBS-CM and lysed with 500µL RIPA buffer supplemented with protease inhibitor cocktail.

Immediately after the quenching step, cells on the strip plate and the total plate were washed 1X with NT buffer. Cells on the strip plate were incubated with MESNA in NT buffer for 30min at 4°C to remove surface bound biotin. Cells on the total plate were incubated with NT buffer for 30 min at 4°C. Cells on the strip plate and the total plate were washed 3X in NT buffer, 3X in PBS, and lysed with 500µL RIPA buffer supplemented with protease inhibitor cocktail.

Protein concentration for each of the 3 lysates was determined with a BCA. For each lysate, 450µg of protein was added to a Pierce Snap Cap Spin Column containing washed

NeutrAvidin resin (300µL) and incubated at 4°C overnight, shaking. The next day, the columns were placed in clean 1.5ml microcentrifuge tubes, and the flowthroughs containing the unbiotinylated proteins were collected by centrifuging 2min 1000xg. The resin was washed 3X with Wash Buffer 1 and 3X with Wash Buffer 2. Biotinylated proteins were eluted from the resin with 75µl 1X SDS buffer by shaking for 1hr at room temperature. Biotinylated fractions were collected by centrifuging at 1000xg for 2min.

The unbiotinylated and biotinylated fractions from the three plates were resolved with PAGE. Blots were probed with anti-GFP. The percentage of Kv4.2g internalized was calculated as the optical density (OD) of the biotinylated Kv4.2g signal from the internalized plate divided by the OD of the biotinylated Kv4.2g signal from the total surface expression plate multiplied by 100. The stripping efficiency was calculated as the OD of the biotinylated Kv4.2g signal from the strip plate divided by the OD of the biotinylated Kv4.2g signal from the total surface expression plate, subtracted from 1 and multiplied by 100. Only data from experiments where the stripping efficiency was >90% were included.

3.3.10 Statistical analysis

GraphPad PRISM 9 software was used for statistical analysis of data. Normality and homogeneity of variance was assessed for each data set. Data points > 2 standard deviations from the mean were considered outliers and were excluded. In all cases, the significance threshold was set at $p<0.05$.

3.4 Results

3.4.1 SUMOylation of Kv4.2g at K579 increases IA Gmax in the presence of auxiliary subunits, KChIP2a and DPP10

The effect of Kv4.2g SUMOylation may be context-dependent. To investigate if/how SUMO modulates Kv4.2g in ternary complexes, we transiently transfected HEK cells with 3 plasmids encoding Kv4.2g, KChIP2a, and DPP10. SUMOylation of target proteins can be increased in cell culture when SUMO and Ubc9 are overexpressed (Dai et al., 2009; Parker et al., 2016; Welch et al., 2019), and SUMOylation was or was not enhanced in this experiment by co-expressing two additional plasmids encoding SUMO and Ubc9. Whole-cell patch-clamp recordings were performed to characterize the currents in the two treatment groups (Figure 3.1A). There was a significant 35% increase in IA maximal conductance (Gmax) when SUMO and Ubc9 were co-expressed with the Kv4.2g ternary complex relative to cells only expressing the Kv4.2g ternary complex (Figure 3.1B). SUMO and Ubc9 co-expression had no significant effect on the voltage of half-activation (V50 act), the voltage of half-inactivation (V50 inact), the slopes of the activation and inactivation curves, or the fast ($\boldsymbol{\tau}$ fast) and slow ($\boldsymbol{\tau}$ slow) time constants of inactivation (Figure 3.1C-E).

The increase in IA Gmax could be due to SUMOylation of Kv4.2g, KChIP2a or DPP10. Kv4.2g is known to be SUMOylated at K437 and K579 (Welch et al., 2019). We asked whether SUMOylation of Kv4.2g K437 and/or K579 mediated the significant increase in IA Gmax by repeating the patch-clamp experiments with three Kv4.2g mutants: K437R, K579R and K437R+K579R (Figure 3.2). Incorporating the Kv4.2g double mutant into the ternary complex abolished the SUMOylation-induced increase in IA Gmax, suggesting that SUMOylation of Kv4.2g was necessary for the enhancement. Augmenting SUMOylation in HEK cells expressing

Kv4.2g K437R still produced a significant increase in IA Gmax, but not when the ternary complex contained Kv4.2g K579R. These data suggested that SUMOylation of Kv4.2g K579 produced a significant increase in the current mediated by the ternary complex.

3.4.2 SUMOylation of Kv4.2g K579 does not enhance Kv4.2 protein expression

SUMOylation can increase IA Gmax by increasing protein expression. We next asked whether SUMOylation regulated steady-state Kv4.2g protein levels. Kv4.2g channels were immunoprecipitated from HEK cells transiently transfected with Kv4.2g + KChIP2a + DPP10 with or without SUMO + Ubc9. The immunoprecipitates (IPs) were used in western blot experiments that employed anti-GFP to visualize Kv4.2g (Figure 3.3A). Total protein in the whole cell lysate was estimated by staining with SYPRO Ruby, as described in Materials and Methods (Figure 3.3B). The steady-state Kv4.2g was defined as the OD for the anti-GFP signal divided by the OD for SYPRO Ruby stain (Figure 3.3C). There was no significant difference in steady-state levels of Kv4.2g between the two treatment groups (Figure 3.3C). These data indicate that Kv4.2g SUMOylation did not increase protein expression.

3.4.3 SUMOylation of Kv4.2g at K579 increases ternary complex surface expression by reducing internalization

Since SUMOylation did not increase protein expression, we next asked whether the significant increase in IA Gmax was mediated by an increase in Kv4.2g surface expression. To do this, we performed cell surface biotinylation assays on HEK cells expressing the ternary complex with or without SUMO+Ubc9. Surface proteins were biotinylated, cells were lysed, and the extracellular fraction was isolated using NeutrAvidin resin. Proteins that did not bind to the NeutrAvidin resin were considered to be intracellular. Intracellular and extracellular fractions from each treatment group were used in western blot experiments (Figure 3.4A). Blots were cut

horizontally at ~50kD and the upper portion of the blot was probed for Kv4.2g. After obtaining the OD for the Kv4.2g signal, the blot was stripped and re-probed for Na^+K^+-ATPase. The lower portion of the blot was probed for actin to ensure there was no intracellular contamination in the extracellular fraction. Kv4.2g surface expression was defined as the Kv4.2g OD in the extracellular fraction divided by the Na^+K^+-ATPase OD in the extracellular fraction. A plot of the data indicated that Kv4.2g surface expression increased by 30% when SUMOylation was enhanced (Figure 3.4B). This is consistent with the SUMOylation-induced ~35% increase in IA Gmax (Figure 3.1).

The experiment was repeated using the mutants, Kv4.2g K437R (Figure 3.4C-D) or Kv4.2g K579R (Figure 3.4E-F). Enhanced SUMOylation still elicited an increase in surface expression when the ternary complex comprised Kv4.2g K437R (Figure 3.4D) but not Kv4.2g K579R (Figure 3.4F). These data indicated that SUMOylation of the ternary complex at Kv4.2 K579 increased channel surface expression and IA Gmax.

Membrane protein SUMOylation is known to modulate that protein's surface expression by regulating both exocytosis from the Golgi to the plasma membrane (Zhou et al., 2018) and internalization from the plasma membrane (Dustrude et al., 2016; Ma et al., 2016). We first tested if SUMOylation reduced internalization. Current data suggest that Kv4.2 undergoes clathrin-mediated endocytosis (J. H. Hu et al., 2020; J. Kim et al., 2007; Nestor & Hoffman, 2012). We therefore performed patch clamp recordings to measure IA when clathrin-mediated endocytosis was inhibited with Pitstop2, a cell-permeable clathrin inhibitor. Application of Pitstop2 (20µm, 20min) to HEK cells expressing Kv4.2g + KChIP2a + DPP10 produced a significant 57% increase in IA Gmax compared to control (Figure 3.5) (Table 3.2). To test if Pitstop2 mimicked and occluded the effects of SUMOylation, SUMO was delivered to HEK

cells expressing the ternary complex by including the peptide in the recording pipette (4.2μM). Pitstop2 was or was not pre-applied for 20min followed by whole-cell patch clamp. Treatment with SUMO or Pitstop2 or SUMO+Pitstop2 produced a similar increase in IA Gmax relative to untreated controls; however, IA Gmax was not significantly different between these three treatment groups (Figure 3.5) (Table 3.2). Thus, Pitstop2 mimicked and occluded the effect of SUMO. Because the effects of SUMO and Pitstop were not additive, these data support the hypothesis that SUMOylation increased channel surface expression and IA Gmax largely by reducing internalization, rather than increasing exocytosis. It should be noted that the level of internalization depends upon the rates of two opposing processes: endocytosis and recycling from the endosome back to the plasma membrane. Since recycling is downstream of endocytosis, and Pitstop2 blocks endocytosis, these data do not indicate if SUMO regulates endocytosis and/or recycling.

In order to further test whether SUMOylation of Kv4.2 at K579 was necessary to reduce ternary complex internalization, Kv4.2 internalization was analyzed with a biotin assay. The assay was performed on two treatment groups: HEK cells expressing the Kv4.2g ternary complex or the Kv4.2g ternary complex + SUMO + Ubc9. Three plates of cells were used for one experiment in one treatment group. The 1st plate was used to measure internalized channels. Cells were treated with biotin on ice to label surface proteins and prevent endocytosis. Labeled cells were then placed at 18°C for 2.5hr to allow for internalization with reduced degradation (Le et al., 1999). Upon completion of the incubation, cells were treated with MESNA to cleave biotin from surface proteins. Biotinylated Kv4.2g channels that were internalized during the 18°C internalization step were protected from cleavage by MESNA, and following cell lysis internalized biotinylated proteins were isolated using NeutrAvidin resin. The 2nd plate was used

to measure total Kv4.2g surface expression. Immediately following biotinylation on ice, cells on this plate were lysed and biotinylated proteins were isolated using NeutrAvidin resin. Since there was no incubation at an elevated temperature, biotinylated proteins should largely represent surface expression. The 3rd plate served as a control to determine stripping efficiency. Immediately following biotinylation on ice, cells on this plate were treated with MESNA to remove all biotin from surface expressed proteins. NeutrAvidin resin was once again used to isolate any remaining biotinylated proteins. The unbiotinylated and biotinylated fractions from the three plates were resolved with PAGE followed by western blot experiments using anti-GFP to visualize Kv4.2g (Figure 3.6A). MESNA stripping efficiency was determined by dividing the OD for the biotinylated Kv4.2g signal on the stripped plate (3rd plate) by the OD for the biotinylated Kv4.2g signal on the total plate (2nd plate), subtracting from 1 and multiplying by 100. An experiment was not used if the stripping efficiency was < 90% (11% of experiments). If stripping efficiency was >90%, then the percentage of internalized Kv4.2g channels was determined by dividing the OD for the biotinylated Kv4.2g signal on the internalization plate (1st plate) by the OD for the biotinylated Kv4.2g signal on the total plate (2nd plate) and multiplying by 100. Plotting the data for both treatment groups showed that enhancing SUMOylation significantly decreased Kv4.2g internalization by 64% relative to control (Figure 3.6B). In order to determine if SUMOylation of Kv4.2g K579 was necessary for this effect, these experiments were repeated using the Kv4.2g K579R mutant (Figure 3.6C). Plotting the data for the two treatment groups showed that enhancing SUMOylation had no significant effect on internalization when K579 was mutated to R (Figure 3.6D). In addition, the mutation alone significantly reduced internalization by ~20% (% internalized: TC, 33.3%±1.61 vs. TC K579R, 26.4%±1.95; p=0.037, t-test). Together these data suggest that K579 influences Kv4.2g

interactions with a protein(s) that regulates/mediates internalization, and post-translationally decorating K579 with SUMO significantly reduces internalization.

3.4.4 The effect of K579 SUMOylation on Kv4.2g internalization is downstream of cargo recruitment and vesicle formation

Internalization of Kv4.2g in the previous experiment was largely determined by the rates of two opposing processes: endocytosis and recycling of the endocytosed channel back to the plasma membrane. Note that degradation during the 2.5hr period should be greatly diminished. Current evidence suggests that Kv4.2 channels undergo clathrin-mediated endocytosis (J. H. Hu et al., 2020; J. Kim et al., 2007; Nestor & Hoffman, 2012). Adaptor protein 2 complex (AP2) is the major clathrin adaptor that recruits cargo and participates in vesicle formation (Mettlen, Chen, Srinivasan, Danuser, & Schmid, 2018). To begin to test if Kv4.2 K579 SUMOylation reduced internalization by inhibiting endocytosis, we examined whether or not SUMOylation altered the interaction between Kv4.2g and AP2. Standard IP experiments with an antibody against GFP were performed on HEK cells co-expressing Kv4.2g + KChIP2a + DPP10 with and without SUMO+Ubc9. IP products were resolved with PAGE and western blots were probed with an antibody against the α-subunit of AP2, α adaptin, and the blot was stripped and re-probed for Kv4.2g (Figure 3.7A). The OD for α adaptin was divided by the OD for Kv4.2g to determine the amount of α adaptin that associated with Kv4.2g. Plotting the data for the two treatment groups showed that SUMOylation did not significantly alter the amount of α adaptin associated with Kv4.2g (Figure 3.7B). Thus, the effect of K579 SUMOylation on Kv4.2g internalization must be downstream of cargo recruitment into clathrin-coated pits.

3.4.5 The effect of Kv4.2 SUMOylation is context-dependent

The effect of Kv4.2 SUMOylation varies depending upon whether it is heterologously expressed alone or co-expressed with KChIP2a and DPP10 in HEK cells. Enhanced SUMOylation elicited a decrease vs. increase in IA Gmax in HEK cells that expressed Kv4.2g alone vs. Kv4.2g + KChIP2a + DPP10, respectively (Figure 3.8A). Enhancing SUMOylation also increased Kv4.2g surface expression to different extents when Kv4.2g was expressed alone or co-expressed with auxiliary subunits (Figure 3.8B). We ascertained the specific effect of SUMOylation at K437 and K579 under each condition.

SUMOylation of K437 had no effect on IA Gmax under either condition, i.e., SUMOylation still produced significant changes in IA Gmax when K437 was mutated to R (compare Figure 3.8C with 3.8A). On the other hand, SUMOylation of K437 enhanced Kv4.2g surface expression when it was expressed alone, but not when it was co-expressed with KChIP2a + DPP10, i.e., the increase in surface expression was blocked by mutating K437 only when Kv4.2g was expressed alone (compare Figure 3.8D vs. 3.8B). Together, these data indicate that SUMOylation of K437 increased the insertion of electrically silent channels/subunits only when the pore-forming α-subunit was expressed alone. It is not clear if K437 can be SUMOylated when Kv4.2g is incorporated into the ternary complex, because mutating K437 did not prevent the SUMOylation induced increase in surface expression (compare Figure 3.8D, right vs. 3.8B, right) or IA Gmax (compare Figure 3.8C, right vs. 3.8A, right) when the α-subunit was co-expressed with KChIP2a and DPP10.

SUMOylation of K579 decreased vs. increased IA Gmax when the α -subunit was expressed alone vs. with the other components of the ternary complex, i.e, when K579 was mutated to R, SUMOylation no longer produced a significant change in IA Gmax under either

condition (compare Figure 3.8E vs. 3.8A). SUMOylation of K579 had no effect on surface expression when the α -subunit was expressed alone, but increased surface expression when Kv4.2g was co-expressed with auxiliary subunits, i.e., when K579 was mutated to R, SUMOylation still produced the significant increase in surface expression when the α -subunit was expressed alone, but not when expressed with ternary complex components (compare Figure 3.8F vs. 3.8B). Together, these data showed that in the absence of auxiliary subunits, K579 SUMOylation decreased IA Gmax without altering surface expression. In contrast, in the presence of KChIP2a and DPP10, K579 SUMOylation increased IA Gmax by reducing internalization (Figures 3.5-3.6). Based on all of these results, we conclude that the effect of Kv4.2 SUMOylation at K437 and K579 is context-dependent.

3.5 Discussion

The biophysical properties of neuronal IA are reproduced in a heterologous system by a ternary complex containing Kv4, KChIP and DPLP subunits (Jerng & Pfaffinger, 2014). It is not clear if all functional channels exist in ternary complexes in native neurons, and how the ternary complex interacts with a larger assemblage of variable accessory subunits and regulator proteins as the channel is assembled, trafficked and modulated in the plasma membrane. Post-translational SUMOylation is likely to play a fundamental role in mediating dynamic interactions within Kv4 macromolecular complexes. This is the first report to examine if/how post-translational SUMOylation modulates the Kv4.2 ternary complex. The current study demonstrated that SUMOylating Kv4.2 K579 reduced internalization and thereby enhanced channel surface expression and IA Gmax. In addition, the effect of SUMOylation depended upon which proteins were available to interact with Kv4.2.

3.5.1 K579 SUMOylation enhances Kv4.2 surface expression by reducing internalization

Increasing SUMOylation of Kv4.2g at K579 in HEK cells expressing Kv4.2g + KChIP2a + DPP10 produced a significant ~35-70% increase in IA Gmax. SUMOylation did not alter steady-state Kv4.2g protein levels but produced a significant ~30-50% increase in surface expression. Modulation of K579 SUMOylation status could be a basis for many of the mechanisms regulating Kv4.2 surface expression in a variety of physiologically relevant models. Different studies report either a decrease or increase in Kv4.2 surface expression following a seizure. In the hippocampus, Kv4.2 surface expression is decreased following kainate-induced status epilepticus (SE) (Joshi et al., 2018; Lugo et al., 2008), while Kv4.2 surface expression is increased following lithium-pilocarpine-induced SE (Joshi et al., 2018). These effects could be mediated by decreasing vs. increasing SUMOylation at K579, respectively. Enhanced excitatory input also regulates Kv4.2 surface expression. Glutamate application to cultured rat cortical or hippocampal neurons results in an increase or decrease in Kv4.2 surface expression, respectively (Lei et al., 2008; Shen et al., 2008). LTP induction or stimulation with AMPA induces Kv4.2 internalization in hippocampal neurons (Hammond et al., 2008; J. Kim et al., 2007). In some of these examples, post-translational phosphorylation is involved in regulating Kv4.2 surface expression (Hammond et al., 2008; Lugo et al., 2008). This is noteworthy because the phosphorylation state of a protein determines its ability to be SUMOylated (Flotho & Melchior, 2013). For example, activation of PKA prevents the SUMOylation-dependent regulation of IA in an invertebrate neuron (Parker et al., 2019). In hippocampal neurons, PKA-dependent phosphorylation of S552 by itself can produce Kv4.2 internalization (Hammond et al., 2008); and preventing K579 SUMOylation should enhance Kv4.2 internalization. These data suggest

that the S552 phosphorylation state may regulate the K579 SUMOylation state, and thereby, ternary complex surface expression.

The surface expression of several membrane proteins is regulated by their SUMOylation state. SUMOylation of HCN2 (Parker et al., 2017), NaV1.7 (Dustrude et al., 2016), mGluR7 (Choi et al., 2016), the dopamine transporter (Cartier et al., 2019), and smoothened (Ma et al., 2016) increased their surface expression, whereas GluR6 SUMOylation decreased its surface expression (Martin, Nishimune, Mellor, & Henley, 2007). In the 3 cases where the mechanism was examined, post-translational SUMOylation increased surface expression by reducing ubiquitination of the membrane protein (Cartier et al., 2019; Dustrude et al., 2016; Ma et al., 2016), either by enhancing the membrane protein's interaction with a de-ubiquitinase (Ma et al., 2016) or by diminishing its interaction with a ubiquitin ligase (Dustrude et al., 2016).

Ubiquitin serves as a trafficking signal recognized by many components of the endocytic and lysosome-targeting machinery (Ferron, Koshti, & Zamponi, 2021; Mettlen et al., 2018). In some cases, multiple ubiquitins on a membrane protein may serve as an endocytic signal, and several endocytic adaptors possess ubiquitin binding domains and recruit ubiquitinated cargo into clathrin-coated pits (Piper, Dikic, & Lukacs, 2014). Thus, decreasing the ubiquitination of a membrane protein can lead to a decrease in its endocytosis. A ubiquitin signal is also used to regulate membrane protein recycling. After endocytosis and vesicle fusion with the early endosome, a membrane protein can either be recycled back to the plasma membrane or it can be recognized by the endosomal ESCRT protein complex and incorporated into vacuoles that remain in the organelle as it matures into the lysosome (Foot, Henshall, & Kumar, 2017; Mettlen et al., 2018). Proteins in the ESCRT system have ubiquitin binding domains that recognize ubiquitin-tagged cargo. Thus, decreasing a membrane protein's ubiquitination can also lead to an

increase in its recycling. To summarize, membrane protein de-ubiquitination generally inhibits internalization by reducing endocytosis and/or increasing recycling.

This study indicated that decorating K579 with SUMO reduced Kv4.2 internalization. The BDM-PUB online prediction tool indicates that Kv4.2 K579 is not a potential site for ubiquitination; and therefore, it is unlikely that K579 is ubiquitinated to produce an endocytic/lysosome sorting signal that may be blocked by competitive SUMOylation (Flotho & Melchior, 2013). However, when exogenously expressed in HEK cells, Kv4.2 interacts with several endogenous de-ubiquitinases (USP9X, USP7, USP24, USP48, USP10, USP10, USP5, USP15), as well as ubiquitin ligases (ITCH, CAND1, UBE3C, UB20, UBE4B, UBE2M) (J. H. Hu et al., 2020). Thus, SUMOylation at K579 could reduce Kv4.2 ubiquitination by enhancing an interaction between Kv4.2 and a de-ubiquitinase and/or by blocking an interaction with a ubiquitin ligase.

Kv4.2 most likely does not require ubiquitination in order to undergo endocytosis. Kv4.2 appears to directly associate with AP2 through conserved motifs. The interface between the α/σ subunits binds cargos with the [D/E](XXX)$_{3\text{-}5}$L[LI] consensus motif (Azarnia Tehran, Lopez-Hernandez, & Maritzen, 2019; Beacham, Partlow, & Hollopeter, 2019), and this motif is present in the C-terminus of Kv4.2 channels (amino acids 475-482). The di-leucine residues in this motif are necessary for Kv4.2 dendritic localization and for activity dependent Kv4.2 internalization (Hammond et al., 2008; Rivera et al., 2003). Kv4.2 also possesses the YXXϕ motif (x is any amino acid and ϕ is an amino acid with a bulky hydrophobic side chain) that directly binds the μ subunit of the AP2 complex (Mettlen et al., 2018). In addition, our data showed that SUMOylation did not change the amount of binding between Kv4.2 and AP2; therefore, the effect of SUMOylation on internalization must be downstream of cargo recruitment into the

vesicle. K579 SUMOylation could potentially reduce Kv4.2g endocytosis by inhibiting vesicle maturation and/or membrane fission, but this seems unlikely. It is more probable that K579 SUMOylation reduces internalization by promoting Kv4.2g recycling, perhaps by reducing Kv4.2g ubiquitination.

3.5.2 The effect of SUMOylation is context-dependent

Given that the role of SUMO is to regulate protein-protein interactions, it is no surprise that the effect of Kv4.2 SUMOylation varied depending upon whether or not it was co-expressed with KChIP2a and DPP10. Kv4.2 surface expression is regulated by SUMOylation of either K579 or K437, depending upon whether Kv4.2 is or is not co-expressed with KChIP2a + DPP10, respectively. When Kv4.2 is expressed alone, SUMOylation of K579 regulates channel gating by blocking an unknown interaction to reduce IA Gmax (Welch et al., 2019). It is possible that SUMOylation of K579 blocks a different protein-protein interaction to increase surface expression when Kv4.2 is in the ternary complex, such as an interaction between Kv4.2 and a ubiquitin ligase.

Other types of post-translational modifications of Kv4.2 also appear to be context-dependent. For example, phosphorylation of Kv4.2 S552 only has an effect when Kv4.2 is co-expressed with KChIP in oocytes (L.A. Schrader, A.E. Anderson, A. Mayne, P.J. Pfaffinger, & J.D. Sweatt, 2002). This may be because S552 phosphorylation regulates K579 SUMOylation, whose effect is context-dependent. Context-dependence may be physiologically relevant as recent work suggests that distinct subpopulations of Kv4 channels may exist, wherein Kv4.2 may be dissociated from other components of the ternary complex (J. H. Hu et al., 2020).

3.5.3 Summary

In sum, the effect of Kv4.2 SUMOylation varies depending on the available interactome. When expressed with ternary complex components in HEK cells, Kv4.2g SUMOylation at K579 reduces channel internalization and increases Kv4.2g surface expression and IA Gmax. Future experiments will examine whether SUMOylation increases Kv4.2g recycling by regulating its ubiquitination status by either blocking the channel's association with a ubiquitin ligase and/or facilitating an interaction with a de-ubiquitinase.

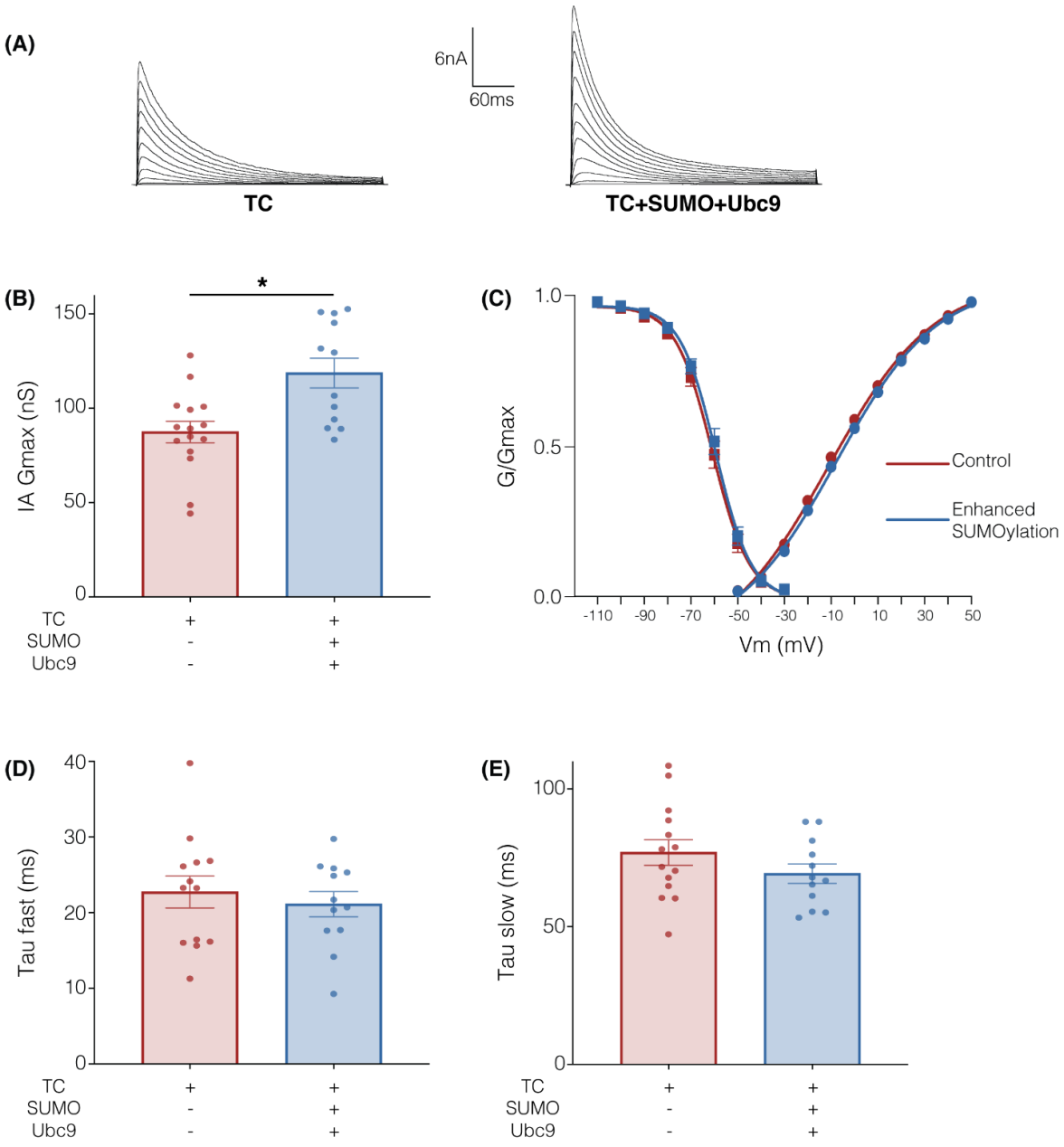

Figure 3.1 Enhanced SUMOylation increases IA Gmax mediated by the ternary complex (TC).

Whole cell-patch clamping was performed on HEK cells transiently transfected with Kv4.2g + KChIP2a + DPP10 in order to measure the current mediated by the TC. SUMOylation was (+) or was not (-) enhanced by co-expressing SUMO + Ubc9. **(A)** Representative current traces for each treatment group. **(B)** Plots of mean±SEM IA Gmax. Each dot represents one cell from ≥3 transfections. Asterisks indicate significant differences. TC: control, 87.4nS ±5.7 vs SUMO+Ubc9, 118.7nS ±7.9, t-test p=0.003. **(C)** Activation (circle) and steady-state inactivation (square) curves. The points on the curve represent the mean±SEM for the cells shown in panel (B). Plots of the mean±SEM fast **(D)** and slow **(E)** time constants of inactivation.

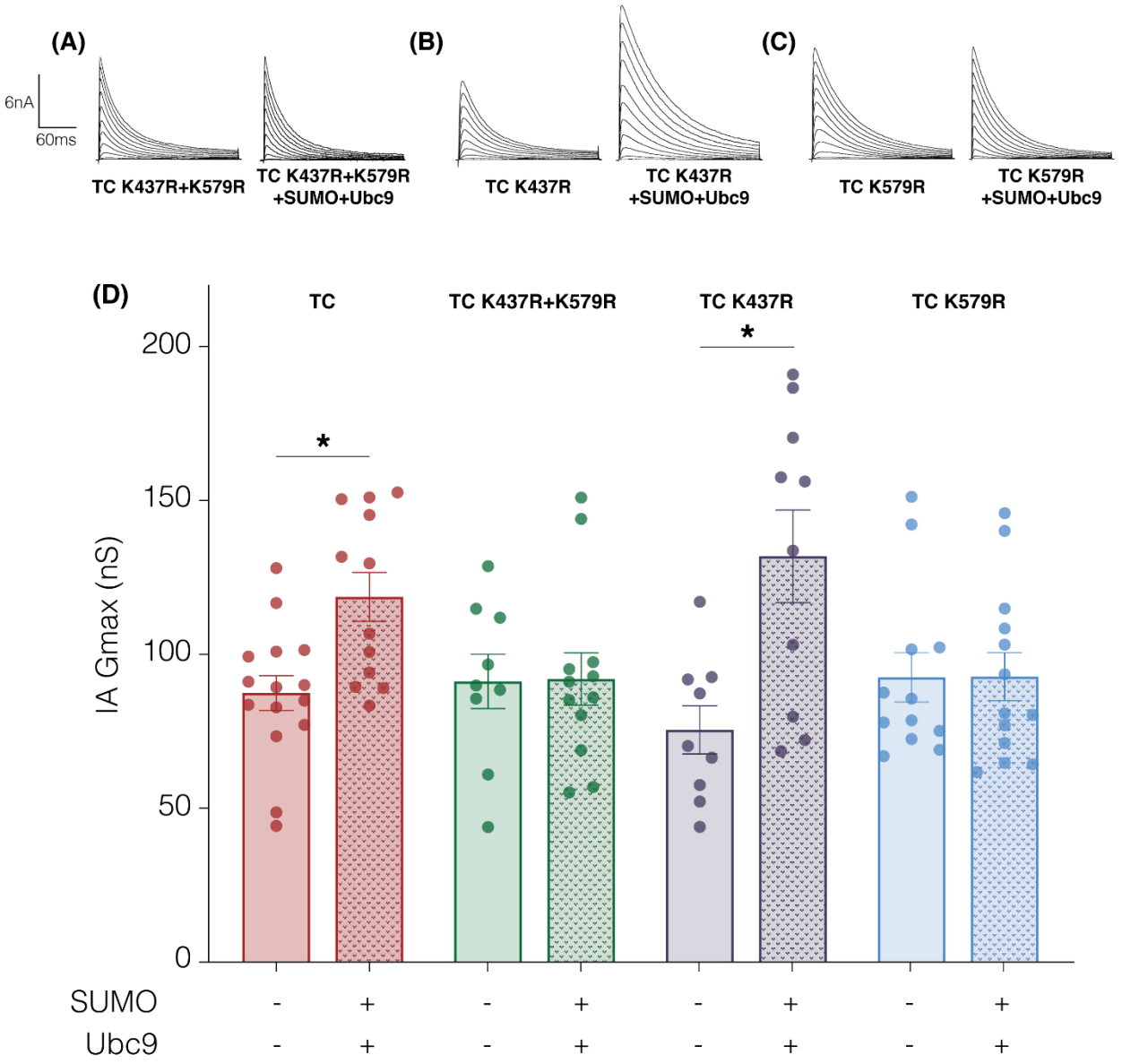

Figure 3.2 SUMOylation of Kv4.2g at K579 increases IA Gmax mediated by the TC. Kv4.2g SUMOylation sites at K437 and K579 were disrupted using site directed mutagenesis. Mutant plasmids were co-expressed with wild type KChIP2a and DPP10 in HEK cells to generate mutant TCs. **(A-C)** Representative current traces for mutant TCs when SUMOylation was or was not increased by co-transfecting SUMO+Ubc9. **(D)** Bar graph showing the mean±SEM IA Gmax for each treatment group. Each dot represents one cell collected from ≥3 transfections. Asterisk, significant differences. TC K437R+K579R: control, 91.23nS±8.832 vs SUMO+Ubc9, 92.0nS±8.509, t-test p=0.95; TC K437R: control, 75.48nS±7.816 vs SUMO+Ubc9, 131.9nS±15.03, t-test p=0.005; TC K579R: control, 92.55nS±8.015 vs SUMO+Ubc9, 92.78nS±7.794, t-test p=0.98.

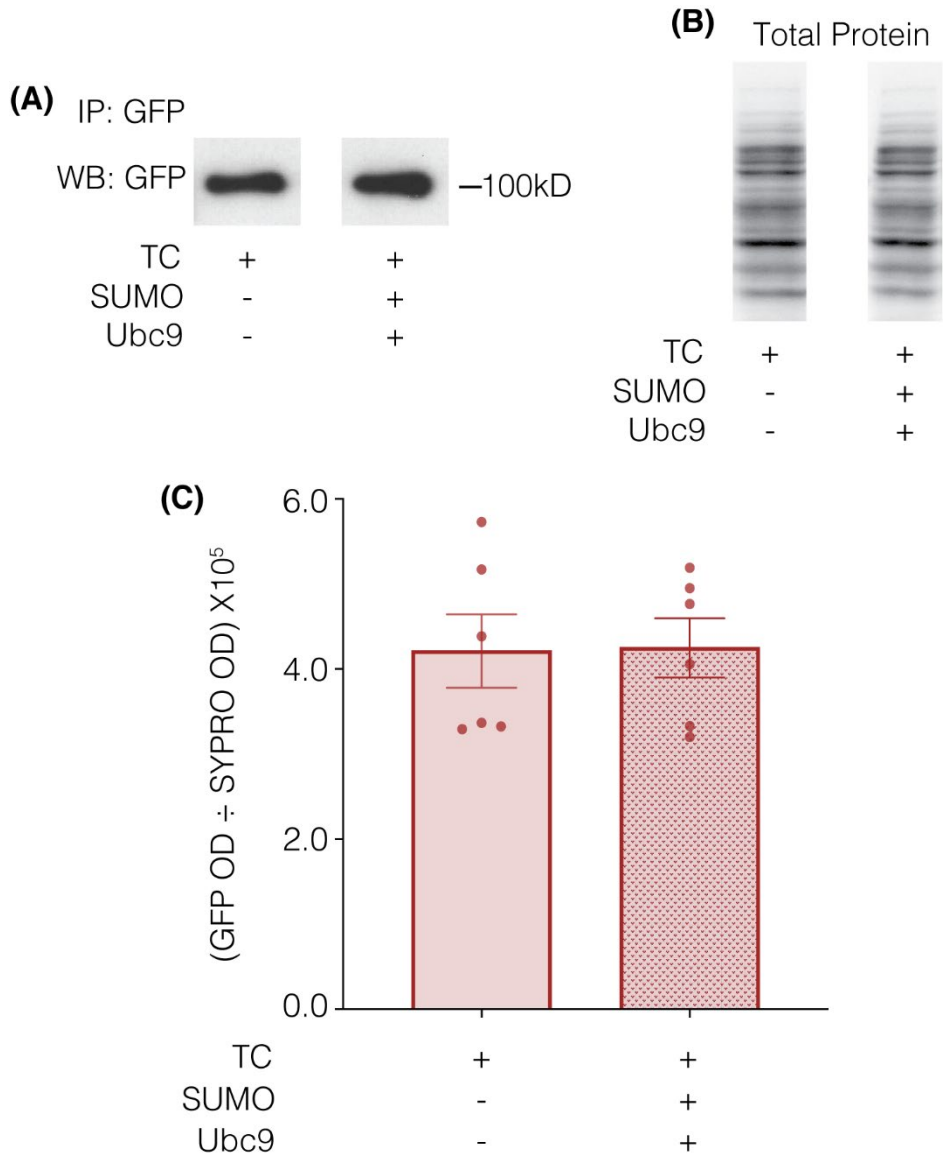

Figure 3.3 Kv4.2g steady-state levels are not altered by enhancing ternary complex SUMOylation.

Kv4.2g IPs were performed on lysates from HEK cells co-expressing Kv4.2g + KChIP2a + DPP10 with (+) or without (-) SUMO+Ubc9. Lysates and IP products were used in western blot experiments. Total protein in lysate lanes was visualized with SYPRO Ruby blot stain. Kv4.2g in IP lanes was visualized with anti-GFP. Kv4.2g protein expression was quantified by dividing the OD for the Kv4.2g signal by the OD for the lysate total protein signal. **(A)** Representative western blots showing Kv4.2g IP products. **(B)** Representative SYPRO Ruby total protein staining. **(C)** Bar graph showing mean ±SEM Kv4.2g protein expression. Each data point represents one independent experiment. TC: control, 4.212 $X10^{-5}$±0.432 $X10^{-5}$ vs. SUMO+Ubc9, 4.249 $X10^{-5}$±0.348 $X10^{-5}$; t-test p=0.948.

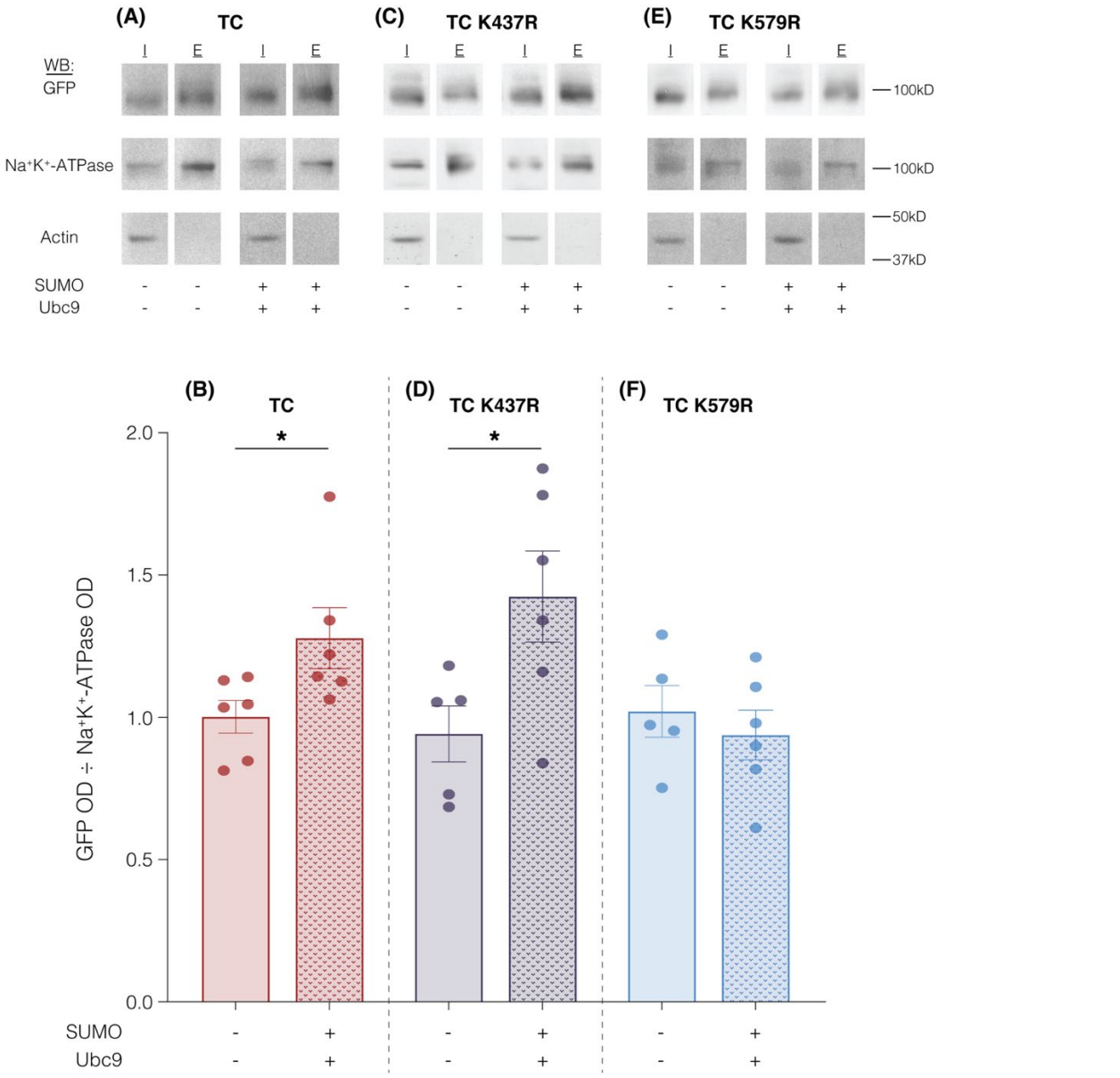

Figure 3.4 SUMOylation of Kv4.2g at K579 increases TC surface expression.

SUMOylation was (+) or was not (-) increased in HEK cells expressing wild-type TC, TC K437R, or TC K579R. Surface proteins were biotinylated, cells were lysed, and extracellular fractions (E) were isolated using NeutrAvidin resin. Proteins that did not bind to the NeutrAvidin resin were considered to be the intracellular fraction (I). **(A, C, and E)** Western blots containing E and I from one representative experiment for each treatment group. The upper portion of the blot (above 50kD) was used to visualize Kv4.2g with anti-GFP; it was then stripped and re-probed with anti-Na^+/K^+-ATPase. The lower portion of the blot (below 50kD) was probed for actin. **(B, D, and F)** Bar graphs showing the mean±SEM Kv4.2g surface expression [extracellular Kv4.2g OD/extracellular Na^+/K^+-ATPase OD]. Each dot is one independent experiment. Asterisk, significantly different. TC: control, 1.002±0.06 vs SUMO+Ubc9, 1.28±0.11, t-test p=0.046; TC K437R: control, 0.94±0.10 vs SUMO+Ubc9, 1.43±0.16, t-test p=0.037; TC K579R: control, 1.021±0.09 vs SUMO+Ubc9, 0.938±0.08, t-test p=0.528.

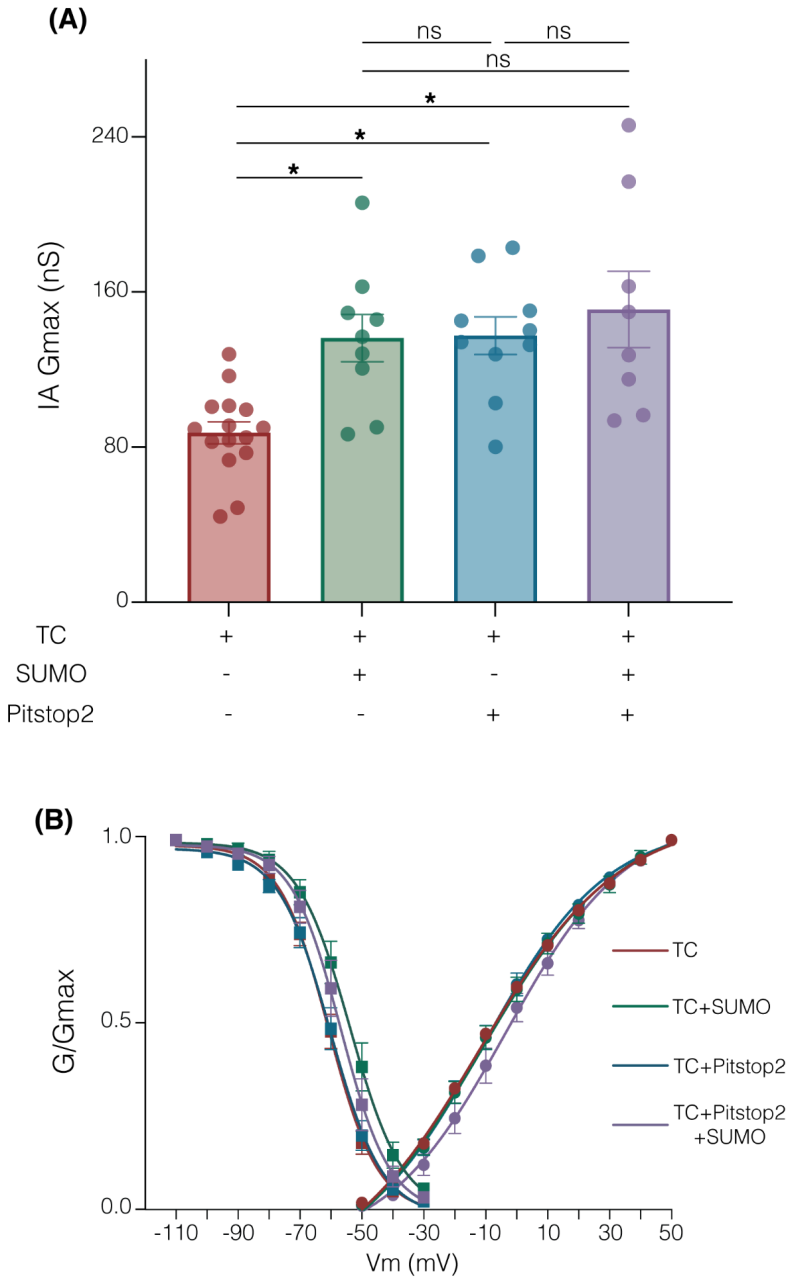

Figure 3.5 SUMOylation of the Kv4.2g ternary complex increases IA Gmax by preventing internalization of the TC.

HEK cells were transiently transfected with plasmids encoding the three TC components. Whole cell patch clamp recordings were performed on transfected cells with and without SUMO(2 or 3) peptides in the patch pipette and Pitstop2, a cell permeable endocytic inhibitor, in the superfusate. **(A)** Plot showing the mean±SEM IA Gmax for each treatment group. Asterisks indicate significance. One-Way ANOVA with Tukey's post hoc, $F(3,38)=7.681$, $p=0.0004$; TC: 87.44nS±5.67, TC+SUMO: 136.3nS±12.20, TC+Pitstop2: 137.5nS ± 9.78, TC+Pitstop2+SUMO: 151.0nS±19.64. **(B)** Activation (circle) and steady-state inactivation (square) curves for each treatment group. Each data point represents the mean±SEM for all data points analyzed.

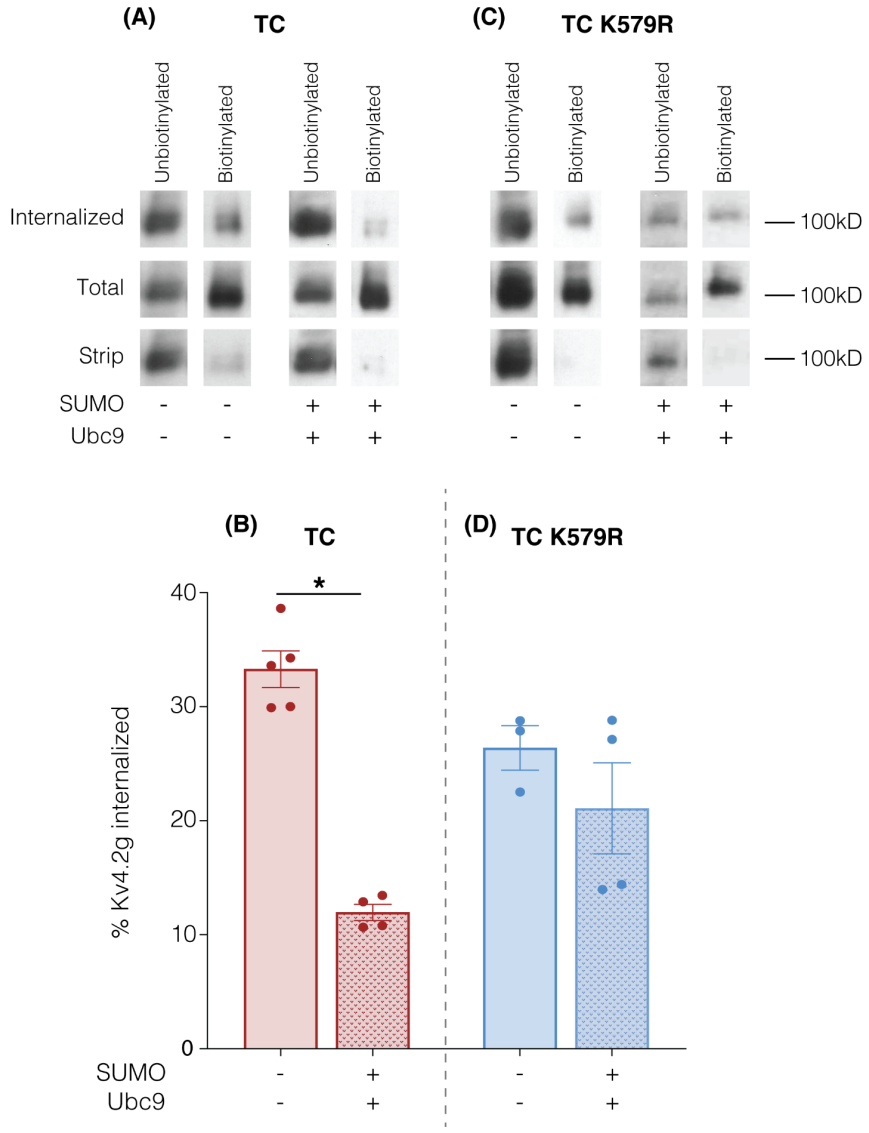

Figure 3.6 Ternary complex SUMOylation of Kv4.2g at K579 reduces channel internalization.

HEK cells were co-transfected with plasmids encoding the three TC or TC K579R components. SUMOylation was (+) or was not (-) enhanced by co-expressing SUMO and Ubc9. Assays to measure internalization in the two treatment groups were performed as detailed in the text. **(A and C)** Western blots containing the unbiotinylated and biotinylated fractions from the internalized, total, and strip plate lysates for a representative experiment in each treatment group for wild-type and mutant TCs. Blots were probed with anti-GFP to visualize Kv4.2g α-subunits. **(B and D)** Bar graph representing the mean±SEM percent internalization: (OD internalized, biotinylated fraction ÷ OD total, biotinylated fraction) x 100. The data for an experiment were only included if the stripping efficiency was >90%: [1-(OD strip, biotinylated fraction ÷ OD total, biotinylated fraction)] x100. Each data point represents one independent experiment. Asterisk, significantly different. TC: control, 33.28%±1.608 vs. SUMO+Ubc9, 11.95%±0.716, t-test p=<0.0001; TC K579R: control, 26.38%±1.954 vs. SUMO+Ubc9, 21.08%±3.99, t-test p=0.337.

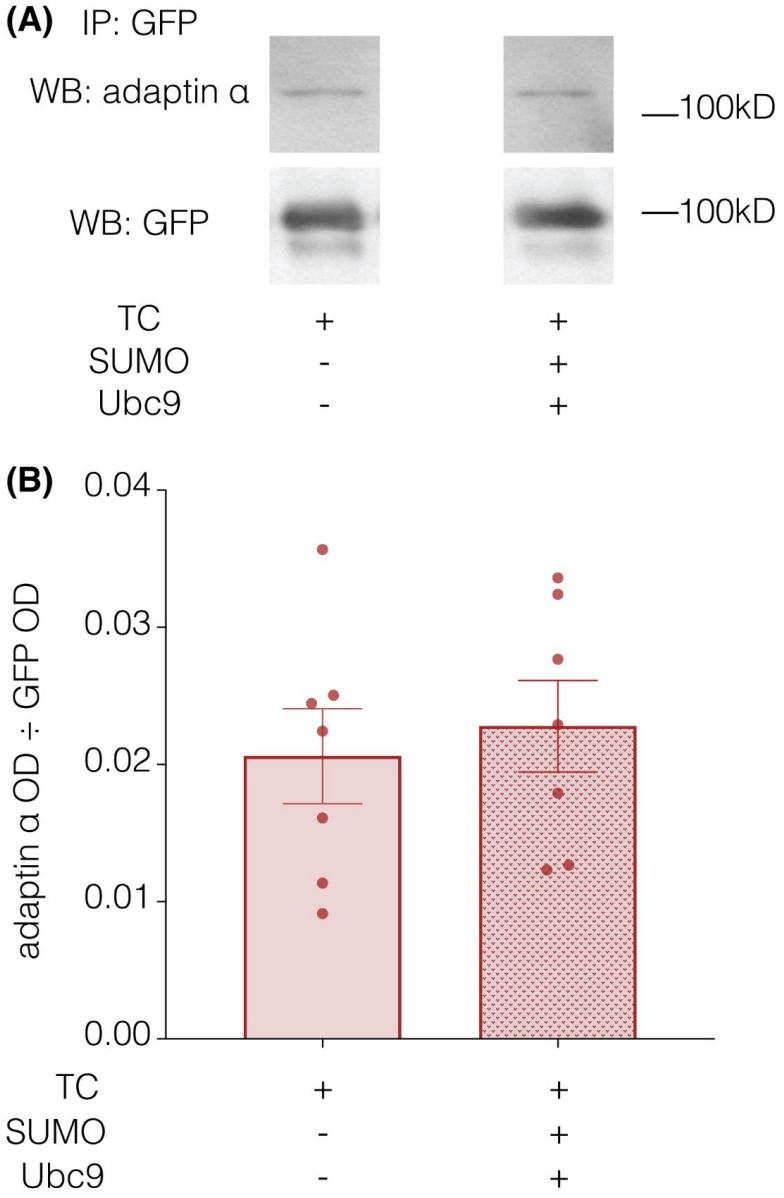

Figure 3.7 Enhancing SUMOylation of the TC does not change the fraction of Kv4.2g associated with adaptin α.

HEK cells were co-transfected with the TC components, and SUMOylation was (+) or was not (-) increased by co-expressing SUMO and Ubc9. Kv4.2g IP was obtained from cell lysates using an anti-GFP antibody, and IP products were resolved with PAGE. Western blots were probed for adaptin α and then stripped and re-probed for Kv4.2g. **(A)** Representative western blots for adaptin α and Kv4.2g for control and enhanced SUMOylation treatment groups. **(B)** Bar graphs plotting the mean±SEM of adaptin α that co-immunoprecipitates with Kv4.2g for each treatment group [OD adaptin α ÷ OD Kv4.2g]. Each data point is one independent experiment. TC: control, 0.0206±0.0035 vs. SUMO+Ubc9, 0.0227±0.0033; t-test p=0.657.

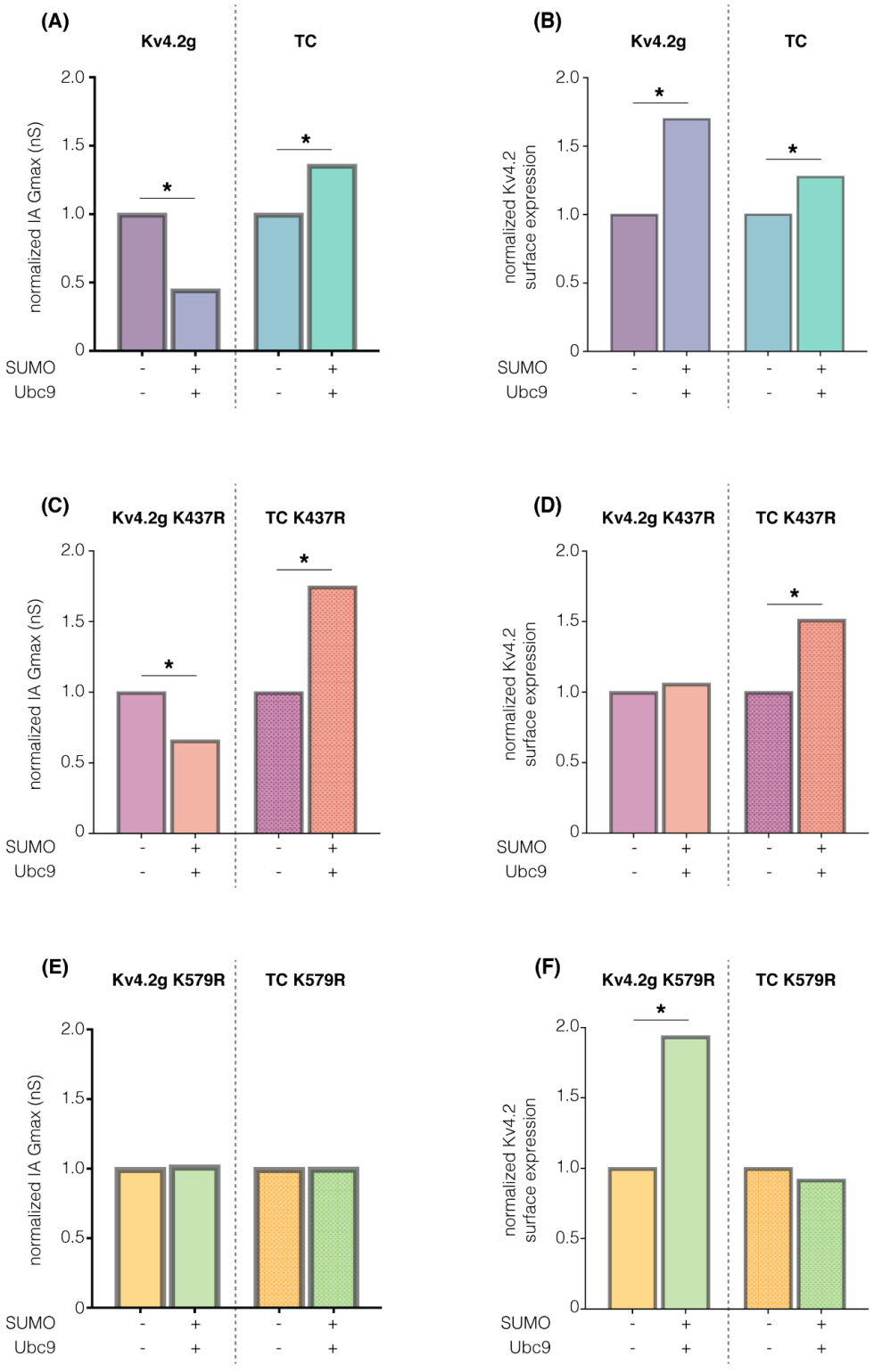

Figure 3.8 SUMOylation produces distinct effects on IA and surface expression when expressed alone or as a member of the ternary complex.

Bar graphs show normalized IA Gmax **(A)** or normalized surface expression **(B)** in HEK cells expressing only Kv4.2g or all 3 components of the wild-type TC when SUMOylation was

(+) or was not (-) increased by co-expressing SUMO+Ubc9. Bar graphs show normalized IA Gmax **(C and E)** or normalized surface expression **(D and F)** in HEK cells expressing the indicated Kv4.2g mutant or Kv4.2g mutant ternary complex with (+) and without (-) co-expression of SUMO+Ubc9. Asterisk, significantly different. Data for Kv4.2g lacking KChIP2a and DPP10 were adapted from (Welch et al., 2019).

Table 3.1 Primary antibodies

Antigen	Immunogen	Host species	Verified by	Manufacturer, catalog number	Concentration
GFP	Recombinant full-length protein corresponding to GFP	Rabbit, polyclonal	Specificity verified by company. On WB, the antibody recognizes recombinant GFP from HEK lysates.	abcam, ab290	IP- 1uL antibody per 0.5mg protein WB- 1: 20,000
Na^+/K^+-ATPase	Full length Rabbit alpha 1 Sodium Potassium ATPase	Mouse, monoclonal	Specificity verified by company. Positive signal on WB using HEK cell lysate	abcam, ab7671	WB- 1:3000
Actin	Peptide mapped to C-terminus of human actin	Rabbit, polyclonal	Specificity verified by company. Positive signal on WB using C32 cell lysate	Santa Cruz Biotechnology, sc-1616-R	WB- 1:2000
BSA	Bovine serum albumin	Rabbit, polyclonal	Specificity verified by company. On WB, the antibody recognizes BSA protein.	ThermoFisher, A11133	WB- 1:20,000
Adaptin-α	Mouse adaptin α, amino acids 38-215	Mouse, monoclonal	Specificity verified by company. WB shows positive signal using rat cerebellum lysate	BD Biosciences, 610502	WB- 1:2000

Table 3.2 Whole-cell patch clamp data when clathrin-mediated endocytosis was blocked using Pitstop2

	TC	TC+ Pitstop2	TC+ SUMO	TC+ Pitstop2+ SUMO
Gmax (nS)	87.44±5.7	137.5±9.8 [T]	136.3±12.2 [T]	151.0±19.6 [T]
V50 act (mV)	-11.05±1.5	-11.53±2.4	-9.945±2.6	-6.067±4.1
Slope act	22.33±0.74	19.57±1.4	22.58±1.5	18.84±1.5
V50 inact (mV)	-60.75±1.4	-60.23±1.8	-54.03±2.0	-56.74±2.5
Slope inact	-6.984±0.33	-7.078±0.26	-7.839±0.73	-6.507±0.33
τ fast (ms)	22.72±2.1	19.66±2.2	23.13±3.4	20.32±2.4
τ slow (ms)	76.89±4.6	92.10±18.9	94.94±15.6	79.70±4.3

TC is the ternary complex and includes Kv4.2g, KChIP2a, and DPP10

[T] Significantly different from Kv4.2g+KChIP2a+DPP10. One-way ANOVA with Tukey's multiple comparisons test, F (3,38)= 7.681, p=0.0004

4 DISCUSSION

In this dissertation work, we have shown Kv4.2 channels are decorated by SUMO-2/3 in rat brain membrane preparations and have characterized the effect of SUMO on a Kv4.2-GFP (Kv4.2g) fusion protein heterologously expressed in human embryonic kidney (HEK) cells. Co-transfecting plasmids containing SUMO-2/3 and Ubc9 in HEK cells expressing Kv4.2g alone produced a significant 60% increase in Kv4.2g SUMOylation that was accompanied by a 22-50% decrease in IA maximal conductance (Gmax) and a significant 70-95% increase in channel surface expression. Using prediction software, we identified two evolutionary conserved SUMOylation sites on Kv4.2g, K437 and K579. Using site-directed mutagenesis, we characterized the effect of SUMOylation at both of these sites. SUMOylation at K437 had no effect on IA Gmax but mediated the insertion of electrically silent channels into the plasma membrane. SUMOylation at K579 had no effect on Kv4.2g surface expression but was responsible for the significant decrease in IA Gmax. Mutating K579 to R mimicked and occluded the effect of SUMOylation, suggesting that SUMOylation at K579 blocks an inter/intramolecular interaction. Next, we determined effect of ternary complex SUMOylation by co-expressing Kv4.2g with potassium channel interacting protein (KChIP2a) and dipeptidyl peptidase-like protein (DPP10). Surprisingly, increasing SUMOylation in HEK cells expressing the ternary complex produced a significant 30-70% increase in IA Gmax and 30-50% increase in Kv4.2g surface expression that was accompanied by a 65% reduction in internalization, and SUMOylation of Kv4.2g K579 was responsible for these effects. Blocking clathrin-mediated endocytosis mimicked and occluded the effect of SUMO on IA Gmax, however the amount of adaptor protein 2 (AP2) associated with Kv4.2g was not affected by SUMO, suggesting that the effect of Kv4.2 internalization is downstream of cargo recruitment and vesicle formation. Our

findings raise two important questions. First, why is the effect of Kv4.2g SUMOylation different in the presence of auxiliary subunits? Second, how does SUMOylation control ternary complex internalization?

4.1 The effect of Kv4.2g SUMOylation is context dependent

The effect of Kv4.2g K437 SUMOylation is context dependent. When the α-subunit is expressed alone, SUMOylation of Kv4.2g K437 produces a 70-95% increase in channel surface expression and has no effect on IA Gmax. We did not specifically address the mechanism, however as discussed in Chapter 2, it is likely the case that Kv4.2g SUMOylation at K437 promotes a protein-protein interaction. Alternatively, SUMO at K437 could compete with another post-translational modification, such as ubiquitination, acetylation and methylation, for addition to that same K residue (D. D. Anderson et al., 2012; W. Wang et al., 2014). K437 is not predicted to be acetylated or methylated, but is a predicted ubiquitination site. As discussed in Chapter 3, ubiquitin plays an important role in regulating internalization. Additionally, misfolded proteins in the ER can be targeted for degradation in a process known as endoplasmic reticulum-associated degradation (ERAD), whereby the misfolded protein is recognized, ubiquitinated, translocated from ER, and degraded by the proteasome (Preston & Brodsky, 2017; X. Wu & Rapoport, 2018). In both of these cases, if K437 SUMOylation were competing with ubiquitination for that residue, we would expect Kv4.2g surface expression to be increased in HEK cells expressing Kv4.2g K437R comparted to wild-type Kv4.2 (e.g. less Kv4.2g would be endocytosed and/or more Kv4.2 would be recycled); however as shown in Chapter 2, there was no difference in Kv4.2g surface expression between the two groups.

It is not clear if Kv4.2g can be SUMOylated at K437 when expressed with KChIP2a and DPP10 because mutating that site has no effect on IA Gmax or channel surface expression.

While a weak argument, KChIP2a binding to the Kv4.2g C-terminus could mask K437 and block its ability to be SUMOylated. High resolution structural data on the KChIP-Kv4 C-terminus interface are lacking, but Kv4.2 C-terminal deletions studies do show that residues proximal to amino acid 580 are important for this interaction and for KChIP modulation of IA (Callsen et al., 2005; W. Han et al., 2006). Additionally, it is also unlikely that DPP10s association with Kv4.2g prevents SUMOylation at K437, as the interaction does not involve the C-terminus of the α-subunit (Cotella et al., 2012; Lin et al., 2014; Ren et al., 2005).

The Kv4.2 SUMOylation pattern could also be different in the two states because the Kv4.2 phosphorylation pattern can vary depending upon whether Kv4.2 is expressed alone or with KChIP and DPLP. Phosphorylation controls the ability of a lysine residue to be SUMOylated (Dustrude et al., 2016; Flotho & Melchior, 2013; Konopacki et al., 2011). Phosphorylation can permit or prevent SUMOylation. For example, collapsin response mediator protein 2 (CRMP2) SUMOylation at K374 is facilitated by cyclin-dependent kinase (Cdk5) phosphorylation at S552 and blocked by Src-family kinase Fyn phosphorylation at Y32 (Dustrude et al., 2016). There are multiple phosphorylation sites on the Kv4.2 C-terminus (S438, S548, S459, S552, S572, S575, T602, T607, T616), and in some cases the ability of heterologously expressed Kv4.2 channels to be phosphorylated depends on the presence of auxiliary subunits. Tandem mass spectrometry reveals phosphorylated S548, S572, and S575 are only detected in COS-1 cells co-expressing Kv4.2+DPP6 or Kv4.2+KChIP2, but not in COS-1 cells only expressing Kv4.2 (Seikel & Trimmer, 2009). It could be the case that phosphorylation at one or multiple site(s) on the Kv4.2g C-terminus antagonizes K437 SUMOylation when the channel is expressed as a ternary complex. Additionally, K437 is located within a Calcium

Calmodulin kinase II (CaMKII) consensus motif (RXXS/T), and CAMKII phosphorylation at S438 or S459 could block ternary complex SUMOylation of Kv4.2g K437 (Varga et al., 2004).

The effect of Kv4.2g K579 SUMOylation is also context dependent. As previously stated in Chapter 3, it seems unlikely that SUMO is competing with another post-translational modification for K579, as this site does not fall within a ubiquitination, methylation, or acetylation consensus motif. While a weak argument, K579 falls within the proposed Kv4.2 C-terminus-KChIP2a binding region (Callsen et al., 2005; W. Han et al., 2006), and it could be the case that conformational change in the C-terminus when interacting with KChIP2a permits K579 SUMOylation to modulate a new interaction. In some cases, the effect of a post-translational modification on Kv4 varies in the presence or absence of auxiliary subunits. For example, AKAP79/150 is a scaffolding protein that interacts with Kv4.2 and tethers PKA and calcineurin for dynamic (de)phosphorylation of the channel. In COS-7 cells, AKAP79/150 co-expressed with Kv4.2+KChIP4 results in increased Kv4.2 stability and surface expression (Lin, Sun, Wikenheiser, Kung, & Hoffman, 2010). However, in COS-7 cells expressing Kv4.2 alone, AKAP79/150 has an inhibitory effect, reducing Kv4.2 surface expression and reducing IA (Lin et al., 2011). In both cases, Kv4.2 phosphorylation at S552 mediated the effect. As described in Chapter 3, in *Xenopus* oocytes, KChIP3 co-expression with the α-subunit is needed for PKA phosphorylation at S552 to produce a functional effect on IA, which in this cases involves decreasing current amplitude by causing a rightward shift in the voltage of half-activation and increasing time constant of inactivation (L. A. Schrader, A. E. Anderson, A. Mayne, P. J. Pfaffinger, & J. D. Sweatt, 2002).

4.2 SUMOylation modulates ternary complex interactions

As previously discussed in Chapter 3, SUMOylation can increase an ion channel's surface expression by reducing its ubiquitination (Cartier et al., 2019; Dustrude et al., 2016; Ma et al., 2016), either by blocking an interaction with a ubiquitin ligase or facilitating an interaction with a de-ubiquitinase. For example, loss of CRMP2 SUMOylation triggers Nav1.7 clathrin-mediated endocytosis by recruiting E3 ubiquitin ligase Nedd4-2 and endocytic proteins Numb and Esp15 (Dustrude et al., 2016). Activation of the smoothened (smo) receptor disrupts its interaction with Ulp1, a de-SUMOylation enzyme, resulting in SUMOylation of the smo receptor. Smo receptor SUMOylation recruits de-ubiquitinase UBPY, which antagonizes smo ubiquitination, thus stabilizing smo surface expression and preventing its internalization and degradation (Ma et al., 2016). As proposed in Chapter 3, SUMOylation could be blocking an interaction with a ubiquitin ligase and/or facilitating an interaction with a de-ubiquitinase to control ternary complex internalization.

This leads to the question, which ubiquitin ligases and/or de-ubiquitinases could be controlling ternary complex internalization? As previously stated in Chapter 3, Multiple ubiquitin ligases (ITCH, CAND1, UBE3C, UB20, UBE4B, UBE2M) and de-ubiquitinases (USP9X, USP7, USP24, USP48, USP10, USP5, USP15) interact with the α-subunit (J. H. Hu et al., 2020). This section will focus on how these ubiquitin ligases and de-ubiquitinases are involved in internalization. E3 ubiquitin ligase ITCH is expressed in multiple cellular compartments including the endosomes, and ITCHs association with a cargo protein peaks after the cargo is endocytosed (Angers, Ramjaun, & McPherson, 2004; Tong, Taylor, & Moran, 2014). ITCH recognizes proline rich consensus sequences, PPXY(PY), and also interacts with phosphorylated serine or threonine followed by proline motifs (phospho-S/T P) (Melino et al.,

2008). Several of the latter motifs are present on the Kv4.2g C-terminus near K579 (phosho-Thr602/proline-603; phosho-Thr607/proline-608; and phosphor-Ser616/proline 617), and it could be the case K579 SUMOylation blocks ITCH from interacting with and ubiquitinating the α-subunit. UBE4B is an endosome-associated ubiquitin ligase that interacts with both the ESCRT complex and the internalized proteins to regulates endosomal trafficking (Gireud-Goss et al., 2020), and SUMO could be acting to block an interaction with this protein. It is unclear if ubiquitin ligases CAND1, UBE3C, UB20 regulate internalization.

There are multiple predicted ubiquitination sites on the Kv4.2 C-terminus (K421, K426, K427, K437, K448, K535, K536). Ubiquitination at one or more than one of these residues could be important for internalization, and it could be the case that K579 SUMOylation facilitates an interaction with a de-ubiquitinase to reduce Kv4.2 internalization. For example, USP9X (Kharitidi et al., 2015), USP7 (Y. Han & Yun, 2020), and USP10 (Bomberger, Barnaby, & Stanton, 2009, 2010) can remove ubiquitin from internalized cargo and this could be occurring at the plasma membrane, during vesicle transport or at the early endosome. USP48 can prevent endocytosis by removing ubiquitin on proteins expressed at the plasma membrane (Armando et al., 2014). USP5 is upregulated and its association with Cav3.2 is enhanced in chronic pain models. The increased interaction between Cav3.2 and USP5 reduces channel ubiquitination and leads to an upregulation of the T-type $Ca2^{+}$ current (Garcia-Caballero et al., 2014). Interestingly, it was recently shown that SUMO modulates the Cav3.2-USP5 interaction. USP5 SUMOylation is reduced in dorsal root ganglia (DRG) neurons following peripheral nerve injury, and there is a stronger interaction between Cav3.2 and SUMO-deficient USP5 compared to Cav3.2 and wild-type USP5 (Garcia-Caballero et al., 2019). Little is known about the role of de-ubiquitinases USP15 and USP24 in internalization.

It could also be the case the aforementioned ubiquitin ligases and/or de-ubiquitinases are not involved in reducing Kv4.2g internalization. In this case, stable isotope labeling of amino acids in cell culture (SILAC) and mass spectrometry would be useful in order to quantify changes in the Kv4.2g interactome when the ternary complex is expressed without vs. with SUMO and Ubc9. This type of experiment would provide greater insight into which interactions within the Kv4.2 macromolecular complex were changing and would allow for a more targeted approach when designing experiments to elucidate the role of ternary complex internalization.

Additionally, SUMOylation not only modulates internalization but is involved at multiple trafficking stages, and SUMO could be acting at these steps to enhance channel trafficking to the plasma membrane. SUMO protease SENP2 associates with the ER and Golgi membranes (Odeh et al., 2018). SUMO modulates trafficking from the Golgi to the plasma membrane (Zhou et al., 2018). SUMO can act as a sorting motif for incorporation into transport vesicles (Kunadt et al., 2015). SUMO can interact with phospholipids at the plasma membrane to stabilize a proteins surface expression (i.e. a positively charged interface on SUMO can interact with the negatively charged phospholipid bilayer) (Huang et al., 2012). It could be the case that SUMOylation dynamically organizes interactions with and within the Kv4 macromolecular complex at multiple stages throughout the channel's lifetime. For example, Kv4.2 might be de-SUMOylated by a SENP located in the ER to permit an interaction with a vesicle transport protein, such as a SNARE, to facilitate forward trafficking. It might also be the case that once at the plasma membrane SUMO stabilizes Kv4.2 surface expression by interacting with PI(3,4,5)P3.

4.3 The benefits and limitations of using a heterologous expression system

Much of this dissertation work was performed in HEK cells. HEK cells are widely used by researchers because they provide high reproducibility of results, they are inexpensive and

easy to grow and maintain, and they are easy to transfect and produce high amounts of protein. My work used HEK cells to examine the effects of SUMO on Kv4.2 channels. HEK cells do not endogenously express Kv4.2 channels. This makes it possible to directly test the effects that specific mutations have on Kv4.2, without the interference of endogenous wild-type Kv4.2. Despite these benefits, there are several limitations with using HEK cells, and understanding these limitations is important when interpreting our results. In some cases, we stably expressed Kv4.2g or SUMO deficient Kv4.2g channels in HEK cells. With our stable lines, we were unable to control the number of copies of the Kv4.2 gene integrated into the HEK cell genome, making it impossible to compare across lines. Most of our experiments involve overexpressing SUMO and Ubc9 to examine the effects of SUMOylation on Kv4.2 channels. In this case, it's important to consider the biological context. By increasing the levels of SUMO and Ubc9 in HEK cells, we maximize Kv4.2 SUMOylation, but are we producing an effect that would not normally be observed under physiological conditions? As previously discussed, SUMO is dynamic, and a target proteins SUMOylation status can be regulated by activity and can be altered in disease states. In future studies, it will be interesting to examine SUMO's effect on Kv4.2 and IA when SUMOylation is manipulated in these physiological contexts.

4.4 Conclusion

In summary, this dissertation work presents the novel finding Kv4.2 channels are post-translationally SUMOylated. This work determines the effect of SUMOylation at two C-terminal K residues on Kv4.2, K437 and K579, and shows effect of SUMOylation at both of these residues depends on the available interactome. This work suggests SUMOylation regulates the Kv4.2 macromolecular complex. This is an important finding because very little is known about mechanisms that organize interactions with and within the Kv4.2 macromolecular complex, and

mechanisms targeting these interactions could be important for tuning Kv4.2 expression and gating, which in turn could modulate cellular excitability.

REFERENCES

Aceto, G., Colussi, C., Leone, L., Fusco, S., Rinaudo, M., Scala, F., . . . Grassi, C. (2020). Chronic mild stress alters synaptic plasticity in the nucleus accumbens through GSK3beta-dependent modulation of Kv4.2 channels. *Proc Natl Acad Sci U S A, 117*(14), 8143-8153. doi:10.1073/pnas.1917423117

Adams, J. P., Anderson, A. E., Varga, A. W., Dineley, K. T., Cook, R. G., Pfaffinger, P. J., & Sweatt, J. D. (2000). The A-type potassium channel Kv4.2 is a substrate for the mitogen-activated protein kinase ERK. *J Neurochem, 75*(6), 2277-2287. doi:10.1046/j.1471-4159.2000.0752277.x

Aguilar-Martinez, E., Chen, X., Webber, A., Mould, A. P., Seifert, A., Hay, R. T., & Sharrocks, A. D. (2015). Screen for multi-SUMO-binding proteins reveals a multi-SIM-binding mechanism for recruitment of the transcriptional regulator ZMYM2 to chromatin. *Proc Natl Acad Sci U S A, 112*(35), E4854-4863. doi:10.1073/pnas.1509716112

Amarillo, Y., De Santiago-Castillo, J. A., Dougherty, K., Maffie, J., Kwon, E., Covarrubias, M., & Rudy, B. (2008). Ternary Kv4.2 channels recapitulate voltage-dependent inactivation kinetics of A-type K+ channels in cerebellar granule neurons. *J Physiol, 586*(8), 2093-2106. doi:10.1113/jphysiol.2007.150540

An, W. F., Bowlby, M. R., Betty, M., Cao, J., Ling, H. P., Mendoza, G., . . . Rhodes, K. J. (2000). Modulation of A-type potassium channels by a family of calcium sensors. *Nature, 403*(6769), 553-556. doi:10.1038/35000592

Anderson, A. E., Adams, J. P., Qian, Y., Cook, R. G., Pfaffinger, P. J., & Sweatt, J. D. (2000). Kv4.2 phosphorylation by cyclic AMP-dependent protein kinase. *J Biol Chem, 275*(8), 5337-5346. doi:10.1074/jbc.275.8.5337

Anderson, D., Mehaffey, W. H., Iftinca, M., Rehak, R., Engbers, J. D., Hameed, S., . . . Turner, R. W. (2010). Regulation of neuronal activity by Cav3-Kv4 channel signaling complexes. *Nat Neurosci, 13*(3), 333-337. doi:10.1038/nn.2493

Anderson, D., Rehak, R., Hameed, S., Mehaffey, W. H., Zamponi, G. W., & Turner, R. W. (2010). Regulation of the KV4.2 complex by CaV3.1 calcium channels. *Channels (Austin), 4*(3), 163-167. doi:10.4161/chan.4.3.11955

Anderson, D. D., Eom, J. Y., & Stover, P. J. (2012). Competition between sumoylation and ubiquitination of serine hydroxymethyltransferase 1 determines its nuclear localization and its accumulation in the nucleus. *J Biol Chem, 287*(7), 4790-4799. doi:10.1074/jbc.M111.302174

Angers, A., Ramjaun, A. R., & McPherson, P. S. (2004). The HECT domain ligase itch ubiquitinates endophilin and localizes to the trans-Golgi network and endosomal system. *J Biol Chem, 279*(12), 11471-11479. doi:10.1074/jbc.M309934200

Armando, I., Villar, V. A., Jones, J. E., Lee, H., Wang, X., Asico, L. D., . . . Jose, P. A. (2014). Dopamine D3 receptor inhibits the ubiquitin-specific peptidase 48 to promote NHE3 degradation. *FASEB J, 28*(3), 1422-1434. doi:10.1096/fj.13-243840

Azarnia Tehran, D., Lopez-Hernandez, T., & Maritzen, T. (2019). Endocytic Adaptor Proteins in Health and Disease: Lessons from Model Organisms and Human Mutations. *Cells, 8*(11). doi:10.3390/cells8111345

Bahring, R. (2018). Kv channel-interacting proteins as neuronal and non-neuronal calcium sensors. *Channels (Austin), 12*(1), 187-200. doi:10.1080/19336950.2018.1491243

Bahring, R., Dannenberg, J., Peters, H. C., Leicher, T., Pongs, O., & Isbrandt, D. (2001). Conserved Kv4 N-terminal domain critical for effects of Kv channel-interacting protein 2.2 on channel expression and gating. *J Biol Chem, 276*(26), 23888-23894. doi:10.1074/jbc.M101320200

Beacham, G. M., Partlow, E. A., & Hollopeter, G. (2019). Conformational regulation of AP1 and AP2 clathrin adaptor complexes. *Traffic, 20*(10), 741-751. doi:10.1111/tra.12677

Benson, M. D., Li, Q. J., Kieckhafer, K., Dudek, D., Whorton, M. R., Sunahara, R. K., . . . Martens, J. R. (2007). SUMO modification regulates inactivation of the voltage-gated potassium channel Kv1.5. *Proc Natl Acad Sci U S A, 104*(6), 1805-1810. doi:10.1073/pnas.0606702104

Birnbaum, S. G., Varga, A. W., Yuan, L. L., Anderson, A. E., Sweatt, J. D., & Schrader, L. A. (2004). Structure and function of Kv4-family transient potassium channels. *Physiol Rev, 84*(3), 803-833. doi:10.1152/physrev.00039.2003

Bomberger, J. M., Barnaby, R. L., & Stanton, B. A. (2009). The deubiquitinating enzyme USP10 regulates the post-endocytic sorting of cystic fibrosis transmembrane conductance regulator in airway epithelial cells. *J Biol Chem, 284*(28), 18778-18789. doi:10.1074/jbc.M109.001685

Bomberger, J. M., Barnaby, R. L., & Stanton, B. A. (2010). The deubiquitinating enzyme USP10 regulates the endocytic recycling of CFTR in airway epithelial cells. *Channels (Austin), 4*(3), 150-154. doi:10.4161/chan.4.3.11223

Callsen, B., Isbrandt, D., Sauter, K., Hartmann, L. S., Pongs, O., & Bahring, R. (2005). Contribution of N- and C-terminal Kv4.2 channel domains to KChIP interaction [corrected]. *J Physiol, 568*(Pt 2), 397-412. doi:10.1113/jphysiol.2005.094359

Carrasquillo, Y., Burkhalter, A., & Nerbonne, J. M. (2012). A-type K+ channels encoded by Kv4.2, Kv4.3 and Kv1.4 differentially regulate intrinsic excitability of cortical pyramidal neurons. *J Physiol, 590*(16), 3877-3890. doi:10.1113/jphysiol.2012.229013

Carrillo-Reid, L., Day, M., Xie, Z., Melendez, A. E., Kondapalli, J., Plotkin, J. L., . . . Surmeier, D. J. (2019). Mutant huntingtin enhances activation of dendritic Kv4 K(+) channels in striatal spiny projection neurons. *Elife, 8*. doi:10.7554/eLife.40818

Cartier, E., Garcia-Olivares, J., Janezic, E., Viana, J., Moore, M., Lin, M. L., . . . Kim, Y. H. (2019). The SUMO-Conjugase Ubc9 Prevents the Degradation of the Dopamine Transporter, Enhancing Its Cell Surface Level and Dopamine Uptake. *Front Cell Neurosci, 13*, 35. doi:10.3389/fncel.2019.00035

Celen, A. B., & Sahin, U. (2020). Sumoylation on its 25th anniversary: mechanisms, pathology, and emerging concepts. *FEBS J, 287*(15), 3110-3140. doi:10.1111/febs.15319

Chamberlain, S. E., Gonzalez-Gonzalez, I. M., Wilkinson, K. A., Konopacki, F. A., Kantamneni, S., Henley, J. M., & Mellor, J. R. (2012). SUMOylation and phosphorylation of GluK2 regulate kainate receptor trafficking and synaptic plasticity. *Nat Neurosci, 15*(6), 845-852. doi:10.1038/nn.3089

Chang, C. C., Naik, M. T., Huang, Y. S., Jeng, J. C., Liao, P. H., Kuo, H. Y., . . . Shih, H. M. (2011). Structural and functional roles of Daxx SIM phosphorylation in SUMO paralog-selective binding and apoptosis modulation. *Mol Cell, 42*(1), 62-74. doi:10.1016/j.molcel.2011.02.022

Chang, H. M., & Yeh, E. T. H. (2020). SUMO: From Bench to Bedside. *Physiol Rev, 100*(4), 1599-1619. doi:10.1152/physrev.00025.2019

Chen, C. P., Lee, L., & Chang, L. S. (2006). Effects of metal-binding properties of human Kv channel-interacting proteins on their molecular structure and binding with Kv4.2 channel. *Protein J, 25*(5), 345-351. doi:10.1007/s10930-006-9020-9

Chen, X., Yuan, L. L., Zhao, C., Birnbaum, S. G., Frick, A., Jung, W. E., . . . Johnston, D. (2006). Deletion of Kv4.2 gene eliminates dendritic A-type K+ current and enhances induction of long-term potentiation in hippocampal CA1 pyramidal neurons. *J Neurosci, 26*(47), 12143-12151. doi:10.1523/JNEUROSCI.2667-06.2006

Choi, J. H., Park, J. Y., Park, S. P., Lee, H., Han, S., Park, K. H., & Suh, Y. H. (2016). Regulation of mGluR7 trafficking by SUMOylation in neurons. *Neuropharmacology, 102*, 229-235. doi:10.1016/j.neuropharm.2015.11.021

Chu, P. J., Rivera, J. F., & Arnold, D. B. (2006). A role for Kif17 in transport of Kv4.2. *J Biol Chem, 281*(1), 365-373. doi:10.1074/jbc.M508897200

Coetzee, W. A., Amarillo, Y., Chiu, J., Chow, A., Lau, D., McCormack, T., . . . Rudy, B. (1999). Molecular diversity of K+ channels. *Ann N Y Acad Sci, 868*, 233-285. doi:10.1111/j.1749-6632.1999.tb11293.x

Colledge, M., Dean, R. A., Scott, G. K., Langeberg, L. K., Huganir, R. L., & Scott, J. D. (2000). Targeting of PKA to glutamate receptors through a MAGUK-AKAP complex. *Neuron, 27*(1), 107-119. doi:10.1016/s0896-6273(00)00013-1

Cotella, D., Radicke, S., Bortoluzzi, A., Ravens, U., Wettwer, E., Santoro, C., & Sblattero, D. (2010). Impaired glycosylation blocks DPP10 cell surface expression and alters the electrophysiology of Ito channel complex. *Pflugers Arch, 460*(1), 87-97. doi:10.1007/s00424-010-0824-2

Cotella, D., Radicke, S., Cipriani, V., Cavaletto, M., Merlin, S., Follenzi, A., . . . Sblattero, D. (2012). N-glycosylation of the mammalian dipeptidyl aminopeptidase-like protein 10 (DPP10) regulates trafficking and interaction with Kv4 channels. *Int J Biochem Cell Biol, 44*(6), 876-885. doi:10.1016/j.biocel.2012.02.011

Cox, O. F., & Huber, P. W. (2018). Developing Practical Therapeutic Strategies that Target Protein SUMOylation. *Curr Drug Targets*. doi:10.2174/1389450119666181026151802

Craig, T. J., Anderson, D., Evans, A. J., Girach, F., & Henley, J. M. (2015). SUMOylation of Syntaxin1A regulates presynaptic endocytosis. *Sci Rep, 5*, 17669. doi:10.1038/srep17669

Craig, T. J., Jaafari, N., Petrovic, M. M., Jacobs, S. C., Rubin, P. P., Mellor, J. R., & Henley, J. M. (2012). Homeostatic synaptic scaling is regulated by protein SUMOylation. *J Biol Chem, 287*(27), 22781-22788. doi:10.1074/jbc.M112.356337

Dai, X. Q., Kolic, J., Marchi, P., Sipione, S., & Macdonald, P. E. (2009). SUMOylation regulates Kv2.1 and modulates pancreatic beta-cell excitability. *J Cell Sci, 122*(Pt 6), 775-779. doi:10.1242/jcs.036632

Desterro, J. M., Thomson, J., & Hay, R. T. (1997). Ubch9 conjugates SUMO but not ubiquitin. *FEBS Lett, 417*(3), 297-300. Retrieved from https://www.ncbi.nlm.nih.gov/pubmed/9409737

https://ac.els-cdn.com/S0014579397013057/1-s2.0-S0014579397013057-main.pdf?_tid=b37da3f8-4735-41b0-9d88-a91a4427bba7&acdnat=1543250579_446b469e16700be00ea389dfa54a6ff4

Dustrude, E. T., Moutal, A., Yang, X., Wang, Y., Khanna, M., & Khanna, R. (2016). Hierarchical CRMP2 posttranslational modifications control NaV1.7 function. *Proc Natl Acad Sci U S A, 113*(52), E8443-E8452. doi:10.1073/pnas.1610531113

Dustrude, E. T., Wilson, S. M., Ju, W., Xiao, Y., & Khanna, R. (2013). CRMP2 protein SUMOylation modulates NaV1.7 channel trafficking. *J Biol Chem, 288*(34), 24316-24331. doi:10.1074/jbc.M113.474924

El-Haou, S., Balse, E., Neyroud, N., Dilanian, G., Gavillet, B., Abriel, H., . . . Hatem, S. N. (2009). Kv4 potassium channels form a tripartite complex with the anchoring protein SAP97 and CaMKII in cardiac myocytes. *Circ Res, 104*(6), 758-769. doi:10.1161/CIRCRESAHA.108.191007

Feligioni, M., Mattson, M. P., & Nistico, R. (2013). SUMOylation in neuroplasticity and neurological disorders. *Neuromolecular Med, 15*(4), 637-638. Retrieved from https://www.ncbi.nlm.nih.gov/pubmed/24354012

Ferron, L., Koshti, S., & Zamponi, G. W. (2021). The life cycle of voltage-gated Ca(2+) channels in neurons: an update on the trafficking of neuronal calcium channels. *Neuronal Signal, 5*(1), NS20200095. doi:10.1042/NS20200095

Flotho, A., & Melchior, F. (2013). Sumoylation: a regulatory protein modification in health and disease. *Annu Rev Biochem, 82*, 357-385. doi:10.1146/annurev-biochem-061909-093311

Flowerdew, S. E., & Burgoyne, R. D. (2009). A VAMP7/Vti1a SNARE complex distinguishes a non-conventional traffic route to the cell surface used by KChIP1 and Kv4 potassium channels. *Biochem J, 418*(3), 529-540. doi:10.1042/BJ20081736

Foeger, N. C., Marionneau, C., & Nerbonne, J. M. (2010). Co-assembly of Kv4 {alpha} subunits with K+ channel-interacting protein 2 stabilizes protein expression and promotes surface retention of channel complexes. *J Biol Chem, 285*(43), 33413-33422. doi:10.1074/jbc.M110.145185

Foeger, N. C., Norris, A. J., Wren, L. M., & Nerbonne, J. M. (2012). Augmentation of Kv4.2-encoded currents by accessory dipeptidyl peptidase 6 and 10 subunits reflects selective cell surface Kv4.2 protein stabilization. *J Biol Chem, 287*(12), 9640-9650. doi:10.1074/jbc.M111.324574

Foot, N., Henshall, T., & Kumar, S. (2017). Ubiquitination and the Regulation of Membrane Proteins. *Physiol Rev, 97*(1), 253-281. doi:10.1152/physrev.00012.2016

Ford, L., Ling, E., Kandel, E. R., & Fioriti, L. (2019). CPEB3 inhibits translation of mRNA targets by localizing them to P bodies. *Proc Natl Acad Sci U S A, 116*(36), 18078-18087. doi:10.1073/pnas.1815275116

Forster, L. A., Jansen, L. R., Rubaharan, M., Murphy, A. Z., & Baro, D. J. (2020). Alterations in SUMOylation of the hyperpolarization-activated cyclic nucleotide-gated ion channel 2 during persistent inflammation. *Eur J Pain, 24*(8), 1517-1536. doi:10.1002/ejp.1606

Francois-Moutal, L., Dustrude, E. T., Wang, Y., Brustovetsky, T., Dorame, A., Ju, W., . . . Khanna, R. (2018). Inhibition of the Ubc9 E2 SUMO-conjugating enzyme-CRMP2 interaction decreases NaV1.7 currents and reverses experimental neuropathic pain. *Pain, 159*(10), 2115-2127. doi:10.1097/j.pain.0000000000001294

Fukuda, I., Ito, A., Hirai, G., Nishimura, S., Kawasaki, H., Saitoh, H., . . . Yoshida, M. (2009). Ginkgolic acid inhibits protein SUMOylation by blocking formation of the E1-SUMO intermediate. *Chem Biol, 16*(2), 133-140. doi:10.1016/j.chembiol.2009.01.009

Garcia-Caballero, A., Gadotti, V. M., Stemkowski, P., Weiss, N., Souza, I. A., Hodgkinson, V., . . . Zamponi, G. W. (2014). The deubiquitinating enzyme USP5 modulates neuropathic and inflammatory pain by enhancing Cav3.2 channel activity. *Neuron, 83*(5), 1144-1158. doi:10.1016/j.neuron.2014.07.036

Garcia-Caballero, A., Zhang, F. X., Chen, L., M'Dahoma, S., Huang, J., & Zamponi, G. W. (2019). SUMOylation regulates USP5-Cav3.2 calcium channel interactions. *Mol Brain, 12*(1), 73. doi:10.1186/s13041-019-0493-9

Gardoni, F., Mauceri, D., Marcello, E., Sala, C., Di Luca, M., & Jeromin, A. (2007). SAP97 directs the localization of Kv4.2 to spines in hippocampal neurons: regulation by CaMKII. *J Biol Chem, 282*(39), 28691-28699. doi:10.1074/jbc.M701899200

Girach, F., Craig, T. J., Rocca, D. L., & Henley, J. M. (2013). RIM1alpha SUMOylation is required for fast synaptic vesicle exocytosis. *Cell Rep, 5*(5), 1294-1301. doi:10.1016/j.celrep.2013.10.039

Gireud-Goss, M., Reyes, S., Tewari, R., Patrizz, A., Howe, M. D., Kofler, J., . . . Bean, A. J. (2020). The ubiquitin ligase UBE4B regulates amyloid precursor protein ubiquitination, endosomal trafficking, and amyloid beta42 generation and secretion. *Mol Cell Neurosci, 108*, 103542. doi:10.1016/j.mcn.2020.103542

Gong, X., Ahner, A., Roldan, A., Lukacs, G. L., Thibodeau, P. H., & Frizzell, R. A. (2016). Non-native Conformers of Cystic Fibrosis Transmembrane Conductance Regulator NBD1 Are Recognized by Hsp27 and Conjugated to SUMO-2 for Degradation. *J Biol Chem, 291*(4), 2004-2017. doi:10.1074/jbc.M115.685628

Gonzalez, W. G., Pham, K., & Miksovska, J. (2014). Modulation of the voltage-gated potassium channel (Kv4.3) and the auxiliary protein (KChIP3) interactions by the current activator NS5806. *J Biol Chem, 289*(46), 32201-32213. doi:10.1074/jbc.M114.577528

Gross, C., Yao, X., Pong, D. L., Jeromin, A., & Bassell, G. J. (2011). Fragile X mental retardation protein regulates protein expression and mRNA translation of the potassium channel Kv4.2. *J Neurosci, 31*(15), 5693-5698. doi:10.1523/JNEUROSCI.6661-10.2011

Guo, D., Li, M., Zhang, Y., Yang, P., Eckenrode, S., Hopkins, D., . . . Wang, C. Y. (2004). A functional variant of SUMO4, a new I kappa B alpha modifier, is associated with type 1 diabetes. *Nat Genet, 36*(8), 837-841. doi:10.1038/ng1391

Gutman, G. A., Chandy, K. G., Grissmer, S., Lazdunski, M., McKinnon, D., Pardo, L. A., . . . Wang, X. (2005). International Union of Pharmacology. LIII. Nomenclature and molecular relationships of voltage-gated potassium channels. *Pharmacol Rev, 57*(4), 473-508. doi:10.1124/pr.57.4.10

Hall, A. M., Throesch, B. T., Buckingham, S. C., Markwardt, S. J., Peng, Y., Wang, Q., . . . Roberson, E. D. (2015). Tau-dependent Kv4.2 depletion and dendritic hyperexcitability in a mouse model of Alzheimer's disease. *J Neurosci, 35*(15), 6221-6230. doi:10.1523/JNEUROSCI.2552-14.2015

Hammond, R. S., Lin, L., Sidorov, M. S., Wikenheiser, A. M., & Hoffman, D. A. (2008). Protein kinase a mediates activity-dependent Kv4.2 channel trafficking. *J Neurosci, 28*(30), 7513-7519. doi:10.1523/JNEUROSCI.1951-08.2008

Han, W., Nattel, S., Noguchi, T., & Shrier, A. (2006). C-terminal domain of Kv4.2 and associated KChIP2 interactions regulate functional expression and gating of Kv4.2. *J Biol Chem, 281*(37), 27134-27144. doi:10.1074/jbc.M604843200

Han, Y., & Yun, C. C. (2020). Ubiquitin-specific peptidase 7 (USP7) and USP10 mediate deubiquitination of human NHE3 regulating its expression and activity. *FASEB J, 34*(12), 16476-16488. doi:10.1096/fj.202001875R

Hasdemir, B., Fitzgerald, D. J., Prior, I. A., Tepikin, A. V., & Burgoyne, R. D. (2005). Traffic of Kv4 K+ channels mediated by KChIP1 is via a novel post-ER vesicular pathway. *J Cell Biol, 171*(3), 459-469. doi:10.1083/jcb.200506005

Hatano, N., Ohya, S., Muraki, K., Clark, R. B., Giles, W. R., & Imaizumi, Y. (2004). Two arginines in the cytoplasmic C-terminal domain are essential for voltage-dependent regulation of A-type K+ current in the Kv4 channel subfamily. *J Biol Chem, 279*(7), 5450-5459. doi:10.1074/jbc.M302034200

Hecker, C. M., Rabiller, M., Haglund, K., Bayer, P., & Dikic, I. (2006). Specification of SUMO1- and SUMO2-interacting motifs. *J Biol Chem, 281*(23), 16117-16127. doi:10.1074/jbc.M512757200

Hendriks, I. A., D'Souza, R. C., Chang, J. G., Mann, M., & Vertegaal, A. C. (2015). System-wide identification of wild-type SUMO-2 conjugation sites. *Nat Commun, 6*, 7289. doi:10.1038/ncomms8289

Henley, J. M., Carmichael, R. E., & Wilkinson, K. A. (2018). Extranuclear SUMOylation in Neurons. *Trends Neurosci, 41*(4), 198-210. doi:10.1016/j.tins.2018.02.004

Henley, J. M., Seager, R., Nakamura, Y., Talandyte, K., Nair, J., & Wilkinson, K. A. (2021). SUMOylation of synaptic and synapse-associated proteins: An update. *J Neurochem, 156*(2), 145-161. doi:10.1111/jnc.15103

Hickey, C. M., Wilson, N. R., & Hochstrasser, M. (2012). Function and regulation of SUMO proteases. *Nat Rev Mol Cell Biol, 13*(12), 755-766. doi:10.1038/nrm3478

Hoffman, D. A., Magee, J. C., Colbert, C. M., & Johnston, D. (1997). K+ channel regulation of signal propagation in dendrites of hippocampal pyramidal neurons. *Nature, 387*(6636), 869-875. doi:10.1038/43119

Holmqvist, M. H., Cao, J., Hernandez-Pineda, R., Jacobson, M. D., Carroll, K. I., Sung, M. A., . . . An, W. F. (2002). Elimination of fast inactivation in Kv4 A-type potassium channels by an auxiliary subunit domain. *Proc Natl Acad Sci U S A, 99*(2), 1035-1040. doi:10.1073/pnas.022509299

Hu, H. J., Alter, B. J., Carrasquillo, Y., Qiu, C. S., & Gereau, R. W. t. (2007). Metabotropic glutamate receptor 5 modulates nociceptive plasticity via extracellular signal-regulated kinase-Kv4.2 signaling in spinal cord dorsal horn neurons. *J Neurosci, 27*(48), 13181-13191. doi:10.1523/JNEUROSCI.0269-07.2007

Hu, J. H., Malloy, C., Tabor, G. T., Gutzmann, J. J., Liu, Y., Abebe, D., . . . Hoffman, D. A. (2020). Activity-dependent isomerization of Kv4.2 by Pin1 regulates cognitive flexibility. *Nat Commun, 11*(1), 1567. doi:10.1038/s41467-020-15390-x

Huang, J., Yan, J., Zhang, J., Zhu, S., Wang, Y., Shi, T., . . . Yu, J. (2012). SUMO1 modification of PTEN regulates tumorigenesis by controlling its association with the plasma membrane. *Nat Commun, 3*, 911. doi:10.1038/ncomms1919

Jaafari, N., Konopacki, F. A., Owen, T. F., Kantamneni, S., Rubin, P., Craig, T. J., . . . Henley, J. M. (2013). SUMOylation is required for glycine-induced increases in AMPA receptor surface expression (ChemLTP) in hippocampal neurons. *PLoS One, 8*(1), e52345. doi:10.1371/journal.pone.0052345

Jansen, L. R., Forster, L. A., Smith, X. L., Rubaharan, M., Murphy, A. Z., & Baro, D. J. (2021). Changes in peripheral HCN2 channels during persistent inflammation. *Channels (Austin), 15*(1), 165-179. doi:10.1080/19336950.2020.1870086

Jardin, C., Horn, A. H., & Sticht, H. (2015). Binding properties of SUMO-interacting motifs (SIMs) in yeast. *J Mol Model, 21*(3), 50. doi:10.1007/s00894-015-2597-1

Jentsch, S., & Psakhye, I. (2013). Control of nuclear activities by substrate-selective and protein-group SUMOylation. *Annu Rev Genet, 47*, 167-186. doi:10.1146/annurev-genet-111212-133453

Jerng, H. H., Kunjilwar, K., & Pfaffinger, P. J. (2005). Multiprotein assembly of Kv4.2, KChIP3 and DPP10 produces ternary channel complexes with ISA-like properties. *J Physiol, 568*(Pt 3), 767-788. doi:10.1113/jphysiol.2005.087858

Jerng, H. H., & Pfaffinger, P. J. (2008). Multiple Kv channel-interacting proteins contain an N-terminal transmembrane domain that regulates Kv4 channel trafficking and gating. *J Biol Chem, 283*(51), 36046-36059. doi:10.1074/jbc.M806852200

Jerng, H. H., & Pfaffinger, P. J. (2012). Incorporation of DPP6a and DPP6K variants in ternary Kv4 channel complex reconstitutes properties of A-type K current in rat cerebellar granule cells. *PLoS One, 7*(6), e38205. doi:10.1371/journal.pone.0038205

Jerng, H. H., & Pfaffinger, P. J. (2014). Modulatory mechanisms and multiple functions of somatodendritic A-type K (+) channel auxiliary subunits. *Front Cell Neurosci, 8*, 82. doi:10.3389/fncel.2014.00082

Jerng, H. H., Qian, Y., & Pfaffinger, P. J. (2004). Modulation of Kv4.2 channel expression and gating by dipeptidyl peptidase 10 (DPP10). *Biophys J, 87*(4), 2380-2396. doi:10.1529/biophysj.104.042358

Johnson, E. S., & Gupta, A. A. (2001). An E3-like factor that promotes SUMO conjugation to the yeast septins. *Cell, 106*(6), 735-744. doi:10.1016/s0092-8674(01)00491-3

Joshi, S., Rajasekaran, K., Hawk, K. M., Chester, S. J., & Goodkin, H. P. (2018). Status epilepticus: Role for etiology in determining response to benzodiazepines. *Ann Neurol, 83*(4), 830-841. doi:10.1002/ana.25213

Kahyo, T., Nishida, T., & Yasuda, H. (2001). Involvement of PIAS1 in the sumoylation of tumor suppressor p53. *Mol Cell, 8*(3), 713-718. doi:10.1016/s1097-2765(01)00349-5

Kamitani, T., Nguyen, H. P., Kito, K., Fukuda-Kamitani, T., & Yeh, E. T. (1998). Covalent modification of PML by the sentrin family of ubiquitin-like proteins. *J Biol Chem, 273*(6), 3117-3120. Retrieved from https://www.ncbi.nlm.nih.gov/pubmed/9452416

Kanda, H., Ling, J., Chang, Y. T., Erol, F., Viatchenko-Karpinski, V., Yamada, A., . . . Gu, J. G. (2021). Kv4.3 Channel Dysfunction Contributes to Trigeminal Neuropathic Pain Manifested with Orofacial Cold Hypersensitivity in Rats. *J Neurosci, 41*(10), 2091-2105. doi:10.1523/JNEUROSCI.2036-20.2021

Kaulin, Y. A., De Santiago-Castillo, J. A., Rocha, C. A., Nadal, M. S., Rudy, B., & Covarrubias, M. (2009). The dipeptidyl-peptidase-like protein DPP6 determines the unitary conductance of neuronal Kv4.2 channels. *J Neurosci, 29*(10), 3242-3251. doi:10.1523/JNEUROSCI.4767-08.2009

Kerscher, O. (2007). SUMO junction-what's your function? New insights through SUMO-interacting motifs. *EMBO Rep, 8*(6), 550-555. doi:10.1038/sj.embor.7400980

Kharitidi, D., Apaja, P. M., Manteghi, S., Suzuki, K., Malitskaya, E., Roldan, A., . . . Pause, A. (2015). Interplay of Endosomal pH and Ligand Occupancy in Integrin alpha5beta1 Ubiquitination, Endocytic Sorting, and Cell Migration. *Cell Rep, 13*(3), 599-609. doi:10.1016/j.celrep.2015.09.024

Kim, J., Jung, S. C., Clemens, A. M., Petralia, R. S., & Hoffman, D. A. (2007). Regulation of dendritic excitability by activity-dependent trafficking of the A-type K+ channel subunit Kv4.2 in hippocampal neurons. *Neuron, 54*(6), 933-947. doi:10.1016/j.neuron.2007.05.026

Kim, K. R., Kim, Y., Jeong, H. J., Kang, J. S., Lee, S. H., Kim, Y., . . . Ho, W. K. (2021). Impaired pattern separation in Tg2576 mice is associated with hyperexcitable dentate

gyrus caused by Kv4.1 downregulation. *Mol Brain, 14*(1), 62. doi:10.1186/s13041-021-00774-x

Kitazawa, M., Kubo, Y., & Nakajo, K. (2015). Kv4.2 and accessory dipeptidyl peptidase-like protein 10 (DPP10) subunit preferentially form a 4:2 (Kv4.2:DPP10) channel complex. *J Biol Chem, 290*(37), 22724-22733. doi:10.1074/jbc.M115.646794

Kohling, R., & Wolfart, J. (2016). Potassium Channels in Epilepsy. *Cold Spring Harb Perspect Med, 6*(5). doi:10.1101/cshperspect.a022871

Konopacki, F. A., Jaafari, N., Rocca, D. L., Wilkinson, K. A., Chamberlain, S., Rubin, P., . . . Henley, J. M. (2011). Agonist-induced PKC phosphorylation regulates GluK2 SUMOylation and kainate receptor endocytosis. *Proc Natl Acad Sci U S A, 108*(49), 19772-19777. doi:10.1073/pnas.1111575108

Kruse, M., Schulze-Bahr, E., Corfield, V., Beckmann, A., Stallmeyer, B., Kurtbay, G., . . . Pongs, O. (2009). Impaired endocytosis of the ion channel TRPM4 is associated with human progressive familial heart block type I. *J Clin Invest, 119*(9), 2737-2744. doi:10.1172/JCI38292

Kuang, Q., Purhonen, P., & Hebert, H. (2015). Structure of potassium channels. *Cell Mol Life Sci, 72*(19), 3677-3693. doi:10.1007/s00018-015-1948-5

Kunadt, M., Eckermann, K., Stuendl, A., Gong, J., Russo, B., Strauss, K., . . . Schneider, A. (2015). Extracellular vesicle sorting of alpha-Synuclein is regulated by sumoylation. *Acta Neuropathol, 129*(5), 695-713. doi:10.1007/s00401-015-1408-1

Kunjilwar, K., Strang, C., DeRubeis, D., & Pfaffinger, P. J. (2004). KChIP3 rescues the functional expression of Shal channel tetramerization mutants. *J Biol Chem, 279*(52), 54542-54551. doi:10.1074/jbc.M409721200

Kuryshev, Y. A., Gudz, T. I., Brown, A. M., & Wible, B. A. (2000). KChAP as a chaperone for specific K(+) channels. *Am J Physiol Cell Physiol, 278*(5), C931-941. doi:10.1152/ajpcell.2000.278.5.C931

Le, T. L., Yap, A. S., & Stow, J. L. (1999). Recycling of E-cadherin: a potential mechanism for regulating cadherin dynamics. *J Cell Biol, 146*(1), 219-232. Retrieved from https://www.ncbi.nlm.nih.gov/pubmed/10402472
https://www.ncbi.nlm.nih.gov/pmc/articles/PMC2199726/pdf/9901088.pdf

Lee, L., Chen, K. C., & Chang, L. S. (2009). Functional roles of EF-hands in human potassium channel-interacting protein 2.2. *Protein Pept Lett, 16*(9), 1081-1087. Retrieved from https://www.ncbi.nlm.nih.gov/pubmed/19508229

Lee, L., Dale, E., Staniszewski, A., Zhang, H., Saeed, F., Sakurai, M., . . . Arancio, O. (2014). Regulation of synaptic plasticity and cognition by SUMO in normal physiology and Alzheimer's disease. *Sci Rep, 4*, 7190. doi:10.1038/srep07190

Lei, Z., Deng, P., & Xu, Z. C. (2008). Regulation of Kv4.2 channels by glutamate in cultured hippocampal neurons. *J Neurochem, 106*(1), 182-192. doi:10.1111/j.1471-4159.2008.05356.x

Li, K., Jiang, Q., Bai, X., Yang, Y. F., Ruan, M. Y., & Cai, S. Q. (2017). Tetrameric Assembly of K(+) Channels Requires ER-Located Chaperone Proteins. *Mol Cell, 65*(1), 52-65. doi:10.1016/j.molcel.2016.10.027

Liang, Y. C., Lee, C. C., Yao, Y. L., Lai, C. C., Schmitz, M. L., & Yang, W. M. (2016). SUMO5, a Novel Poly-SUMO Isoform, Regulates PML Nuclear Bodies. *Sci Rep, 6*, 26509. doi:10.1038/srep26509

Lin, L., Long, L. K., Hatch, M. M., & Hoffman, D. A. (2014). DPP6 domains responsible for its localization and function. *J Biol Chem, 289*(46), 32153-32165. doi:10.1074/jbc.M114.578070

Lin, L., Sun, W., Kung, F., Dell'Acqua, M. L., & Hoffman, D. A. (2011). AKAP79/150 impacts intrinsic excitability of hippocampal neurons through phospho-regulation of A-type K+ channel trafficking. *J Neurosci, 31*(4), 1323-1332. doi:10.1523/JNEUROSCI.5383-10.2011

Lin, L., Sun, W., Wikenheiser, A. M., Kung, F., & Hoffman, D. A. (2010). KChIP4a regulates Kv4.2 channel trafficking through PKA phosphorylation. *Mol Cell Neurosci, 43*(3), 315-325. doi:10.1016/j.mcn.2009.12.005

Loriol, C., Casse, F., Khayachi, A., Poupon, G., Chafai, M., Deval, E., . . . Martin, S. (2014). mGlu5 receptors regulate synaptic sumoylation via a transient PKC-dependent diffusional trapping of Ubc9 into spines. *Nat Commun, 5*, 5113. doi:10.1038/ncomms6113

Loriol, C., Khayachi, A., Poupon, G., Gwizdek, C., & Martin, S. (2013). Activity-dependent regulation of the sumoylation machinery in rat hippocampal neurons. *Biol Cell, 105*(1), 30-45. doi:10.1111/boc.201200016

Lu, H., Liu, B., You, S., Xue, Q., Zhang, F., Cheng, J., & Yu, B. (2009). The activity-dependent stimuli increase SUMO modification in SHSY5Y cells. *Biochem Biophys Res Commun, 390*(3), 872-876. doi:10.1016/j.bbrc.2009.10.065

Lugo, J. N., Barnwell, L. F., Ren, Y., Lee, W. L., Johnston, L. D., Kim, R., . . . Anderson, A. E. (2008). Altered phosphorylation and localization of the A-type channel, Kv4.2 in status epilepticus. *J Neurochem, 106*(4), 1929-1940. doi:10.1111/j.1471-4159.2008.05508.x

Ma, G., Li, S., Han, Y., Li, S., Yue, T., Wang, B., & Jiang, J. (2016). Regulation of Smoothened Trafficking and Hedgehog Signaling by the SUMO Pathway. *Dev Cell, 39*(4), 438-451. doi:10.1016/j.devcel.2016.09.014

Marionneau, C., Carrasquillo, Y., Norris, A. J., Townsend, R. R., Isom, L. L., Link, A. J., & Nerbonne, J. M. (2012). The sodium channel accessory subunit Navbeta1 regulates neuronal excitability through modulation of repolarizing voltage-gated K(+) channels. *J Neurosci, 32*(17), 5716-5727. doi:10.1523/JNEUROSCI.6450-11.2012

Martin, S., Nishimune, A., Mellor, J. R., & Henley, J. M. (2007). SUMOylation regulates kainate-receptor-mediated synaptic transmission. *Nature, 447*(7142), 321-325. doi:10.1038/nature05736

Martin, S., Wilkinson, K. A., Nishimune, A., & Henley, J. M. (2007). Emerging extranuclear roles of protein SUMOylation in neuronal function and dysfunction. *Nat Rev Neurosci, 8*(12), 948-959. doi:10.1038/nrn2276

Matic, I., Schimmel, J., Hendriks, I. A., van Santen, M. A., van de Rijke, F., van Dam, H., . . . Vertegaal, A. C. (2010). Site-specific identification of SUMO-2 targets in cells reveals an inverted SUMOylation motif and a hydrophobic cluster SUMOylation motif. *Mol Cell, 39*(4), 641-652. doi:10.1016/j.molcel.2010.07.026

Melino, G., Gallagher, E., Aqeilan, R. I., Knight, R., Peschiaroli, A., Rossi, M., . . . Bernassola, F. (2008). Itch: a HECT-type E3 ligase regulating immunity, skin and cancer. *Cell Death Differ, 15*(7), 1103-1112. doi:10.1038/cdd.2008.60

Mendes, A. V., Grou, C. P., Azevedo, J. E., & Pinto, M. P. (2016). Evaluation of the activity and substrate specificity of the human SENP family of SUMO proteases. *Biochim Biophys Acta, 1863*(1), 139-147. doi:10.1016/j.bbamcr.2015.10.020

Mettlen, M., Chen, P. H., Srinivasan, S., Danuser, G., & Schmid, S. L. (2018). Regulation of Clathrin-Mediated Endocytosis. *Annu Rev Biochem, 87*, 871-896. doi:10.1146/annurev-biochem-062917-012644

Meulmeester, E., Kunze, M., Hsiao, H. H., Urlaub, H., & Melchior, F. (2008). Mechanism and consequences for paralog-specific sumoylation of ubiquitin-specific protease 25. *Mol Cell, 30*(5), 610-619. doi:10.1016/j.molcel.2008.03.021

Morohashi, Y., Hatano, N., Ohya, S., Takikawa, R., Watabiki, T., Takasugi, N., . . . Iwatsubo, T. (2002). Molecular cloning and characterization of CALP/KChIP4, a novel EF-hand protein interacting with presenilin 2 and voltage-gated potassium channel subunit Kv4. *J Biol Chem, 277*(17), 14965-14975. doi:10.1074/jbc.M200897200

Moutal, A., Dustrude, E. T., Largent-Milnes, T. M., Vanderah, T. W., Khanna, M., & Khanna, R. (2017). Blocking CRMP2 SUMOylation reverses neuropathic pain. *Mol Psychiatry*. doi:10.1038/mp.2017.117

Nadal, M. S., Amarillo, Y., Vega-Saenz de Miera, E., & Rudy, B. (2006). Differential characterization of three alternative spliced isoforms of DPPX. *Brain Res, 1094*(1), 1-12. doi:10.1016/j.brainres.2006.03.106

Nadal, M. S., Ozaita, A., Amarillo, Y., Vega-Saenz de Miera, E., Ma, Y., Mo, W., . . . Rudy, B. (2003). The CD26-related dipeptidyl aminopeptidase-like protein DPPX is a critical component of neuronal A-type K+ channels. *Neuron, 37*(3), 449-461. Retrieved from https://www.ncbi.nlm.nih.gov/pubmed/12575952

https://ac.els-cdn.com/S0896627302011856/1-s2.0-S0896627302011856-main.pdf?_tid=4a6795ac-930c-4b8e-bef6-4fed20af9b82&acdnat=1537189364_1dae5f3a20f3cc81adb973df15697d5e

Namanja, A. T., Li, Y. J., Su, Y., Wong, S., Lu, J., Colson, L. T., . . . Chen, Y. (2012). Insights into high affinity small ubiquitin-like modifier (SUMO) recognition by SUMO-interacting motifs (SIMs) revealed by a combination of NMR and peptide array analysis. *J Biol Chem, 287*(5), 3231-3240. doi:10.1074/jbc.M111.293118

Nayak, A., & Muller, S. (2014). SUMO-specific proteases/isopeptidases: SENPs and beyond. *Genome Biol, 15*(7), 422. doi:10.1186/s13059-014-0422-2

Nestor, M. W., & Hoffman, D. A. (2012). Differential cycling rates of Kv4.2 channels in proximal and distal dendrites of hippocampal CA1 pyramidal neurons. *Hippocampus, 22*(5), 969-980. doi:10.1002/hipo.20899

Noh, W., Pak, S., Choi, G., Yang, S., & Yang, S. (2019). Transient Potassium Channels: Therapeutic Targets for Brain Disorders. *Front Cell Neurosci, 13*, 265. doi:10.3389/fncel.2019.00265

O'Callaghan, D. W., Hasdemir, B., Leighton, M., & Burgoyne, R. D. (2003). Residues within the myristoylation motif determine intracellular targeting of the neuronal Ca2+ sensor protein KChIP1 to post-ER transport vesicles and traffic of Kv4 K+ channels. *J Cell Sci, 116*(Pt 23), 4833-4845. doi:10.1242/jcs.00803

Odeh, H. M., Coyaud, E., Raught, B., & Matunis, M. J. (2018). The SUMO-specific isopeptidase SENP2 is targeted to intracellular membranes via a predicted N-terminal amphipathic alpha-helix. *Mol Biol Cell, 29*(15), 1878-1890. doi:10.1091/mbc.E17-07-0445

Osawa, M., Dace, A., Tong, K. I., Valiveti, A., Ikura, M., & Ames, J. B. (2005). Mg2+ and Ca2+ differentially regulate DNA binding and dimerization of DREAM. *J Biol Chem, 280*(18), 18008-18014. doi:10.1074/jbc.M500338200

Owerbach, D., McKay, E. M., Yeh, E. T., Gabbay, K. H., & Bohren, K. M. (2005). A proline-90 residue unique to SUMO-4 prevents maturation and sumoylation. *Biochem Biophys Res Commun, 337*(2), 517-520. doi:10.1016/j.bbrc.2005.09.090

Parker, A. R., Forster, L. A., & Baro, D. J. (2019). Modulator-Gated, SUMOylation-Mediated, Activity-Dependent Regulation of Ionic Current Densities Contributes to Short-Term Activity Homeostasis. *J Neurosci, 39*(4), 596-611. doi:10.1523/JNEUROSCI.1379-18.2018

Parker, A. R., Welch, M. A., Forster, L. A., Tasneem, S. M., Dubhashi, J. A., & Baro, D. J. (2016). SUMOylation of the Hyperpolarization-Activated Cyclic Nucleotide-Gated Channel 2 Increases Surface Expression and the Maximal Conductance of the Hyperpolarization-Activated Current. *Front Mol Neurosci, 9*, 168. doi:10.3389/fnmol.2016.00168

Parker, A. R., Welch, M. A., Forster, L. A., Tasneem, S. M., Dubhashi, J. A., & Baro, D. J. (2017). SUMOylation of the Hyperpolarization-Activated Cyclic Nucleotide-Gated Channel 2 Increases Surface Expression and the Maximal Conductance of the Hyperpolarization-Activated Current. *Front Mol Neurosci, 9*, 168. doi:10.3389/fnmol.2016.00168

Petrecca, K., Miller, D. M., & Shrier, A. (2000). Localization and enhanced current density of the Kv4.2 potassium channel by interaction with the actin-binding protein filamin. *J Neurosci, 20*(23), 8736-8744. Retrieved from https://www.ncbi.nlm.nih.gov/pubmed/11102480
http://www.jneurosci.org/content/jneuro/20/23/8736.full.pdf

Ping, Y., Hahm, E. T., Waro, G., Song, Q., Vo-Ba, D. A., Licursi, A., . . . Tsunoda, S. (2015). Linking abeta42-induced hyperexcitability to neurodegeneration, learning and motor deficits, and a shorter lifespan in an Alzheimer's model. *PLoS Genet, 11*(3), e1005025. doi:10.1371/journal.pgen.1005025

Pioletti, M., Findeisen, F., Hura, G. L., & Minor, D. L., Jr. (2006). Three-dimensional structure of the KChIP1-Kv4.3 T1 complex reveals a cross-shaped octamer. *Nat Struct Mol Biol, 13*(11), 987-995. doi:10.1038/nsmb1164

Piper, R. C., Dikic, I., & Lukacs, G. L. (2014). Ubiquitin-dependent sorting in endocytosis. *Cold Spring Harb Perspect Biol, 6*(1). doi:10.1101/cshperspect.a016808

Plant, L. D., Dementieva, I. S., Kollewe, A., Olikara, S., Marks, J. D., & Goldstein, S. A. (2010). One SUMO is sufficient to silence the dimeric potassium channel K2P1. *Proc Natl Acad Sci U S A, 107*(23), 10743-10748. doi:10.1073/pnas.1004712107

Plant, L. D., Dowdell, E. J., Dementieva, I. S., Marks, J. D., & Goldstein, S. A. (2011). SUMO modification of cell surface Kv2.1 potassium channels regulates the activity of rat hippocampal neurons. *J Gen Physiol, 137*(5), 441-454. doi:10.1085/jgp.201110604

Plant, L. D., Marks, J. D., & Goldstein, S. A. (2016). SUMOylation of NaV1.2 channels mediates the early response to acute hypoxia in central neurons. *Elife, 5*. doi:10.7554/eLife.20054

Plant, L. D., Xiong, D., Romero, J., Dai, H., & Goldstein, S. A. N. (2020). Hypoxia Produces Pro-arrhythmic Late Sodium Current in Cardiac Myocytes by SUMOylation of NaV1.5 Channels. *Cell Rep, 30*(7), 2225-2236 e2224. doi:10.1016/j.celrep.2020.01.025

Plant, L. D., Zuniga, L., Araki, D., Marks, J. D., & Goldstein, S. A. (2012). SUMOylation silences heterodimeric TASK potassium channels containing K2P1 subunits in cerebellar granule neurons. *Sci Signal, 5*(251), ra84. doi:10.1126/scisignal.2003431

Pourrier, M., Schram, G., & Nattel, S. (2003). Properties, expression and potential roles of cardiac K+ channel accessory subunits: MinK, MiRPs, KChIP, and KChAP. *J Membr Biol, 194*(3), 141-152. doi:10.1007/s00232-003-2034-8

Preston, G. M., & Brodsky, J. L. (2017). The evolving role of ubiquitin modification in endoplasmic reticulum-associated degradation. *Biochem J, 474*(4), 445-469. doi:10.1042/BCJ20160582

Psakhye, I., & Jentsch, S. (2012). Protein group modification and synergy in the SUMO pathway as exemplified in DNA repair. *Cell, 151*(4), 807-820. doi:10.1016/j.cell.2012.10.021

Qi, Y., Wang, J., Bomben, V. C., Li, D. P., Chen, S. R., Sun, H., . . . Yeh, E. T. (2014). Hyper-SUMOylation of the Kv7 potassium channel diminishes the M-current leading to seizures and sudden death. *Neuron, 83*(5), 1159-1171. doi:10.1016/j.neuron.2014.07.042

Rajan, S., Plant, L. D., Rabin, M. L., Butler, M. H., & Goldstein, S. A. (2005). Sumoylation silences the plasma membrane leak K+ channel K2P1. *Cell, 121*(1), 37-47. doi:10.1016/j.cell.2005.01.019

Ren, X., Hayashi, Y., Yoshimura, N., & Takimoto, K. (2005). Transmembrane interaction mediates complex formation between peptidase homologues and Kv4 channels. *Mol Cell Neurosci, 29*(2), 320-332. doi:10.1016/j.mcn.2005.02.003

Rivera, J. F., Ahmad, S., Quick, M. W., Liman, E. R., & Arnold, D. B. (2003). An evolutionarily conserved dileucine motif in Shal K+ channels mediates dendritic targeting. *Nat Neurosci, 6*(3), 243-250. doi:10.1038/nn1020

Rodgers, E. W., Krenz, W. D., Jiang, X., Li, L., & Baro, D. J. (2013). Dopaminergic tone regulates transient potassium current maximal conductance through a translational mechanism requiring D1Rs, cAMP/PKA, Erk and mTOR. *BMC Neurosci, 14*, 143. doi:10.1186/1471-2202-14-143

Sampson, D. A., Wang, M., & Matunis, M. J. (2001). The small ubiquitin-like modifier-1 (SUMO-1) consensus sequence mediates Ubc9 binding and is essential for SUMO-1 modification. *J Biol Chem, 276*(24), 21664-21669. doi:10.1074/jbc.M100006200

Scala, F., Fusco, S., Ripoli, C., Piacentini, R., Li Puma, D. D., Spinelli, M., . . . D'Ascenzo, M. (2015). Intraneuronal Abeta accumulation induces hippocampal neuron hyperexcitability through A-type K(+) current inhibition mediated by activation of caspases and GSK-3. *Neurobiol Aging, 36*(2), 886-900. doi:10.1016/j.neurobiolaging.2014.10.034

Schrader, L. A., Anderson, A. E., Mayne, A., Pfaffinger, P. J., & Sweatt, J. D. (2002). PKA modulation of Kv4.2-encoded A-type potassium channels requires formation of a supramolecular complex. *J.Neurosci., 22*(23), 10123-10133. Retrieved from PM:12451113

Schrader, L. A., Anderson, A. E., Mayne, A., Pfaffinger, P. J., & Sweatt, J. D. (2002). PKA modulation of Kv4.2-encoded A-type potassium channels requires formation of a supramolecular complex. *J Neurosci, 22*(23), 10123-10133. Retrieved from https://www.ncbi.nlm.nih.gov/pubmed/12451113

https://www.ncbi.nlm.nih.gov/pmc/articles/PMC6758737/pdf/ns2302010123.pdf

Schrader, L. A., Ren, Y., Cheng, F., Bui, D., Sweatt, J. D., & Anderson, A. E. (2009). Kv4.2 is a locus for PKC and ERK/MAPK cross-talk. *Biochem J, 417*(3), 705-715. doi:10.1042/BJ20081213

Seifert, A., Schofield, P., Barton, G. J., & Hay, R. T. (2015). Proteotoxic stress reprograms the chromatin landscape of SUMO modification. *Sci Signal, 8*(384), rs7. doi:10.1126/scisignal.aaa2213

Seifert, C., Storch, S., & Bahring, R. (2020). Modulation of Kv4.2/KChIP3 interaction by the ceroid lipofuscinosis neuronal 3 protein CLN3. *J Biol Chem, 295*(34), 12099-12110. doi:10.1074/jbc.RA120.013828

Seikel, E., & Trimmer, J. S. (2009). Convergent modulation of Kv4.2 channel alpha subunits by structurally distinct DPPX and KChIP auxiliary subunits. *Biochemistry, 48*(24), 5721-5730. doi:10.1021/bi802316m

Shah, M. M., Hammond, R. S., & Hoffman, D. A. (2010). Dendritic ion channel trafficking and plasticity. *Trends Neurosci, 33*(7), 307-316. doi:10.1016/j.tins.2010.03.002

Shen, B., Zhou, K., Yang, S., Xu, T., & Wang, Y. (2008). The Kv4.2 mediates excitatory activity-dependent regulation of neuronal excitability in rat cortical neurons. *J Neurochem, 105*(3), 773-783. doi:10.1111/j.1471-4159.2007.05179.x

Sheng, M., Tsaur, M. L., Jan, Y. N., & Jan, L. Y. (1992). Subcellular segregation of two A-type K+ channel proteins in rat central neurons. *Neuron, 9*(2), 271-284. Retrieved from https://www.ncbi.nlm.nih.gov/pubmed/1497894
http://ac.els-cdn.com/089662739290166B/1-s2.0-089662739290166B-main.pdf?_tid=749b8a9e-5ffb-11e7-aa16-00000aacb35e&acdnat=1499092105_75f081aef320fdf891c92042649f922e

Shibata, R., Misonou, H., Campomanes, C. R., Anderson, A. E., Schrader, L. A., Doliveira, L. C., . . . Trimmer, J. S. (2003). A fundamental role for KChIPs in determining the molecular properties and trafficking of Kv4.2 potassium channels. *J Biol Chem, 278*(38), 36445-36454. doi:10.1074/jbc.M306142200

Smith, S. E., Xu, L., Kasten, M. R., & Anderson, M. P. (2012). Mutant LGI1 inhibits seizure-induced trafficking of Kv4.2 potassium channels. *J Neurochem, 120*(4), 611-621. doi:10.1111/j.1471-4159.2011.07605.x

Soh, H., & Goldstein, S. A. (2008). I SA channel complexes include four subunits each of DPP6 and Kv4.2. *J Biol Chem, 283*(22), 15072-15077. doi:10.1074/jbc.M706964200

Sokolova, O., Accardi, A., Gutierrez, D., Lau, A., Rigney, M., & Grigorieff, N. (2003). Conformational changes in the C terminus of Shaker K+ channel bound to the rat Kvbeta2-subunit. *Proc Natl Acad Sci U S A, 100*(22), 12607-12612. doi:10.1073/pnas.2235650100

Steffensen, A. B., Andersen, M. N., Mutsaers, N., Mujezinovic, A., & Schmitt, N. (2018). SUMO co-expression modifies KV 11.1 channel activity. *Acta Physiol (Oxf), 222*(3). doi:10.1111/apha.12974

Takimoto, K., Hayashi, Y., Ren, X., & Yoshimura, N. (2006). Species and tissue differences in the expression of DPPY splicing variants. *Biochem Biophys Res Commun, 348*(3), 1094-1100. doi:10.1016/j.bbrc.2006.07.157

Takimoto, K., Yang, E. K., & Conforti, L. (2002). Palmitoylation of KChIP splicing variants is required for efficient cell surface expression of Kv4.3 channels. *J Biol Chem, 277*(30), 26904-26911. doi:10.1074/jbc.M203651200

Tang, B. L. (2020). Vesicle transport through interaction with t-SNAREs 1a (Vti1a)'s roles in neurons. *Heliyon, 6*(8), e04600. doi:10.1016/j.heliyon.2020.e04600

Tang, L. T., Craig, T. J., & Henley, J. M. (2015). SUMOylation of synapsin Ia maintains synaptic vesicle availability and is reduced in an autism mutation. *Nat Commun, 6*, 7728. doi:10.1038/ncomms8728

Tatham, M. H., Jaffray, E., Vaughan, O. A., Desterro, J. M., Botting, C. H., Naismith, J. H., & Hay, R. T. (2001). Polymeric chains of SUMO-2 and SUMO-3 are conjugated to protein

substrates by SAE1/SAE2 and Ubc9. *J Biol Chem, 276*(38), 35368-35374. doi:10.1074/jbc.M104214200

Tong, J., Taylor, P., & Moran, M. F. (2014). Proteomic analysis of the epidermal growth factor receptor (EGFR) interactome and post-translational modifications associated with receptor endocytosis in response to EGF and stress. *Mol Cell Proteomics, 13*(7), 1644-1658. doi:10.1074/mcp.M114.038596

Uzoma, I., Hu, J., Cox, E., Xia, S., Zhou, J., Rho, H. S., . . . Zhu, H. (2018). Global Identification of Small Ubiquitin-related Modifier (SUMO) Substrates Reveals Crosstalk between SUMOylation and Phosphorylation Promotes Cell Migration. *Mol Cell Proteomics, 17*(5), 871-888. doi:10.1074/mcp.RA117.000014

Varga, A. W., Yuan, L. L., Anderson, A. E., Schrader, L. A., Wu, G. Y., Gatchel, J. R., . . . Sweatt, J. D. (2004). Calcium-calmodulin-dependent kinase II modulates Kv4.2 channel expression and upregulates neuronal A-type potassium currents. *J Neurosci, 24*(14), 3643-3654. doi:10.1523/JNEUROSCI.0154-04.2004

Wang, C., Pan, Y., Zhang, W., Chen, Y., Li, C., Zhao, F., & Behnisch, T. (2021). Positive Regulatory Domain I-binding Factor 1 Mediates Peripheral Nerve Injury-induced Nociception in Mice by Repressing Kv4.3 Channel Expression. *Anesthesiology, 134*(3), 435-456. doi:10.1097/ALN.0000000000003654

Wang, C. Y., Yang, P., Li, M., & Gong, F. (2009). Characterization of a negative feedback network between SUMO4 expression and NFkappaB transcriptional activity. *Biochem Biophys Res Commun, 381*(4), 477-481. doi:10.1016/j.bbrc.2009.02.060

Wang, H., Yan, Y., Liu, Q., Huang, Y., Shen, Y., Chen, L., . . . Chai, J. (2007). Structural basis for modulation of Kv4 K+ channels by auxiliary KChIP subunits. *Nat Neurosci, 10*(1), 32-39. doi:10.1038/nn1822

Wang, T., Cheng, Y., Dou, Y., Goonesekara, C., David, J. P., Steele, D. F., . . . Fedida, D. (2012). Trafficking of an endogenous potassium channel in adult ventricular myocytes. *Am J Physiol Cell Physiol, 303*(9), C963-976. doi:10.1152/ajpcell.00217.2012

Wang, W., Chen, Y., Wang, S., Hu, N., Cao, Z., Wang, W., . . . Zhang, X. (2014). PIASxalpha ligase enhances SUMO1 modification of PTEN protein as a SUMO E3 ligase. *J Biol Chem, 289*(6), 3217-3230. doi:10.1074/jbc.M113.508515

Wang, W. C., Cheng, C. F., & Tsaur, M. L. (2015). Immunohistochemical localization of DPP10 in rat brain supports the existence of a Kv4/KChIP/DPPL ternary complex in neurons. *J Comp Neurol, 523*(4), 608-628. doi:10.1002/cne.23698

Wang, Y., Gao, Y., Tian, Q., Deng, Q., Wang, Y., Zhou, T., . . . Li, Y. (2018). TRPV1 SUMOylation regulates nociceptive signaling in models of inflammatory pain. *Nat Commun, 9*(1), 1529. doi:10.1038/s41467-018-03974-7

Wasik, U., & Filipek, A. (2014). Non-nuclear function of sumoylated proteins. *Biochim Biophys Acta, 1843*(12), 2878-2885. doi:10.1016/j.bbamcr.2014.07.018

Watts, F. Z. (2013). Starting and stopping SUMOylation. What regulates the regulator? *Chromosoma, 122*(6), 451-463. doi:10.1007/s00412-013-0422-0

Wei, W., Yang, P., Pang, J., Zhang, S., Wang, Y., Wang, M. H., . . . Wang, C. Y. (2008). A stress-dependent SUMO4 sumoylation of its substrate proteins. *Biochem Biophys Res Commun, 375*(3), 454-459. doi:10.1016/j.bbrc.2008.08.028

Welch, M. A., Forster, L. A., Atlas, S. I., & Baro, D. J. (2019). SUMOylating Two Distinct Sites on the A-type Potassium Channel, Kv4.2, Increases Surface Expression and Decreases Current Amplitude. *Front Mol Neurosci, 12*, 144. doi:10.3389/fnmol.2019.00144

Wong, W., Newell, E. W., Jugloff, D. G., Jones, O. T., & Schlichter, L. C. (2002). Cell surface targeting and clustering interactions between heterologously expressed PSD-95 and the Shal voltage-gated potassium channel, Kv4.2. *J Biol Chem, 277*(23), 20423-20430. doi:10.1074/jbc.M109412200

Wu, H., Chen, X., Cheng, J., & Qi, Y. (2016). SUMOylation and Potassium Channels: Links to Epilepsy and Sudden Death. *Adv Protein Chem Struct Biol, 103*, 295-321. doi:10.1016/bs.apcsb.2015.11.009

Wu, X., & Rapoport, T. A. (2018). Mechanistic insights into ER-associated protein degradation. *Curr Opin Cell Biol, 53*, 22-28. doi:10.1016/j.ceb.2018.04.004

Xiong, D., Li, T., Dai, H., Arena, A. F., Plant, L. D., & Goldstein, S. A. N. (2017). SUMOylation determines the voltage required to activate cardiac IKs channels. *Proc Natl Acad Sci U S A, 114*(32), E6686-E6694. doi:10.1073/pnas.1706267114

Yamakawa, T., Saith, S., Li, Y., Gao, X., Gaisano, H. Y., & Tsushima, R. G. (2007). Interaction of syntaxin 1A with the N-terminus of Kv4.2 modulates channel surface expression and gating. *Biochemistry, 46*(38), 10942-10949. doi:10.1021/bi7006806

Yang, E. K., Alvira, M. R., Levitan, E. S., & Takimoto, K. (2001). Kvbeta subunits increase expression of Kv4.3 channels by interacting with their C termini. *J Biol Chem, 276*(7), 4839-4844. doi:10.1074/jbc.M004768200

Yasugi, T., & Howley, P. M. (1996). Identification of the structural and functional human homolog of the yeast ubiquitin conjugating enzyme UBC9. *Nucleic Acids Res, 24*(11), 2005-2010. Retrieved from https://www.ncbi.nlm.nih.gov/pubmed/8668529 https://www.ncbi.nlm.nih.gov/pmc/articles/PMC145898/pdf/242005.pdf

Yuan, L. L., Adams, J. P., Swank, M., Sweatt, J. D., & Johnston, D. (2002). Protein kinase modulation of dendritic K+ channels in hippocampus involves a mitogen-activated protein kinase pathway. *J Neurosci, 22*(12), 4860-4868. Retrieved from https://www.ncbi.nlm.nih.gov/pubmed/12077183

Zagha, E., Ozaita, A., Chang, S. Y., Nadal, M. S., Lin, U., Saganich, M. J., . . . Rudy, B. (2005). DPP10 modulates Kv4-mediated A-type potassium channels. *J Biol Chem, 280*(19), 18853-18861. doi:10.1074/jbc.M410613200

Zemel, B. M., Ritter, D. M., Covarrubias, M., & Muqeem, T. (2018). A-Type KV Channels in Dorsal Root Ganglion Neurons: Diversity, Function, and Dysfunction. *Front Mol Neurosci, 11*, 253. doi:10.3389/fnmol.2018.00253

Zhao, Q., Xie, Y., Zheng, Y., Jiang, S., Liu, W., Mu, W., . . . Ren, J. (2014). GPS-SUMO: a tool for the prediction of sumoylation sites and SUMO-interaction motifs. *Nucleic Acids Res, 42*(Web Server issue), W325-330. doi:10.1093/nar/gku383

Zhou, H. J., Xu, Z., Wang, Z., Zhang, H., Zhuang, Z. W., Simons, M., & Min, W. (2018). SUMOylation of VEGFR2 regulates its intracellular trafficking and pathological angiogenesis. *Nat Commun, 9*(1), 3303. doi:10.1038/s41467-018-05812-2

Zhu, J., Zhu, S., Guzzo, C. M., Ellis, N. A., Sung, K. S., Choi, C. Y., & Matunis, M. J. (2008). Small ubiquitin-related modifier (SUMO) binding determines substrate recognition and paralog-selective SUMO modification. *J Biol Chem, 283*(43), 29405-29415. doi:10.1074/jbc.M803632200